

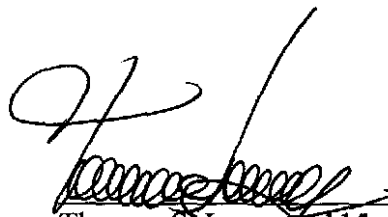
540187

**Analysis Report
Task 3 of AP-110
Evaluation of Water-Level Rise in the Culebra Due to Leakage Through
Poorly Plugged and Abandoned Potash Boreholes**

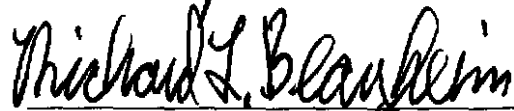
**(AP-110: Analysis Plan for Evaluation of
Culebra Water-Level-Rise Scenarios)**

Task Number 1.4.1.1

Authors:

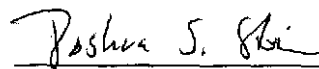

Thomas S. Lowry, 6115
Geohydrology Department

6-2-05
Date


Richard L. Beauheim, 6822
Repository Performance Department

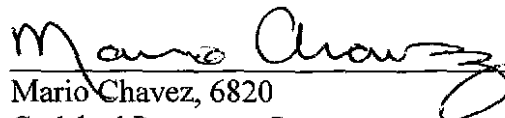
6/9/05
Date

Technical Review:


Joshua S. Stein, 6852
Subsystems Performance Assessment Department

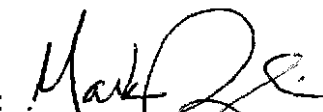
6-2-2005
Date

QA Review:


Mario Chavez, 6820
Carlsbad Programs Group

6/13/05
Date

Management Review:


Mark Rigali, 6822
Manager, Repository Performance Department

6/9/05
Date

Table of Contents

1	Introduction	5
1.1	<i>Background</i>	5
1.2	<i>Water-Level Rise</i>	5
1.3	<i>Outline</i>	8
2	Approach	10
2.1	<i>Overview</i>	10
2.2	<i>Software</i>	15
2.3	<i>File-Naming Conventions</i>	16
2.4	<i>Model Domain and Discretization</i>	18
2.5	<i>Boundary and Initial Conditions</i>	19
3	Data	20
4	Modeling Assumptions and Parameters	22
4.1	<i>Assumptions</i>	22
4.2	<i>Parameters</i>	23
5	Results	24
5.1	<i>Option A</i>	24
5.2	<i>Option B</i>	30
5.3	<i>Option C</i>	35
6	Discussion	41
7	Summary and Conclusions	45
	References:	47
	Appendix A: Fitted Well Data for Calibration	50
	Appendix B: FORTRAN Utility Code - T_Field.f90	54
	Appendix C: FORTRAN Utility Code - Get_heads.f90	55
	Appendix D: FORTRAN Utility Code - exhdsdrw_scratch.f90	57
	Appendix E: FORTRAN Utility Code - mfrun.f90	60
	Appendix F: FORTRAN Utility Code - cut.f90	62
	Appendix G: Linux Shell Script - Ppest_run.sh	63
	Appendix H: Linux Shell Script - clean.sh	64
	Appendix I: Linux Shell Script - runpest.sh	65
	Appendix J: Linux Shell Script - setup.sh	66
	Appendix K: Linux Shell Script - pslave.sh	67
	Appendix L: Linux Shell Script - pmaster.sh	68
	Appendix M: Linux Shell Script - mfrun.sh	69
	Appendix N: Option A Calibrated Filtered Head Rises	70
	Appendix O: Option A Calibration Results	74
	Appendix P: Option B Calibrated Filtered Head Rises	76
	Appendix Q: Option B Calibration Results	80
	Appendix R: Option C Calibrated Filtered Head Rises	82
	Appendix S: Option C Calibration Results	86
	Appendix T: Option C Long-Term Simulations (115 yr)	88

List of Tables

Table 1. Cementing categories for potash and other drillholes in the hydrologic domain.	12
Table 2. The three Options and their respective calibration parameters and variables. Calibration is achieved by adjusting the calibration variables such that the difference between the calibration parameter and the linearized head rise from the data is minimized. The values of variables that are kept fixed during the calibrations are shown in parentheses.	14
Table 3. Major codes used for this analysis.	15
Table 4. Input and output data files used for Task 2. Each directory is listed as its relation to /home3/tslowry/wipp.	18
Table 5. The coordinates of the corners of the numerical model domain in UTM NAD27 coordinate system.	19
Table 6. The coordinates of the corners of the WIPP land withdrawal boundary (LWB) in UTM NAD27 coordinate system.	19
Table 7. Well coordinates in UTM NAD27, and the calculated slope of the head-rise.	20
Table 8. Option A total leakage rates for each group of leaky boreholes.	25
Table 9. Relative error, ε , of each T-field sorted by best (d05r05) to worst (d08r05) for Option A.	26
Table 10. Percentage contribution of each well to the total error for the average case, T-field d05r05 (best fit), T-field d04r08 (median case) and T-field d08r05 (worst fit) for Option A. The results for the four worst-fitting wells for each case are in bold.	28
Table 11. Option B total leakage rates for each group of leaky boreholes.	30
Table 12. Relative error, ε , of each T-field sorted by best (d22r02) to worst (d07r10) for Option B.	31
Table 13. Percentage contribution of each well to the total error for the average case, T-field d22r02 (best fit), T-field d07r10 (median case) and T-field d03r06 (worst fit) for Option B. The results for the four worst-fitting wells for each case are in bold.	33
Table 14. Option C total leakage rates for each group of leaky boreholes and S_s values. S_s^{ND} is the specific storage in Nash Draw, S_s is the specific storage elsewhere.	35
Table 15. Relative error, ε , of each T-field sorted by best (d01r06) to worst (d04r08) for Option C.	36
Table 16. Comparison of specific storage values (m^{-1}) from Lowry and Beauheim (2004) and Option C.	36
Table 17. Percentage contribution of each well to the total error for the average case, T-field d01r06 (best fit), T-field d12r06 (median case) and T-field d04r08 (worst fit) for Option C. The results for the four worst-fitting wells for each case are in bold.	38
Table 18. Comparison of mean calibration parameters for all three options. Percentages show percent of leakage from that group to the total leakage.	41

List of Figures

Figure 1. Locations of Culebra wells used in the CCA modeling.	6
Figure 2. Water-level trends in the Culebra for Nash Draw wells and P-14.	7
Figure 3. Rising Culebra and Magenta water levels at H-6.	7
Figure 4. Categorized potash exploration boreholes in the WIPP region.	11
Figure 5. Modeling domain showing boundary features, monitoring well locations, Nash Draw area, WIPP boundary, and the grouping of the leaky boreholes for use in the calibration process.	13
Figure 6. Comparison of the best-fit T-field (d05r05) and the worst-fit T-field (d08r05) for Option A.	26
Figure 7. Simulated head-rise for T-field d05r05, Option A, versus data head-rise.	27
Figure 8. Contour plots of the normalized ε value as calculated at each well for Option A.	29
Figure 9. Comparison of the best-fit T-field (d22r02) and the worst-fit T-field (d07r10) for Option B.	32
Figure 10. Simulated head-rise for T-field d22r02, Option B, versus data head-rise.	32
Figure 11. Contour plots of the normalized ε value as calculated at each well for Option B.	34
Figure 12. Comparison of the best-fit T-field (d01r06) and the worst-fit T-field (d04r08) for Option C.	37
Figure 13. Simulated head-rise for T-field d01r06, Option C, versus data head-rise.	38
Figure 14. Contour plots of the normalized ε value as calculated at each well for Option C.	39
Figure 15. Histogram of the maximum additional water level rise for the last 100 years of the long-term simulations. The vertical green and red lines represent the median (1.53 m) and mean (2.02 m) values, respectively.	40
Figure 16. Cumulative distribution functions of the major calibration parameters and the maximum simulated water level rise for Options A, B, and C.	42

1 Introduction

This analysis report describes modeling activities performed as part of Task 3 of AP-110, "Analysis Plan for Evaluation of Culebra Water-Level-Rise Scenarios" (Beauheim, 2003a). The purpose of this Task is to evaluate the likelihood that observed rising water levels in the Culebra Dolomite Member of the Rustler Formation near the Waste Isolation Pilot Plant (WIPP) are due to leakage from poorly plugged and abandoned boreholes.

1.1 Background

The Culebra flow model used in performance assessment (PA) calculations for the WIPP Compliance Certification Application (CCA; DOE, 1996) was calibrated to heads assumed to represent steady-state conditions as well as to transient heads arising from hydraulic testing and shaft activities. In the assessment of compliance monitoring parameters (COMP's) for the year 2000 (SNL, 2001), freshwater heads were compared to trigger values established for 28 of 32 monitoring wells (Figure 1) used in generation of the CCA Culebra transmissivity (T) fields (water levels in the other four wells could not be determined because the wells had been removed from the monitoring network, i.e., plugged and abandoned, or converted to monitor units other than the Culebra). Of these 28 measurements, freshwater heads in 21 wells appeared to be outside the trigger value ranges, 20 higher and one lower than expected. Head changes in four of the wells could be explained by problems with well casings and/or leaking packers, leaving 17 wells with unexpectedly high freshwater heads. Exceeding trigger values does not mean that WIPP's continued compliance with EPA regulations is in jeopardy, but that further action must be taken to evaluate the cause(s) and consequences of exceeding the trigger value. Based on requirements for further investigations when trigger values are exceeded and concerns expressed by the Environmental Protection Agency (EPA, 2002) and Environmental Evaluation Group (EEG, 2002), investigative studies were defined to explore possible scenarios that could explain the water-level changes (SNL, 2003).

1.2 Water-Level Rise

Water-level records (hydrographs) from the WIPP wells reveal a variety of changes since monitoring began in the earliest wells in 1977. Hydrographs from the wells within the 16 square miles of the WIPP site typically show myriad effects because of the extensive well testing and shaft activities that occurred in the 1980's. Hydrographs from wells in Nash Draw and P-14 (Figure 2) typically do not show responses to tests conducted on the WIPP site, but nevertheless show broad rising and falling trends over periods of several years. Since 1989, a general long-term rise has been observed in both Culebra and Magenta water levels (Figure 3) over a broad area including Nash Draw. At the time of the CCA, this long-term rise for wells outside of Nash Draw was recognized but was thought to represent the recovery from the accumulation of tests and shaft leakage that had occurred at the WIPP site since the late 1970's. Within Nash Draw, the water-level rise was assumed to be caused by changes in the amounts of potash mill effluent discharged onto tailings piles in or near to Nash Draw (Silva, 1996). As the rise in water levels has continued over recent years, however, observed heads have exceeded the ranges of uncertainty established for the steady-state heads in most of the 32 wells used in calibration of the T fields for the CCA, throwing into question the basic modeling assumption that Culebra heads on the WIPP site were, in the absence of anthropogenic effects, at steady state.

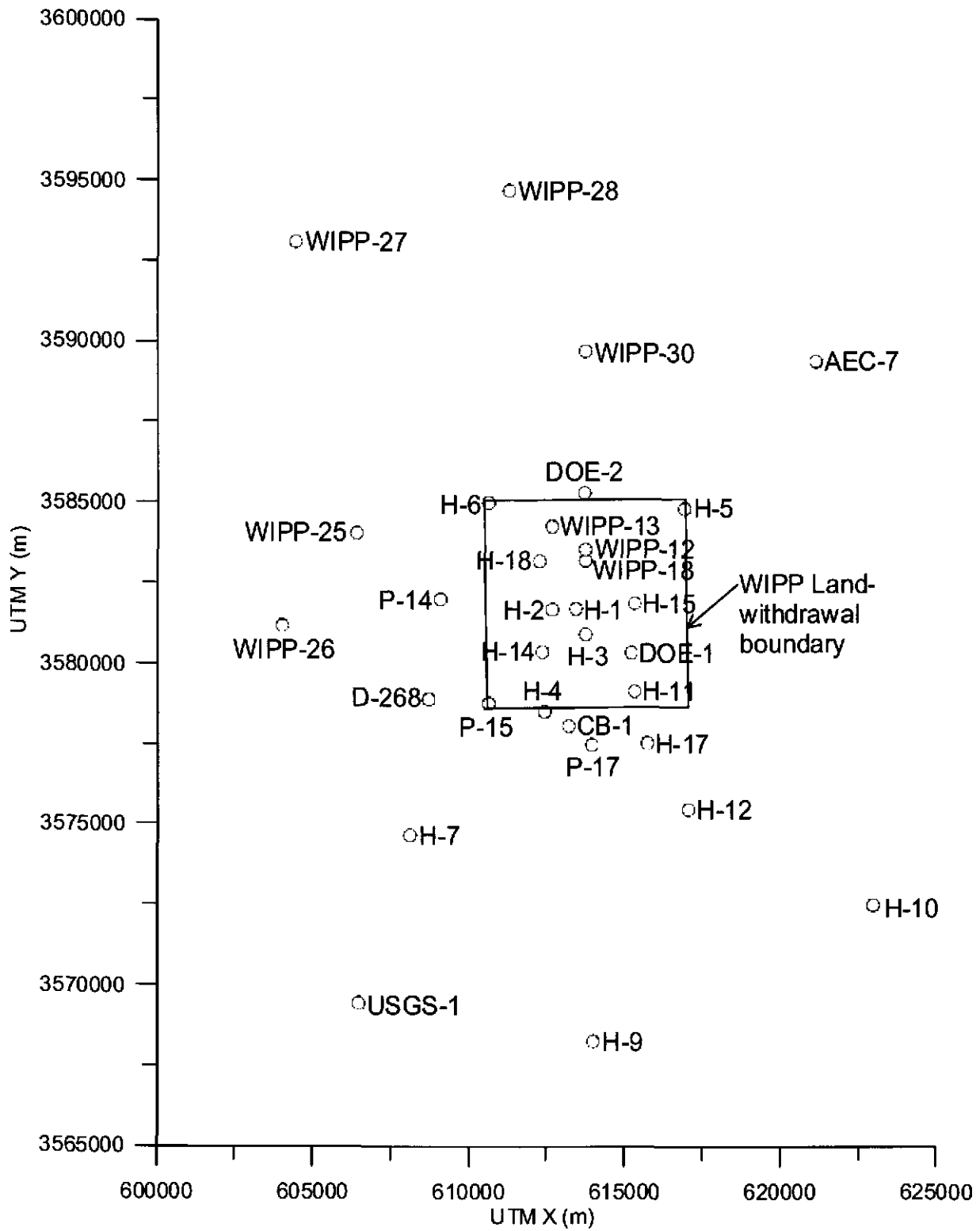


Figure 1. Locations of Culebra wells used in the CCA modeling.

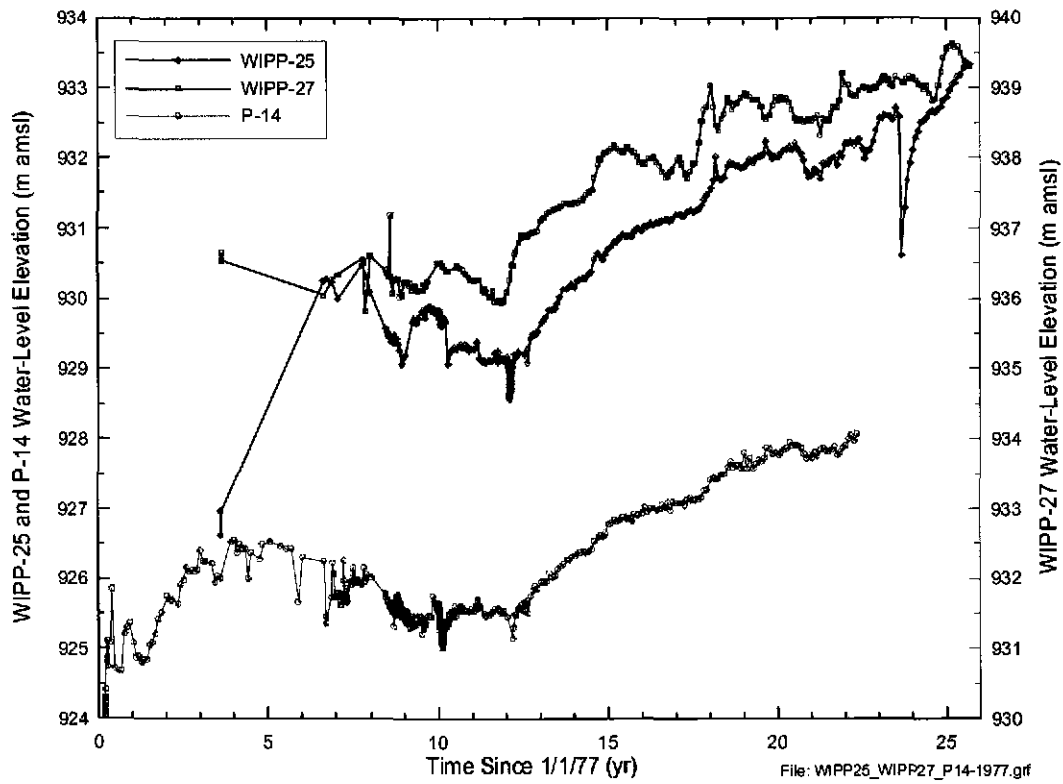


Figure 2. Water-level trends in the Culebra for Nash Draw wells and P-14.

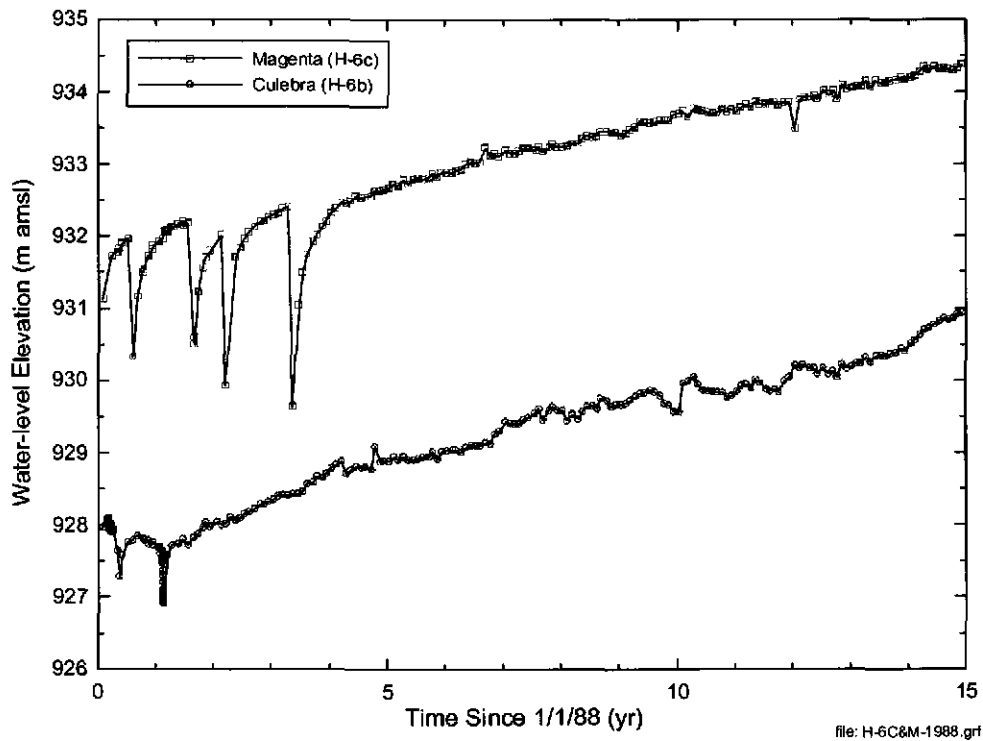


Figure 3. Rising Culebra and Magenta water levels at H-6.

Given the inconsistency between assumed steady-state heads and water levels observed to be continually rising, three scenarios have been postulated that may explain the observations. The scenarios are that the observed water-level rise is due to: 1) leakage into the Culebra of refining process water discharged onto potash tailings piles, probably through subsidence-induced fractures and/or leaky boreholes; 2) leakage into the Culebra of water from units above the Culebra (Magenta and/or Dewey Lake) or below the Culebra (e.g. Salado, Bell Canyon) through poorly plugged and abandoned boreholes; and 3) leakage into the Culebra of water being injected at depth (e.g. into the Bell Canyon Formation) through leaky boreholes. Conceptually, each of these scenarios is possible. However, a quantitative determination needs to be made of the volumes of water required under each of the scenarios to cause the observed water-level rises, and those volumes need to be compared to the volumes that are known, or can be calculated, to be available from the potential sources. Thus, each scenario is being evaluated using numerical flow models to determine if it could plausibly explain the observed water-level changes. This report describes the modeling process and results that were used to examine the part of the second scenario pertaining to leakage into the Culebra of water from overlying units with higher heads (Magenta and/or Dewey Lake) through poorly plugged and abandoned potash boreholes.

1.3 Outline

This report documents the data, methods, and summary results of the work done as Task 3 of Analysis Plan 110 (Beauheim, 2003a). The sections of this report and a brief description of each subsection are:

Section 2: Approach

- 2.1: Overview;** Provides an overview and summary of the modeling approach.
- 2.2: Software;** Describes the software usage and information flow between programs.
- 2.3: File-Naming Conventions;** Describes the file-naming conventions and the input and output files for each program.
- 2.4: Model Domain and Discretization;** Outlines the computational grid and modeling domain
- 2.5: Boundary and Initial Conditions;** Describes the boundary and initial conditions in terms of regional scale coordinates.

Section 3: Data; Describes the well data used in the calibration procedure.

Section 4: Modeling Assumptions and Parameters

- 4.1: Assumptions;** Describes the major assumptions used in the modeling process.
- 4.2: Parameters;** Describes the main modeling parameters and the basis for the values used in the model simulations.

Section 5: Results

- 5.1: Option A;** Results matching total head rises after 15 years, adjusting only leakage rates
- 5.2: Option B;** Results matching last six years' head rises, adjusting only leakage rates

5.3: Option C; Results matching last six years' head rises, adjusting leakage rates and specific storage

Section 6: Discussion; Discusses the implications and results with regard to the objective of this analysis and recommends future work.

Section 7: Summary and Conclusions; Presents a summary and the conclusions of the report.

2 Approach

2.1 Overview

For this analysis, the observed water-level rise in wells in and around the WIPP site is hypothesized to be the result of leakage into the Culebra through poorly plugged or abandoned potash exploration holes. Some of these holes date back to the first half of the twentieth century, when plugging and abandonment practices were not as rigorous as they are today. From a search of BLM records assembled for Washington Regulatory and Environmental Services (WRES) for the Delaware Basin Drilling Surveillance Program, plugging and abandonment records were found for 576 exploration holes in the vicinity of the WIPP site (Figure 4). These holes may provide potential avenues for vertical hydraulic communication among the formations above the Salado. Many of the incompletely plugged potash holes are located near, and in some cases beneath, the Intrepid (formerly Mississippi) East tailings pile.

Powers (2004) evaluated and categorized the potential leaky boreholes based on a number of criteria. Initially, boreholes were immediately eliminated if they either were outside the active portion of the Culebra modeling domain and/or were in areas of Salado dissolution. The latter criterion reflects the belief that all Rustler members may already be hydraulically connected as a result of subsidence and collapse in areas of Salado dissolution, and hence leaky boreholes would not be significant. The remaining boreholes were then categorized based on their plugging record. The categories and their respective criteria are shown in Table 1. For this analysis, boreholes of category 4 (cement interval in drillhole does not match Culebra interval) and category 5 (open hole) were used as the candidate leaky boreholes (Figure 4).

To evaluate the effects of leaking boreholes, we employ the groundwater flow model of the Culebra developed under AP-088 (Beauheim, 2002). The model domain is shown in Figure 5. AP-088 simulated one hundred instances of the model with **MODFLOW-2000 (MF2K;** Harbaugh et al., 2000) using calibrated T-fields from McKenna and Hart (2003). McKenna and Hart (2003) calibrated 137 different realizations of the Culebra T-field to heads measured in late 2000 (treated as “steady-state” heads) and to transient heads associated with seven pumping tests. Beauheim (2003b) developed and applied acceptance criteria to identify the 100 realizations that were used for performance assessment calculations for the WIPP Compliance Recertification Application (CRA; DOE, 2004). The 100 T-field realizations from Beauheim (2003b) are used in this analysis. Borehole leakage is modeled by utilizing the well package of **MF2K**. Each leaky borehole is assumed to be an injection well with the leakage rate into the Culebra equivalent to the injection rate.

Determination of the flow rate necessary in each borehole to match the observed water-level rise was accomplished through inverse modeling using **Parallel PEST (PEST v5.51;** Doherty, 2002). To simplify the calibration process, the boreholes were placed into four groups, dependent on where they exist within the modeling domain. The first group (Upper group) consists of the 16 boreholes clustered near the top (north end) of the modeling domain, the second group (Mid group) contains six boreholes that are adjacent to the northern boundary of the WIPP site, the third group (Nash Draw group) consists of the three boreholes located in the Nash Draw region to the west and southwest of the WIPP site, and the fourth group (Lower group) is a single borehole located directly south of the WIPP site (Figure 5).

Composite map of Cement Evaluation Types
 (Source is Table Task 1A AP-110.xls)

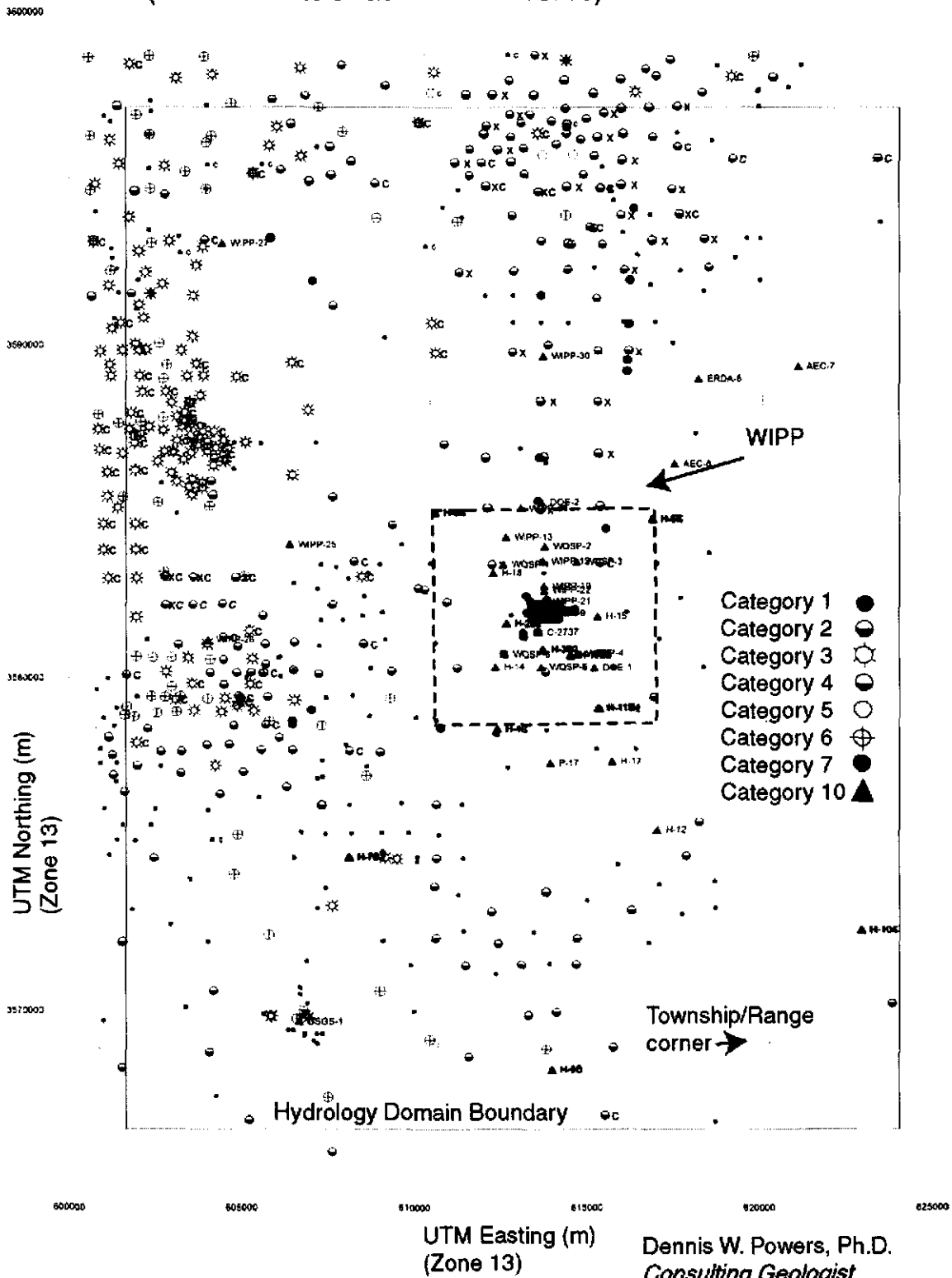


Figure 4. Categorized potash exploration boreholes in the WIPP region.

Table 1. Cementing categories for potash and other drillholes in the hydrologic domain.

Cementing Category	Characteristics
1	Data indicate drillhole was cemented from total depth to surface
2	Data indicate that Culebra interval is completely cemented, with a high degree of certainty
3	Culebra intercepted by drillhole; cement intervals in drillhole; data not clear regarding cementing across Culebra interval [This category is generally a temporary category that is resolved with further checking; some drillholes remain in this category where the plugging history is considered irrelevant because of other factors.]
4	Culebra intercepted by drillhole; cement interval in drillhole does not match Culebra interval
5	Apparent open hole
6	Plugging information not available for drillhole
7	Drillhole is too shallow to intercept Culebra; plugging not considered
10	Drillhole is completed to Culebra for monitoring or water well; plugging not considered
c	This modifier for the basic category indicates that casing has been left in the drillhole; does not apply to surface marker casing; applied to categories 2–6.
x	This modifier for the basic category (either 2 or 4) indicates that the cement plug level is at, or within 3 ft above, the top of Culebra (2x) or is 1–3 ft below the top of Culebra (4x); both x and c modifiers may be attached for a single drillhole.

Due to the stochastic nature of the T-fields and the temporal variability seen in some of the hydrographs, exact calibration of the model to the actual hydrographs at each monitoring well was impossible. Thus, a more general approach to the calibration process was developed that evolved into three different methods (Table 2). The first calibration method (Option A) adjusted the injection rate at each group of leaky boreholes to obtain a temporally averaged best fit to the 15-year linearized slopes of the head rises at each monitoring well. The slopes of the head rises were estimated by fitting a linear-regression line to the data or a subset of the data. Plots of the data and fitted lines are shown in Appendix A.

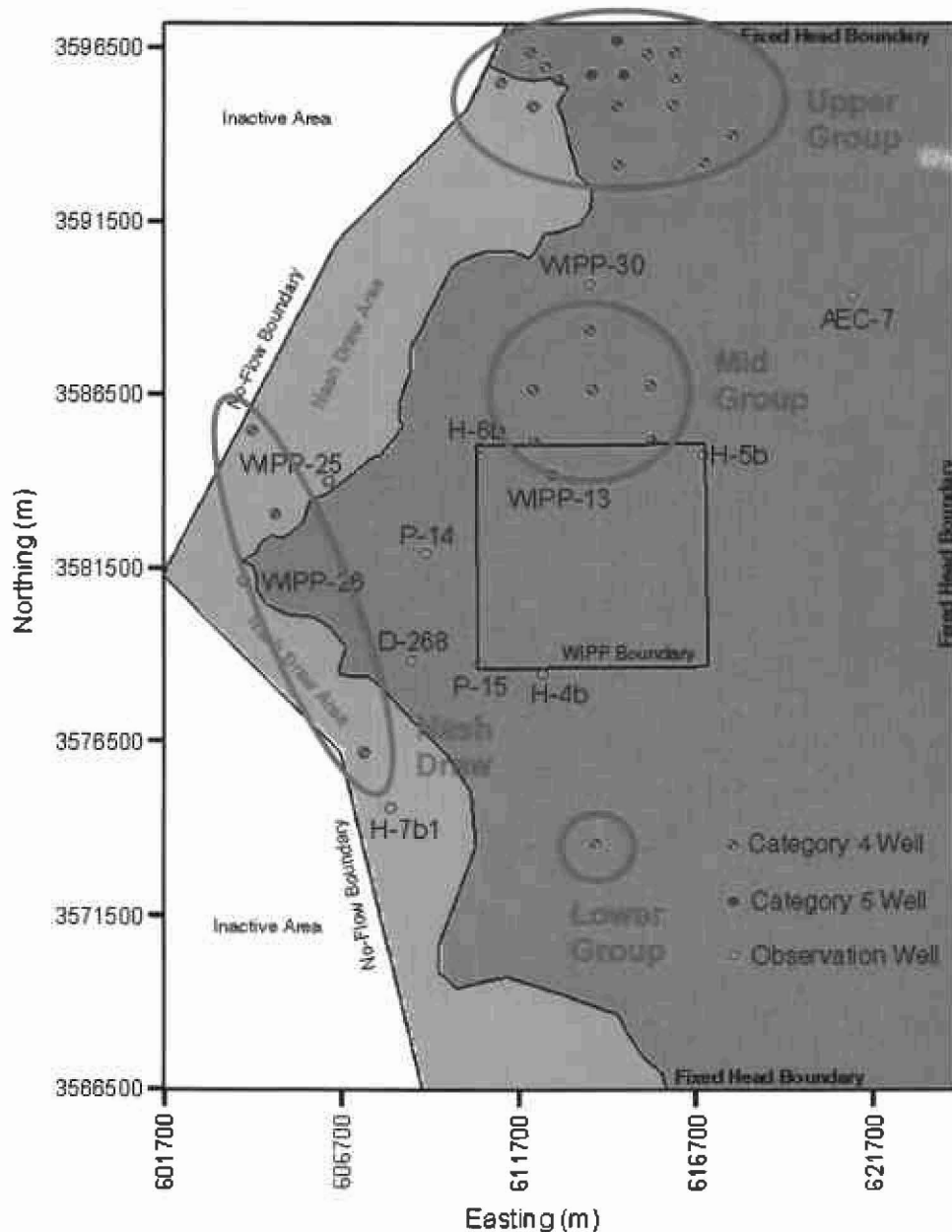


Figure 5. Modeling domain showing boundary features, monitoring well locations, Nash Draw area, WIPP boundary, and the grouping of the leaky boreholes for use in the calibration process.

When the Option A results showed more early-time transient decline in the rate of head rise than was observed in the typical hydrograph, the method was modified (Option B) to fit only the head rise during the last 6 years of the 15-year simulation to the linearized slopes at each monitoring well. This approach implicitly assumes that whatever is causing the water-level rise began long enough in the past that the current hydrographs show only late-time, quasi-steady-state responses. In addition, Option B combines the Nash Draw and Mid groups into one group due to the model's low sensitivity to the injection rates from those boreholes, as established by the Option A simulations.

Table 2. The three options and their respective calibration parameters and variables. Calibration is achieved by adjusting the calibration variables such that the difference between the calibration parameter and the linearized head rise from the data is minimized. The values of variables that are kept fixed during the calibrations are shown in parentheses.

Option	A	B	C
Calibration Parameter			
	Total head rise over length of simulation	Head rise over last six years of simulation	Head rise over last six years of simulation
Calibration Variables			
Leakage in Upper Group	Yes	Yes	Yes
Leakage in Mid Group	Yes	Yes (Mid and ND groups combined)	Yes
Leakage in Nash Draw Group	Yes		Fixed ($2.36 \times 10^{-5} \text{ m}^3/\text{s}$)
Leakage in Lower Group	Yes	Yes	Yes
S_s within Nash Draw	Fixed ($1.29 \times 10^{-6} \text{ m}^{-1}$)	Fixed ($1.29 \times 10^{-6} \text{ m}^{-1}$)	Yes
S_s outside of Nash Draw	Fixed ($1.29 \times 10^{-6} \text{ m}^{-1}$)	Fixed ($1.29 \times 10^{-6} \text{ m}^{-1}$)	Yes

The third option (Option C) includes specific storage (S_s) values for areas inside and outside of the Nash Draw region of the model as calibration parameters in addition to the leakage rates in the Upper, Mid, and Lower groups. Because the model sensitivity could change with different values of specific storage, the Mid group was treated separately from the Nash Draw group. However, because the specific storage values within Nash Draw are presumed to be much higher than outside of Nash Draw, and thus the potential change in model sensitivity to those boreholes is much smaller, the leakage rate in the Nash Draw group was fixed at a value equal to the average from the qualified runs from Option A. Option C also allows for comparison to the calibrations done by Lowry and Beauheim (2004) that simultaneously calibrated a recharge rate from the Intrepid East tailings pile as well as S_s inside and outside of Nash Draw.

2.2 Software

The flow modeling was performed using **MODFLOW 2000 (MF2K)**, version 1.6 (Harbaugh et al., 2000) on the 6115 Linux cluster (lylin102). **MF2K** is a modular, finite-difference code for solving the groundwater flow equation on a two- or three-dimensional rectilinear grid. For calibration, the parallel version of **PEST** (version 5.51) was used. **PEST v5.51** is a parameter-estimation program that systematically changes parameter input values to fit a set of observations and is designed to run each **MF2K** simulation simultaneously on a different computer, allowing for parallel processing over a networked system. The combination of **PEST v5.51** and **MF2K** is the same software package used to calibrate the T-fields in McKenna and Hart (2003). The programs are listed, with the ERMS #'s of their Quality Assurance (QA) packages, in Table 3.

Table 3. Major codes used for this analysis.

Code Name	Description	QA Package ERMS #
MODFLOW 2000, v1.6	Groundwater Flow Model	523867
PEST, v5.51	Parameter Estimation Code	527057

Several FORTRAN utility codes are used for simulation setup and data conversion purposes. These codes are **T_Field.f90** (for Options A and B), **T_Field_stor.f90** (for Option C), **Get_heads.f90** and **exhdsdrw_scratch.f90** (for Option A), and **exhdsdrw_scratch_opt.f90** (for Options B and C). The first, **T_Field[_stor].f90**, is used to read in each T-field from McKenna and Hart (2003) and to write those data to a **MF2K** layer-property flow (LPF) input file (the Option C version also reads and writes values of S_s to the LPF file). **Get_heads.f90** is used to extract head results from a **MF2K** steady-state run, and re-write those values to a **MF2K** basic input file as the starting heads for the transient calibration.

In order for **PEST v5.51** to calibrate to the slopes of the head rises at each well, the head rises must be extracted from the **MF2K** results file. This is done by **exhdsdrw_scratch[_opt].f90**, which reads the **MF2K** output files, extracts the heads and head rises at each well location, and outputs those values to a separate file.

Two post-processing FORTRAN utility codes are used to gather the calibrated values into a form that is suitable for analysis and visualization. The first, **mfrun.f90** (or **mfrun_ob.f90** for Option B or **mfrun_oc.f90** for Option C), is used to read in the calibrated leakage rates (and S_s values for Option C) from each calibration and write them to a **MF2K** well file (and the LPF file for the S_s values in Option C) to perform a final run of the flow model using the calibrated values. The second, **cut.f90**, reads in the simulated head rise from each calibration run and compiles the results into a single file for use in plotting and visualization.

The executable name for each FORTRAN utility code is the prefix of the FORTRAN file name (e.g., the executable of **T_Field.f90** is **T_Field**), with the exception of **cut.f90**, whose executable is named **ctout** to prevent conflicts with the intrinsic Linux command 'cut'. The FORTRAN

utility codes are reproduced in Appendices B through F. Each code is verified by visual inspection.

The Department of Defense Groundwater Modeling System (**GMS**, version 5.0) software is used for visualization and plotting purposes (GMS, 2004). **GMS** is a groundwater modeling and geo-statistical software package that provides a graphical user interface to numerous groundwater modeling codes. **GMS** is not used to perform any calculations or data conversions.

Several Linux shell scripts are used to control the data flow and program execution and to automate the simulation over all 100 T-field realizations. Those scripts are **Ppest_run.sh**, **clean.sh**, **runpest.sh**, **setup.sh**, **pslave.sh**, **pmaster.sh**, and **mfrun.sh**. **Ppest_run.sh** is the parent script to all other scripts except for **mfrun.sh** and provides the run control sequence for the entire simulation. All other scripts are called from within **Ppest_run.sh** or from another script that is called from within **Ppest_run.sh**. Progressing through the execution sequence, **Ppest_run.sh** first calls **clean.sh** to delete unneeded files from any previous **PEST v5.51** run. It then calls **T_Field** to write the current simulation's transmissivity field to the appropriate **MF2K** input file. **MF2K** is then run in steady-state mode to establish the starting heads for the transient calibration runs. **Get_heads** is then run to extract the steady-state solution and write them to a **MF2K** basic input file. At this point, **Ppest_run.sh** moves control to **runpest.sh**. The main purpose of **runpest.sh** is to set up the **PEST v5.51** simulation by first calling the script **setup.sh**, which writes the appropriate input files to a series of directories where **PEST v5.51** will be executed. It then writes and executes the script **pslave.sh** in each of those directories. This script, which is executed on the slave computers, copies the appropriate files to the local slave hard drives and begins the slave execution of **PEST v5.51**. Finally, **runpest.sh** executes the script **pmaster.sh**, which sets up the master files for **PEST v5.51**, starts the last slave computer, and then executes **PEST v5.51**. Once the calibration is finished, **pmaster.sh** collects the calibrated leakage rates (and S_s values for Option C) and writes them to a file called *well.out* for easy retrieval at the end of the simulations. Options A, B, and C each execute slightly different versions of **pmaster.sh** to account for the different calibration parameters.

After the calibrations are complete, a separate script, **mfrun.sh**, is manually executed. This script creates a directory for each T-field, and then executes **MF2K** in each directory using the calibrated values for that T-field. The FORTRAN utility code **cut.f90** is run after the execution of **mfrun.sh**. The shell scripts are reproduced in Appendices G through M. These scripts differ slightly from those used in Lowry and Beauheim (2004) for evaluating the tailings pile scenario to accommodate the commands of a new queuing system that was installed on the cluster.

2.3 File-Naming Conventions

All calculations were performed on the 6115 Linux cluster (lylin102) within a common directory. To run **PEST v5.51**, each slave computer writes its output to a separate directory. At the end of the **PEST v5.51** calibration, the final results are accumulated in a single file called *well.out* that lists the leakage rate for each borehole, the borehole group (Upper, Mid, Nash Draw, or Lower), the S_s values for Option C, and the T-field name. Once all the **PEST v5.51** calibrations are done, a separate directory for each T-field is created and **MF2K** is run in each directory using the calibrated values for each T-field. The general path for the simulation base

directory, the directory that holds the final results file, as well as the set-up files, scripts, and programs for Option A is:

/home3/tslowry/wipp/lkybrhl

Both Option B and Option C are run under the same base directory of:

/home3/tslowry/wipp/lky_optB

with the output and results of each calibration being saved to

*/home3/tslowry/wipp/lky_optB/Opt**

where the * is either 'B' or 'C' depending on the Option.

The general path for the T-field directories is:

/home3/tslowry/wipp/lkybrhl/d###r##

where *d###r##* is the original base transmissivity field naming convention as described in McKenna and Hart (2003). The ##'s next to 'd' range from 01 to 22 and next to the 'r' range from 01 to 10. The common directory from which the PPEST runs are executed is:

/home3/tslowry/wipp/lkybrhl/ppest1

or

/home3/tslowry/wipp/lky_optB/ppest1

for Options B and C.

In addition, a data directory that contains all the T-fields is located at:

/home3/tslowry/wipp/Tfields

where each T-field file has the naming format of *d###r##.mod*.

To help conserve hard disk space and computer memory, all input and output files for each calibration are deleted once the final results are written to *well.out*. Templates of all input files, which are copied and re-written with the appropriate simulation values for each **PEST v5.51** run to the **PEST v5.51** common directory, are kept in the simulation base directory. The input and output files that will remain archived in the directories are listed in Table 4.

Table 4. Input and output data files used for Task 2. Each directory is listed as its relation to /home3/tslowry/wipp.

Directory	File	Description
/Tfields	d###r###.mod	List of good T-fields in d###r### format
/kylbrhl	Goodruns.txt	List of 100 T-field data files
	filelist.master	List of files necessary for PEST v5.51 simulation
	filelist.slave	List of files for PEST v5.51 slave execution
	filelist.modflow	List of files necessary for MF2K execution
	LBH1.ba6	MF2K basic input file
	LBH1.lpf	MF2K layer property flow input file
	LBH1.nam	MF2K naming file used in PEST v5.51 simulations
	LBH1_home.nam	MF2K naming file used in final calibrated run
	LBH1_steady.nam	MF2K naming file for steady-state runs
	LBH1.dis	MF2K discretization input file
	LBH1_steady.dis	MF2K discretization input file for steady-state runs
	LBH1.lmg	MF2K AMG1R5 solver input file
	LBH1.oc	MF2K output control file
	LBH1.rch	MF2K recharge package input file
	LBH1.wel	MF2K well package input file
	LBH1_new.ins	PEST v5.51 instruction file
	LBH1.pst	PEST v5.51 control file
	LBH1.rmf	PEST v5.51 run management file
	LBH1_run.in	PEST v5.51 executable input file
	LBH1.tmp	PEST v5.51 template file for leakage rates
	well.out	Output of calibrated leakage rates
wellobs.txt	Time series output of calibrated head rise	
Y_Int.txt	Holding file for initial condition at each well	
/kylbrhl/ppest/	*	PEST v5.51 run directory (contains no data files)
/kylbrhl/d###r###	LBH1.glo	MF2K global output file
	LBH1.ccf	MF2K cell-by-cell flow file
	LBH1.drw	MF2K head rise file
	LBH1.hed	MF2K head output file
	wellhdsdrw.txt	Head and head rise output file
	RSE.txt	Root squared error output file

2.4 Model Domain and Discretization

The modeling domain for all three options is the same as that of McKenna and Hart (2003) and consists of 224 cells in the east-west direction (*x*-direction) and 307 cells in the north-south direction (*y*-direction). Each cell is of uniform 100-m size on all sides making the modeling domain 22.4 km wide by 30.7 km tall (Figure 5). The discretization of the flow model domain into 100x100 meter cells leads to a total of 68,768 cells with 14,999 (21.8%) of the cells inactive to the west of the no-flow boundary and 53,769 active cells. The corner coordinates of the

modeling domain and the WIPP land withdrawal boundary (LWB) in UTM NAD 27 (Zone 13) coordinates are given in Table 5 and Table 6, respectively.

Table 5. The coordinates of the corners of the numerical model domain in UTM NAD27 coordinate system.

Domain Corner	X Coordinate (m)	Y Coordinate (m)
Northeast	624,100	3,597,200
Northwest	601,700	3,597,200
Southeast	624,100	3,566,500
Southwest	601,700	3,566,500

Table 6. The coordinates of the corners of the WIPP land withdrawal boundary (LWB) in UTM NAD27 coordinate system.

LWB Corner	X Coordinate (m)	Y Coordinate (m)
Northeast	616,941	3,585,109
Northwest	610,495	3,585,068
Southeast	617,015	3,578,681
Southwest	610,567	3,578,623

2.5 Boundary and Initial Conditions

The initial conditions are the same as those used in McKenna and Hart (2003). As a summary, field head data from the year 2000 consisting of 37 head measurements across the modeling domain were interpolated to the computational grid using kriging. A five-parameter Gaussian function was used to de-trend the head data and a Gaussian variogram model was used to describe the variability of the head residuals with distance. The variogram model was used to estimate the residuals at each node in the grid. The final step added the regional trend back to the estimated residuals using the five-parameter Gaussian function.

The model boundaries along the north, east, and south edges of the domain are considered fixed-head boundaries (Figure 5). The kriged head values used to determine the initial heads were assigned to each constant-head cell and kept fixed for all simulations. The irregular western boundary is considered a no-flow boundary and falls along the groundwater divide associated with Nash Draw. Nash Draw is interpreted as a regional groundwater divide, draining the Rustler units to the east and north (and also by implication via discharge symmetry, to the west). Initial conditions for each T-field were set by executing a steady-state run with each T-field prior to performing the calibration.

3 Data

Observed water levels in Culebra monitoring wells provide both the motivation for this study and the data to which the modeling results are compared. Culebra water levels have been measured and reported by a number of different organizations since well installation for the WIPP project began. Data collected by the U.S. Geological Survey (USGS) have been reported by Mercer and Orr (1979) and Richey (1986; 1987a,b). Data collected by or on behalf of Sandia National Laboratories are reported in Hydro Geo Chem (1985), Intera Technologies and Hydro Geo Chem (1985), Intera Technologies (1986), Saulnier et al. (1987), and Stensrud et al. (1987; 1988a,b; 1990). Data collected by the WIPP Management and Operating Contractor (MOC), now known as Washington TRU Solutions (WTS), are reported in Kehrman (2002).

Most of the well monitoring data show a high degree of variability with a general increasing trend over time. The variability is probably due to both anthropogenic (e.g., pumping tests, mining operations, etc.) and natural (e.g., recharge variability) influences. Capturing the magnitude and variability of the head measurements in each well over time is beyond the ability of this model, mainly due to a lack of spatial and temporal resolution of model input parameters such as transmissivity, recharge rates, etc. Thus, rather than calibrate to the variable head levels in each well, calibration was based on the slope of the linearized head rise over time. This was done to remove the small-scale fluctuations in the data, both spatially and temporally, that are unable to be captured in the model. Twelve wells were chosen surrounding the WIPP site that had sufficiently long data records to reflect the water-level rise over time (Figure 5).

To determine the slope of the water-level change at each well over time, the time-series data were fit using a linear regression model. The raw data and fitted model for each well are shown in Appendix A. In all but one case (H-7b1), the raw data: 1) exhibited highly variable behavior for part of the time sequence, 2) did not show a rising trend until later in the time sequence, or 3) contained outliers that were clearly anomalous. In those cases, the linear regression was performed on a subset of the raw data. The data that were not included in the regression are plotted in red in Appendix A. Each well, its UTM NAD27 coordinates, and slope of the linearized head rise as determined by the regression analysis are listed in Table 7.

Table 7. Well coordinates in UTM NAD27, and the calculated slope of the head-rise.

Well Name	Easting (m)	Northing (m)	Slope (m/yr)
AEC-7	621126	3589381	0.113568
D-268	608702	3578877	0.126283
H-4b	612380	3578483	0.198349
H-5b	616872	3584801	0.118846
H-6b	610594	3585008	0.201408
H-7b1	608124	3574648	0.072852
P-14	609084	3581976	0.229142
P-15	610624	3578747	0.194967
WIPP-13	612644	3584247	0.097052
WIPP-25	606385	3584028	0.227839
WIPP-26	604014	3581162	0.148470
WIPP-30	613721	3589701	0.184103

4 Modeling Assumptions and Parameters

4.1 Assumptions

Besides assumptions inherent in all modeling exercises (e.g. physical processes can be adequately parameterized and estimated on a numerical grid), several other assumptions are specific and important to this Task. Those assumptions are as follows:

1. We assumed that the boundary conditions along the model domain boundary are known and are independent of the T-field being used. This is appropriate because each T-field was calibrated under the same boundary conditions.
2. We assumed that the variations in leakage rates and initiation times between wells within each group are not important. By grouping the wells based on location, the impact of varying leakage rates among individual wells is minimized. The initiation times assumption is supported by the data, which show that the water-level rise for all wells from about 1989 onwards is consistent with the linearized slopes.
3. We assumed that the water-level rise indicated in the data is due only to leakage from the boreholes and not from other sources.
4. For Options A and B, we assumed that a single value of S_s is representative of S_s across the entire modeling domain. The single value of $1.2903 \times 10^{-6} \text{ m}^{-1}$ (storativity = 1×10^{-5}) used in this analysis is the same value used during the calibration of the T-fields (McKenna and Hart, 2003).
5. We assumed that leakage from boreholes can be adequately simulated as injection wells with an injection rate equivalent to the leakage rate into the Culebra. While this may lead to artificially high heads in wells in low-transmissivity areas, this effect is negated by the fact that calibration is to the rate of rise and not the magnitude of the heads. Additionally, this effect is averaged out by the assumption that each borehole in each group has the same leakage rate.
6. For Option B, we assumed that the model is insensitive to the leakage rates from the Mid and Nash Draw boreholes and that despite their disparate geologic locations, combining the two groups has negligible impact on the quality of the calibrations. This is supported by the parameter sensitivity output produced from the calibration of Option A.
7. For Option C, we assumed that the Nash Draw boreholes can be adequately represented using a fixed injection rate of $2.36298 \times 10^{-5} \text{ m}^3/\text{s}$, which is the average of the Nash Draw borehole injection rates from the qualified Option A runs. Again, this approach is supported by the low sensitivity of the calibration to leakage rates in the Nash Draw boreholes.

Option A calibrates the 15-year simulated head rise to the slope by minimizing the total residual between the measured and simulated slopes using the following equation:

$$R = \frac{1}{n} \sum_{i=1}^n \left(S_i - \frac{d_{15i}}{15} \right)^2 \quad (1)$$

where R is the residual between the measured and simulated slopes, n is the number of monitoring wells, S_i is the linearized data slope at well i , and d_{15i} is the simulated head rise after 15 years at well i . Options B and C calibrate the last 6 years of the simulated head rise by minimizing R using:

$$R = \frac{1}{n} \sum_{i=1}^n \left(S_i - \frac{d_{15i} - d_{9i}}{6} \right)^2 \quad (2)$$

where d_{9i} is the head rise after nine years from the start of the simulation and all other terms are described above.

4.2 Parameters

The conceptual model assumes that the boundary conditions are known and that each T-field is equally possible. Options A and B assume that S_s is constant across the region at $1.2903 \times 10^{-6} \text{ m}^{-1}$. Option C assumes two adjustable values for S_s , one within Nash Draw and the other outside of Nash Draw. Thus, Option A used four adjustable parameters: the leakage rate from each group of boreholes. Option B used three adjustable parameters because the Nash Draw and Mid groups are considered as a single group. Option C used five adjustable parameters: the leakage rates in the Upper, Mid, and Lower borehole groups (the rate for the Nash Draw group was fixed) and the two values for S_s . The leakage rate for the Nash Draw group was fixed at $2.36298 \times 10^{-5} \text{ m}^3/\text{s}$ per borehole for Option C.

To estimate reasonable calibration bounds on leakage rates, several T-fields were calibrated using an initial leakage rate for all boreholes of $5 \times 10^{-6} \text{ m}^3/\text{s}$. The initial calibrations showed that the calibration problems were not sensitive to the initial value and that the model did not need stringent upper and lower limits to converge in a timely manner to achieve suitable results. Thus, for all calibrations, the initial leakage rate was set to $1 \times 10^{-5} \text{ m}^3/\text{s}$ for all boreholes, with upper and lower limits of $1.0 \text{ m}^3/\text{s}$ and $1 \times 10^{-10} \text{ m}^3/\text{s}$, respectively.

5 Results

Inverse modeling using **PEST v5.51** only guarantees that an objective function reaches a minimum value. It does not guarantee that the calibrated values will reflect reality or other observations that are not included in the calibration process. Thus, calibration runs were filtered if the calibrated value of any of the parameters reached its maximum or minimum allowable limit. By reaching the maximum or minimum value of any of the input parameters, no guarantee can be made that PEST found an optimal solution.

5.1 Option A

For Option A, the filtering criteria resulted in 48 filtered T-fields. However, for reasons that will be explained below, exceptions were made to the first criterion if it was the Mid group that reached its minimum and the root mean squared error (ε) for the calibration was under 0.70 m. The ε value is calculated with the following formula:

$$\varepsilon = \sqrt{\frac{\sum_{i=1}^N \sum_{j=1}^T (D_{i,j}^d - D_{i,j}^m)(D_{i,j}^d - D_{i,j}^m)}{N \times T}} \quad (3)$$

where D^d is the observed head rise from the data, D^m is the modeled head rise, N is the number of observation wells, and T is the number of observations over time (one observation per year). This formula differs slightly from that used in Lowry and Beauheim (2004) in that it averages over time and space rather than just over space. This helps compensate for the fact that specific storage was kept constant during the calibration process. After applying the exception rule, 18 additional calibrations were deemed qualified, resulting in a total of 66 qualified T-fields. The simulated head rises are compared to the linearized head rises and plotted for each well in Appendix N. The 66 T-fields and the leakage rate per borehole for each group are listed in Appendix O.

For the 66 qualified runs, the range of total leakage from all boreholes was from 8.10×10^{-5} to 3.28×10^{-3} m³/s, with an average of 4.41×10^{-4} m³/s. Of this, 58.4% came from the Upper group of boreholes, 0.3% came from the Mid group, 21.9% from the Nash Draw group, and 19.4% from the Lower group. We were able to apply the exceptions to the first filtering criterion because the Mid group had such a minor influence on the dynamics of the system. A breakdown of the total leakage rate for each group of boreholes, along with the overall total leakage rate, is shown in Table 8.

Table 8. Option A total leakage rates for each group of leaky boreholes.

	Leakage by Group (m³/s)				
Statistic	Upper	Mid	Nash Draw	Lower	Total
Average	2.93x10 ⁻⁴	6.39x10 ⁻⁷	7.09x10 ⁻⁵	7.63x10 ⁻⁵	4.41x10 ⁻⁴
Median	2.31x10 ⁻⁴	3.00x10 ⁻⁹	5.95x10 ⁻⁵	6.47x10 ⁻⁵	3.55x10 ⁻⁴
Maximum	3.17x10 ⁻³	4.94x10 ⁻⁶	2.56x10 ⁻⁴	3.10x10 ⁻⁴	3.28x10 ⁻³
Minimum	1.33x10 ⁻⁵	6.00x10 ⁻¹⁰	5.19x10 ⁻⁹	7.60x10 ⁻⁶	8.10x10 ⁻⁵
Std. Dev.	4.01x10 ⁻⁴	1.34x10 ⁻⁶	6.56x10 ⁻⁵	5.64x10 ⁻⁵	4.05x10 ⁻⁴

Examination of the plots in Appendix N shows that the rate of simulated head rise declines over time in a typical transient response to a leakage beginning at a specific time. In some cases, most of the total simulated head rise occurs in only the first few years, rather than the constant and consistent head rise over time that is shown in the data. Because the optimization function was trying, in effect, to match a straight line with a curved line, the simulated early-time rates were too high and the simulated late-time rates were too low. Options B and C were developed to put more emphasis on matching the simulated late-time rates of head rise to the linearized hydrographs.

To compare the relative fits among the T-fields, the ε value was calculated for each T-field using equation (1). Those T-fields with the lowest ε values fit the data the best, while those with the highest ε values fit the data the worst. The relative errors ranged from 0.510 to 0.698 m, with T-field d05r05 providing the best fit and T-field d08r05 providing the worst. The T-fields with their corresponding ε values are listed in Table 9.

Figure 6 shows visualizations of the best-fit and worst-fit T-fields, expressed in $\log_{10} T$ (m²/s) values. The d05r05 T-field is much more uniform and homogeneous than the d08r05 T-field, with the T values in the Nash Draw area for d05r05 being smaller and closer to the T values in the middle of the domain than the Nash Draw T values for d08r05.

Table 9. Relative error, ϵ , of each T-field sorted by best (d05r05) to worst (d08r05) for Option A.

T-field	ϵ (m)	T-field	ϵ (m)	T-field	ϵ (m)	T-field	ϵ (m)
d05r05	0.510	d09r10	0.588	d08r03	0.631	d08r07	0.664
d05r02	0.515	d03r10	0.589	d06r02	0.636	d06r03	0.665
d02r10	0.539	d04r02	0.593	d03r06	0.636	d06r07	0.667
d03r09	0.550	d06r04	0.595	d09r08	0.637	d12r02	0.668
d22r02	0.555	d01r07	0.597	d09r06	0.645	d10r04	0.670
d08r09	0.558	d09r02	0.604	d07r07	0.646	d11r07	0.672
d11r02	0.561	d01r02	0.605	d07r08	0.647	d01r10	0.679
d05r03	0.561	d11r01	0.607	d01r06	0.649	d11r10	0.682
d02r02	0.562	d12r08	0.612	d06r10	0.650	d09r03	0.683
d02r07	0.573	d05r01	0.613	d04r10	0.650	d04r07	0.684
d01r08	0.575	d10r10	0.617	d07r05	0.653	d10r03	0.684
d03r07	0.577	d08r06	0.621	d11r08	0.653	d07r02	0.688
d08r01	0.580	d07r09	0.626	d12r07	0.654	d07r10	0.694
d03r03	0.583	d04r06	0.626	d07r01	0.656	d09r04	0.697
d12r01	0.584	d05r07	0.628	d09r05	0.659	d08r05	0.698
d09r07	0.585	d08r04	0.628	d04r05	0.663		
d04r03	0.588	d04r08	0.629	d10r08	0.663		

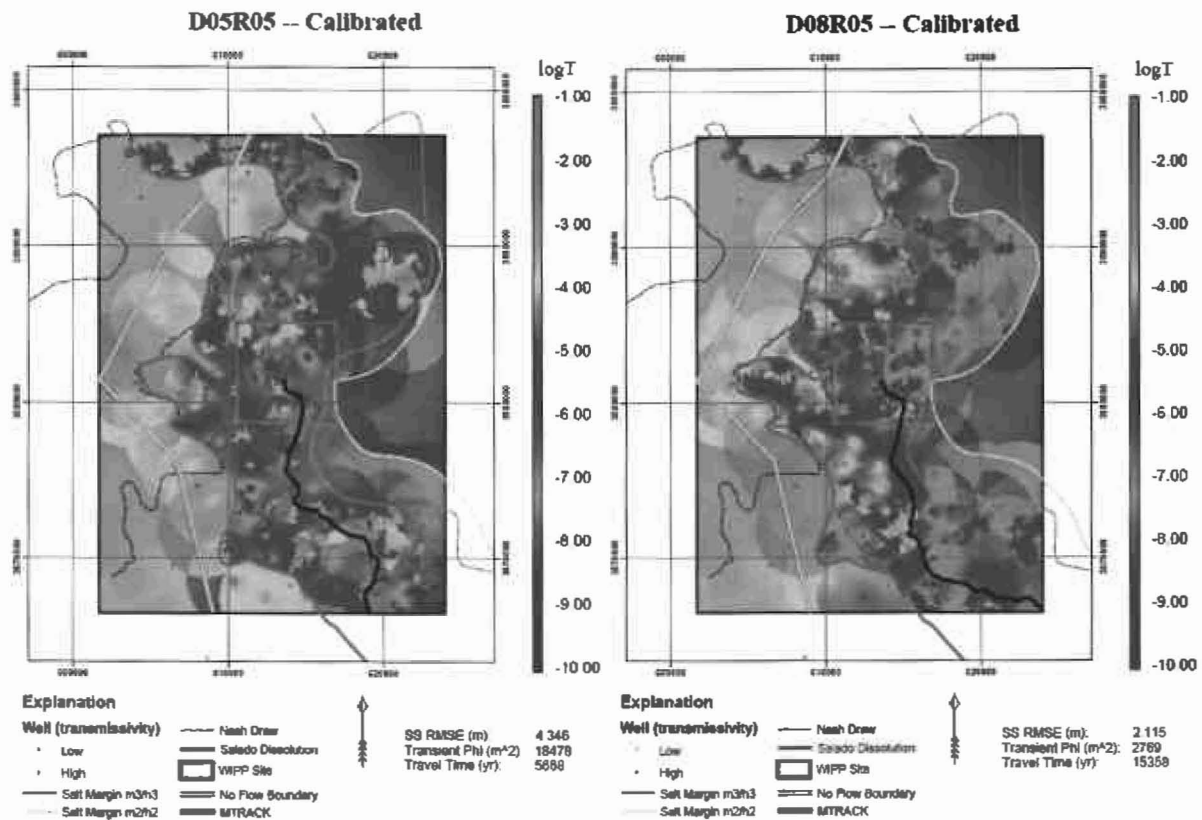


Figure 6. Comparison of the best-fit T-field (d05r05) and the worst-fit T-field (d08r05) for Option A.

Figure 7 shows the linearized head rise slope from the data versus the simulated head rise slopes for T-field d05r05. Immediately apparent is that the simulated slopes fall in a relatively narrow, and lower range as compared to the data slopes. This again is the result of trying to match a quasi-steady-state response with a transient simulation.

To gain some understanding of the error associated with the calibration process, we compare the percentage contribution of each monitoring well to ε for three T-fields and the averaged case. The three T-fields are d05r05 (best fit), d08r05 (worst fit), and d04r08 (median fit). Table 10 lists the percentage contribution to ε of each well for the four cases. Looking at the four worst-fit wells for each case, only P-14 and WIPP-25 are common across all four cases. For the average case, wells P-14 and WIPP-25 together account for 30.8% of the total error. For d05r05, d08r05, and d04r08, P-14 and WIPP-25 together account for 40.7%, 26.3%, and 30.0%, respectively. The fact that those two wells account for a significantly higher percentage of the error for the best-fit T-field (d05r05) indicates that the lower ε score for d05r05 is due to a better fit on the remaining 10 monitoring wells. Additionally, the fact that those two wells are difficult to fit across all T-fields suggests that the Salado dissolution re-entrant (and associated high Culebra T) connecting those two wells that was hardwired into all T-fields by Holt and Yarbrough (2003) may not be an accurate representation of conditions in that area. P-14 and WIPP-25 were also difficult to fit for the tailings-pile scenario (Lowry and Beauheim, 2004). A contour plot showing the total error for the average case and for T-fields d05r05, d04r08, and d08r05 is shown in Figure 8. The hard-to-fit P-14 and WIPP-25 wells can easily be seen in all the plots.

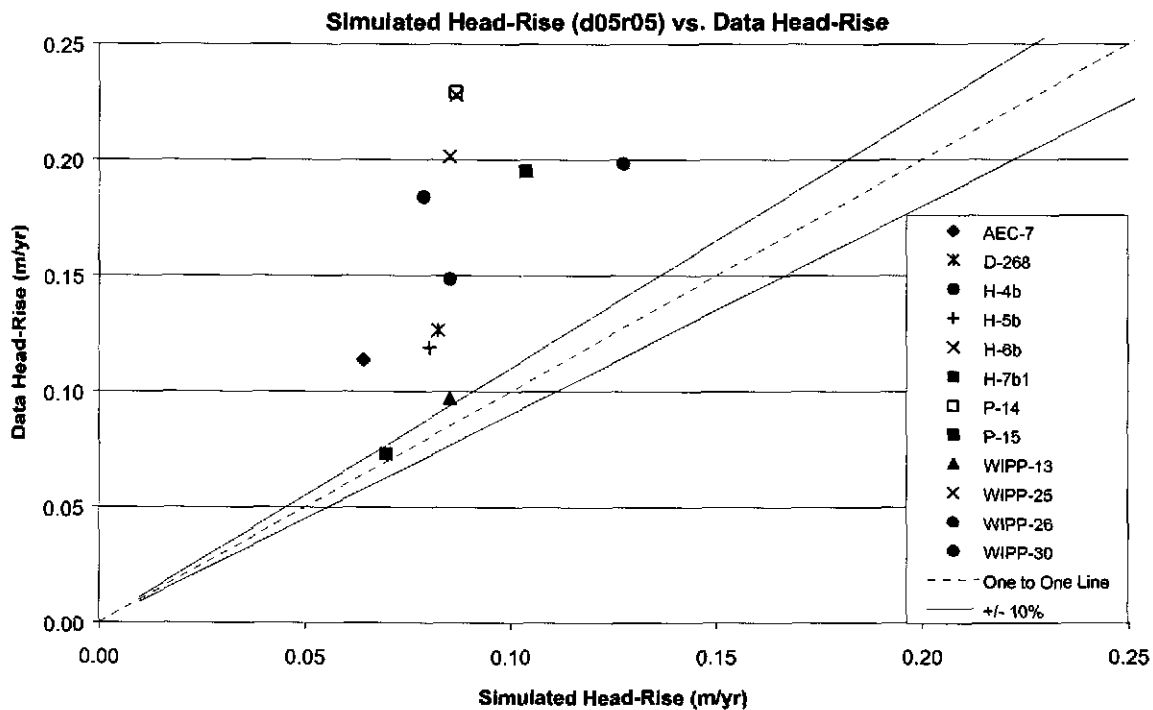


Figure 7. Simulated head-rise for T-field d05r05, Option A, versus data head-rise.

Table 10. Percentage contribution of each well to the total error for the average case, T-field d05r05 (best fit), T-field d04r08 (median case) and T-field d08r05 (worst fit) for Option A. The results for the four worst-fitting wells for each case are in bold.

Well #	Average	d05r05	d04r08	d08r05
AEC-7	3.55%	4.72%	0.79%	11.90%
D-268	4.71%	5.27%	4.94%	4.07%
H-4b	10.26%	4.96%	11.57%	10.37%
H-5b	2.69%	2.18%	3.40%	0.93%
H-6b	8.75%	10.61%	9.90%	8.79%
H-7b1	7.58%	2.82%	7.92%	6.16%
P-14	15.68%	20.58%	15.45%	13.97%
P-15	9.90%	5.49%	10.83%	9.32%
WIPP-13	8.81%	7.17%	7.22%	9.29%
WIPP-25	15.10%	20.10%	14.51%	12.28%
WIPP-26	6.04%	7.99%	6.83%	5.75%
WIPP-30	6.92%	8.11%	6.64%	7.16%

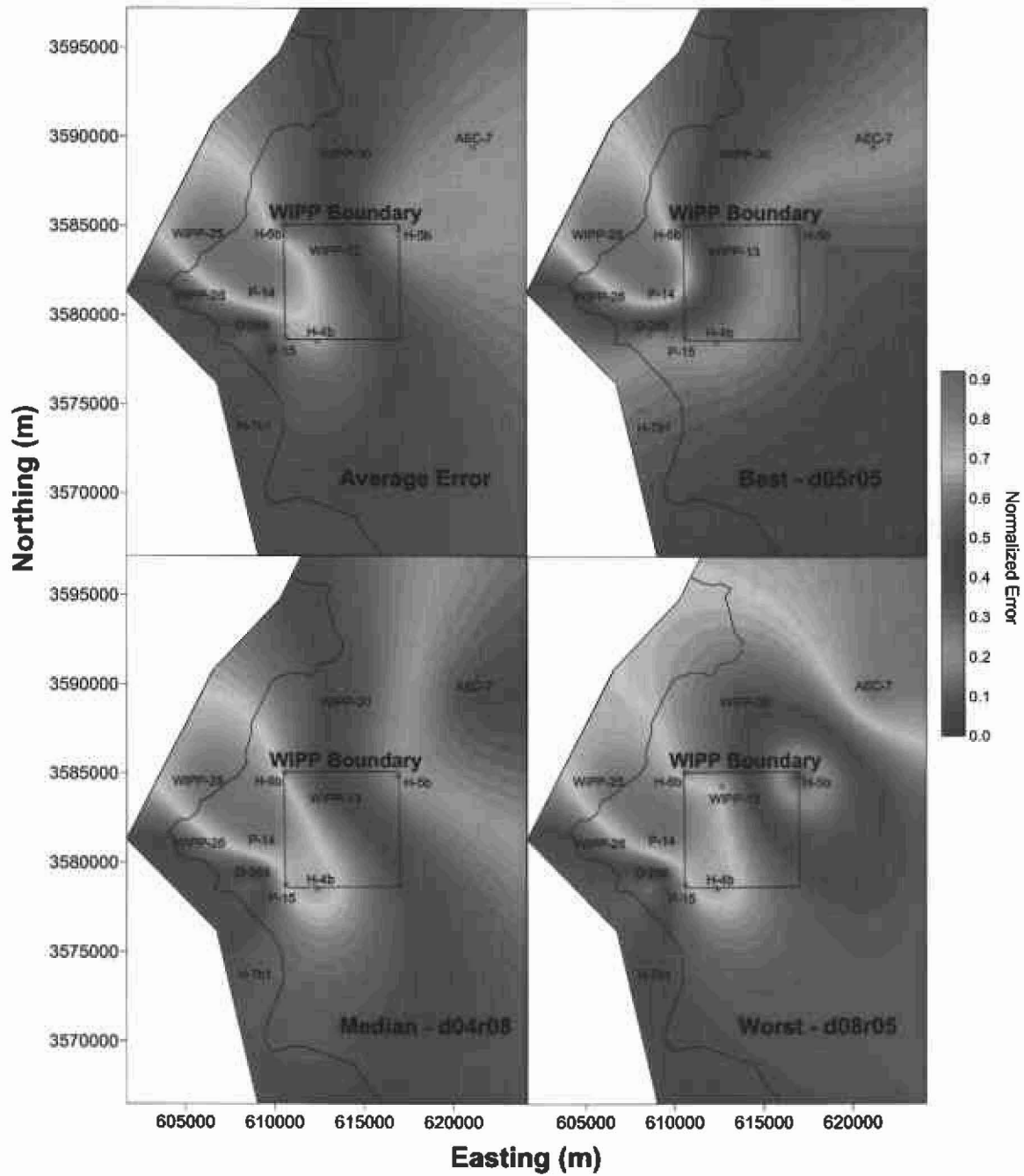


Figure 8. Contour plots of the normalized ϵ value as calculated at each well for Option A.

5.2 Option B

Option B required fitting the rate of head rise for the last six years of the simulation to the linearized head rise as calculated through the regression analysis of the data. This provides no limitation to the total amount of head rise over the 15-year simulation time. To meet the late-time water-level rise, the calibration in some cases produced very high leakage rates which resulted in high total head rises over the 15-year simulations (i.e., there was a very rapid water-level rise in the early years, which leveled off in the later years). This is a result of the storage coefficient remaining fixed. Thus, an extra filtering criterion was established that omitted a T-field if the total simulated head rise for the 15-year period was greater than 50 m in any one well. This value was chosen to omit simulations that were grossly inappropriate (i.e., Culebra heads exceeded Magenta and/or Dewey Lake heads). The extra criteria eliminated 18 T-fields with maximum water-level rises across all wells ranging from 52.9 to 248.3 m. This resulted in 77 qualified runs for Option B. The range of total leakage from all boreholes was from 2.46×10^{-4} to 1.22×10^{-2} m³/s, with an average of 3.12×10^{-3} m³/s. Because the Mid and Nash Draw boreholes were calibrated as a single group, the total flow for each group was determined by multiplying the calibrated leakage rate for each borehole by the number of boreholes in each group (six for the Mid group and three for the Nash Draw group). Of the total leakage, 25.6% came from the Upper group of boreholes and 74.4% from the Lower group. The Mid/Nash Draw group resulted in leakage rates that were four orders of magnitude smaller than the rates for the Upper and Lower groups. The Lower group had a much higher percentage of the total leakage in Option B than in Option A. A breakdown of the total leakage rate for each group of boreholes is shown in Table 11.

Table 11. Option B total leakage rates for each group of leaky boreholes.

Statistic	Leakage by Group (m ³ /s)				
	Upper	Mid	Nash Draw	Lower	Total
Average	8.00×10^{-4}	7.24×10^{-8}	3.62×10^{-8}	2.32×10^{-3}	3.12×10^{-3}
Median	8.85×10^{-5}	5.78×10^{-8}	2.89×10^{-8}	1.63×10^{-3}	2.26×10^{-3}
Maximum	1.22×10^{-2}	5.65×10^{-7}	2.82×10^{-7}	1.02×10^{-2}	1.22×10^{-2}
Minimum	7.54×10^{-8}	6.33×10^{-10}	3.17×10^{-10}	2.50×10^{-6}	2.46×10^{-4}
Std. Dev.	1.80×10^{-3}	9.18×10^{-8}	4.59×10^{-8}	2.33×10^{-3}	2.60×10^{-3}

Plots of the simulated head rises at each well for the last six years of the Option B simulations are compared to the slopes calculated from the data in Appendix P. In most cases, Option B had a difficult time matching the rate of the late-time head-rise.

The relative errors (ϵ) for Option B ranged from 0.745 to 1.458 m, with T-field d22r02 providing the best fit and T-field d07r10 providing the worst. The T-fields with their corresponding ϵ

values are listed in Table 12. Figure 9 shows visualizations of the best-fit and worst-fit T-fields, expressed in $\log_{10} T$ (m^2/s) values.

Figure 10 shows the data slopes versus the calibrated slopes for T-field d22r02. As compared to Option A, the slopes are not as biased and tend to reflect a wider range of head rises. However, most values lie outside the region of 10% error. This may indicate that the assumption of a spatially constant S_s is too simplistic. It may also mean that grouping the leaky boreholes based on their location may not provide sufficient detail to capture the local dynamics.

To gain some understanding of the error associated with the calibration process, we compare the percentage contribution of each monitoring well to ε for three T-fields and the averaged case. The three T-fields are d22r02 (best fit), d07r10 (worst fit), and d03r06 (median fit). Table 13 lists the percentage contribution to ε of each well for the four cases. Looking at the four worst-fit wells for each case, only P-14 and WIPP-25 are common across all four cases. Similar to Option A, wells P-14 and WIPP-25 are consistently difficult to fit across all T-fields and, on average, together account for 35.3% of the total error. For d22r02, d07r10, and d03r06, P-14 and WIPP-25 together account for 31.9%, 32.8%, and 36.5% of the total error, respectively. For the best-fitting T-field (d22r02), wells P-14 and WIPP-25 together accounted for less of the total error than in Option A (35.3% versus 40.7% for T-field d05r05, Option A), but d22r02 also had a large contribution to the total error from well AEC-7 (28.4%). The remaining nine wells outside of P-14, WIPP-25, and AEC-7 contributed, at most, only 8.3% to the total error, meaning the relative fit was better in those areas. A contour plot showing the normalized error for the average case and for T-fields d22r02, d07r10, and d03r06 is shown in Figure 11. The hard-to-fit P-14 and WIPP-25 wells can easily be seen in all the plots.

Table 12. Relative error, ε , sorted by best (d22r02) to worst (d07r10) for Option B.

T-field	ε (m)	T-field	ε (m)	T-field	ε (m)	T-field	ε (m)
d22r02	0.745	d08r01	1.003	d10r10	1.173	d22r08	1.326
d11r10	0.751	d05r05	1.005	d22r06	1.181	d04r10	1.331
d12r08	0.773	d06r04	1.041	d07r08	1.209	d13r01	1.336
d01r02	0.801	d21r02	1.070	d12r02	1.213	d10r08	1.355
d01r07	0.822	d05r03	1.077	d21r07	1.233	d13r08	1.362
d02r02	0.826	d08r09	1.089	d22r09	1.243	d06r03	1.368
d04r02	0.854	d03r03	1.097	d04r06	1.249	d07r07	1.373
d05r02	0.860	d13r05	1.099	d12r07	1.250	d22r07	1.376
d05r07	0.899	d11r01	1.104	d13r02	1.260	d21r03	1.379
d02r07	0.901	d03r07	1.113	d07r01	1.280	d10r02	1.390
d09r10	0.947	d02r10	1.113	d06r06	1.283	d06r07	1.394
d07r09	0.948	d09r05	1.129	d08r04	1.285	d21r05	1.397
d03r09	0.956	d04r08	1.138	d12r06	1.286	d22r10	1.408
d01r08	0.956	d06r02	1.138	d12r03	1.287	d12r05	1.413
d11r06	0.957	d03r10	1.139	d10r07	1.293	d08r02	1.428
d22r05	0.980	d21r10	1.146	d21r01	1.307	d08r06	1.441
d07r02	0.980	d12r01	1.156	d08r03	1.311	d07r10	1.458
d09r02	0.981	d07r05	1.159	d04r05	1.320		
d11r08	0.991	d03r06	1.160	d08r05	1.324		
d11r07	1.000	d04r03	1.167	d01r10	1.325		

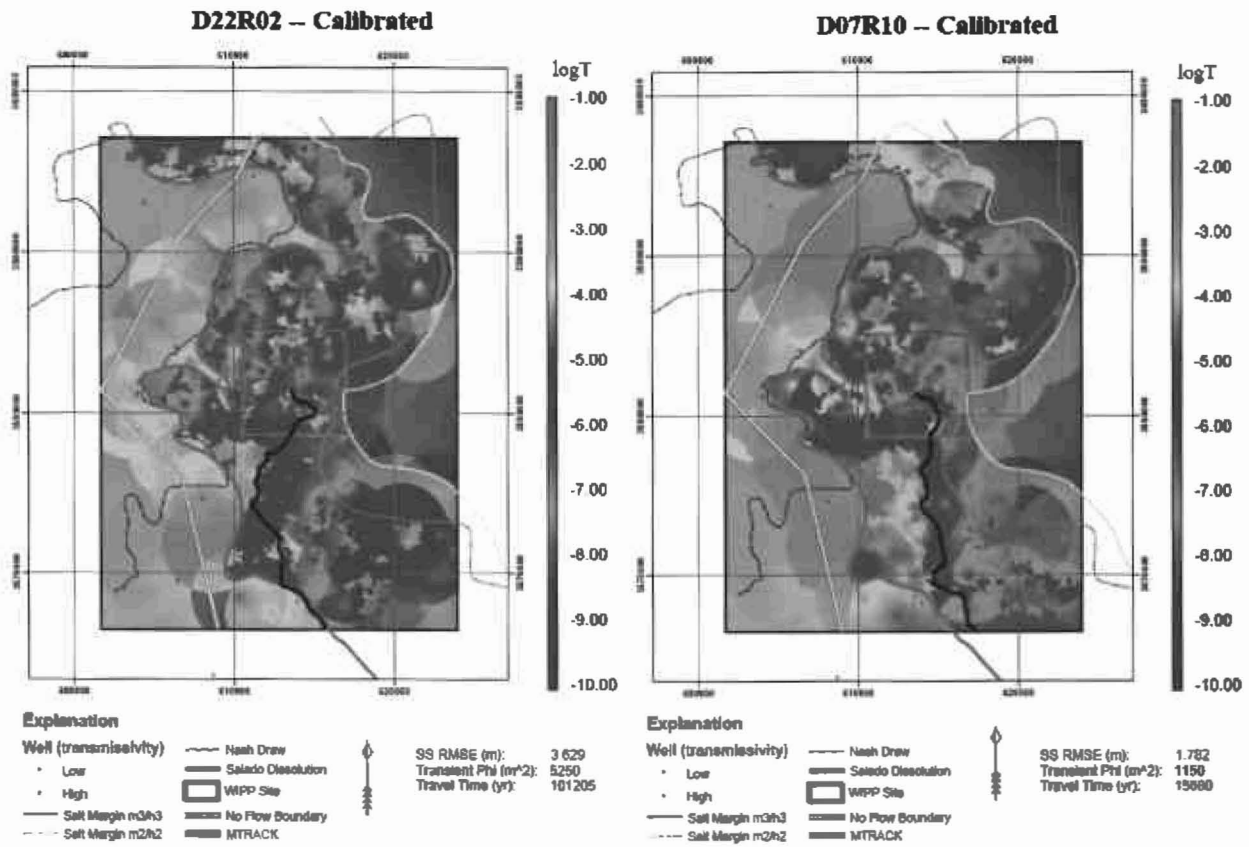


Figure 9. Comparison of the best-fit T-field (d22r02) and the worst-fit T-field (d07r10) for Option B.

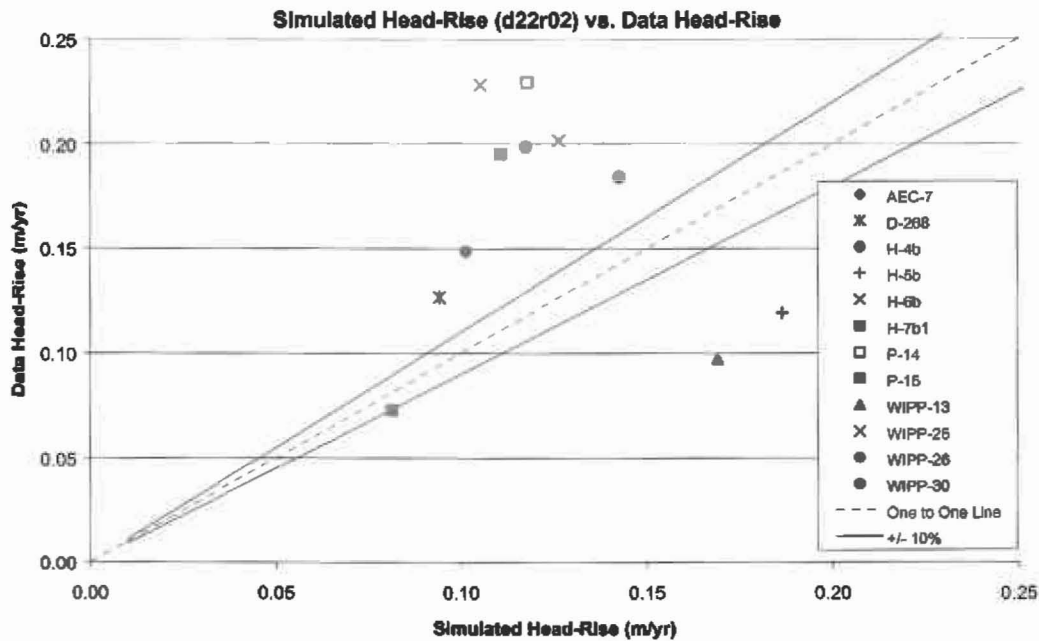


Figure 10. Simulated head-rise for T-field d22r02, Option B, versus data head-rise.

Table 13. Percentage contribution of each well to the total error for the average case, T-field d22r02 (best fit), T-field d07r10 (median case) and T-field d03r06 (worst fit) for Option B. The results for the four worst-fitting wells for each case are in bold.

Well #	Average	d22r02	d07r10	d03r06
AEC-7	7.06%	28.42%	1.12%	20.28%
D-268	4.39%	1.20%	4.98%	2.32%
H-4b	10.75%	7.61%	12.28%	7.11%
H-5b	2.88%	5.31%	2.38%	0.03%
H-6b	10.19%	6.56%	12.66%	10.15%
H-7b1	1.23%	0.08%	1.64%	0.56%
P-14	17.68%	14.42%	16.47%	17.81%
P-15	11.04%	8.27%	11.91%	5.75%
WIPP-13	1.80%	6.03%	2.81%	0.56%
WIPP-25	17.84%	17.51%	16.33%	18.72%
WIPP-26	6.59%	2.59%	6.91%	6.09%
WIPP-30	8.57%	2.01%	10.51%	10.62%

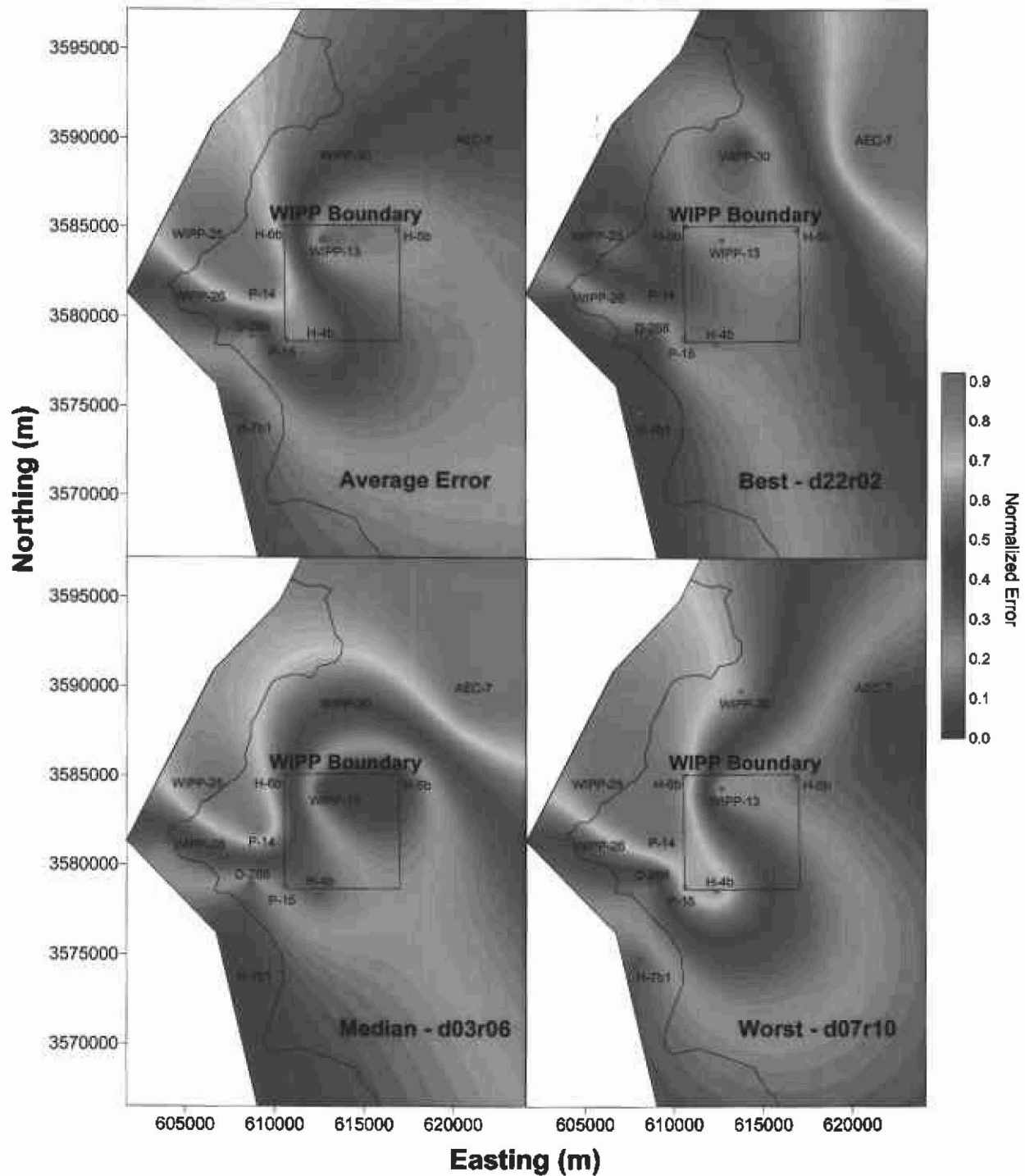


Figure 11. Contour plots of the normalized ϵ value as calculated at each well for Option B.

5.3 Option C

Option C involved fitting the rate of head rise for the last six years of the simulation to the linearized head rises as calculated through the regression analysis of the data, using both leakage rates and specific storage in two areas (inside and outside of Nash Draw) as fitting parameters. The specific storage parameters were calibrated between upper and lower limit values of 1×10^{-4} and $1 \times 10^{-8} \text{ m}^{-1}$. After filtering, Option C resulted in 65 qualified runs. The range of total leakage from all boreholes was from 2.73×10^{-4} to $3.85 \times 10^{-3} \text{ m}^3/\text{s}$, with an average of $1.28 \times 10^{-3} \text{ m}^3/\text{s}$. Of the average total leakage, 28.5% came from the Upper group, 1.9% from the Mid group, 5.5% from the Nash Draw group, and 64.1% from the Lower group. This is somewhat more balanced than the rates from Option B, but again is heavily weighted between the Upper and Lower groups. A breakdown of the total leakage rate for each group of boreholes is shown in Table 14.

Table 14. Option C total leakage rates for each group of leaky boreholes and S_s values. S_s^{ND} is the specific storage in Nash Draw, S_s is the specific storage elsewhere.

Statistic	Leakage by Group (m^3/s)				Specific Storage (m^{-1})	
	Upper	Mid	Lower	Total*	S_s^{ND}	S_s
Average	3.64×10^{-4}	2.42×10^{-5}	8.18×10^{-4}	1.28×10^{-3}	4.91×10^{-5}	6.40×10^{-6}
Median	2.30×10^{-4}	9.10×10^{-6}	6.57×10^{-4}	1.18×10^{-3}	4.72×10^{-5}	3.02×10^{-6}
Maximum	1.59×10^{-3}	3.07×10^{-4}	2.98×10^{-3}	3.85×10^{-3}	9.99×10^{-5}	5.55×10^{-5}
Minimum	8.23×10^{-7}	6.65×10^{-8}	7.19×10^{-5}	2.73×10^{-4}	3.28×10^{-6}	1.02×10^{-8}
Std. Dev.	4.07×10^{-4}	4.55×10^{-5}	6.04×10^{-4}	7.08×10^{-4}	2.51×10^{-5}	8.91×10^{-6}

*Includes the fixed leakage of $7.09 \times 10^{-3} \text{ m}^3/\text{s}$ for the Nash Draw group.

Plots of the head rises at each well for the last six years of the Option C simulations are compared to the slopes calculated from the data in Appendix Q. The plots show that the Option C calibrations tend to be clustered around the data slopes better than either the Option A or Option B calibrations. Overall, Option C consistently produced the best fits.

The relative error (ε) ranged from 0.312 to 0.886 m, with T-field d01r06 providing the best fit and T-field d04r08 providing the worst. Option C had the best-fitting calibrations of all the options, with 61 out of 65 fits being better than any from Options A or B. The T-fields with their corresponding ε values are listed in Table 15. Figure 12 shows visualizations of the best-fit and worst-fit T-fields, expressed in $\log_{10} T$ (m^2/s) values.

The S_s values within and outside of Nash Draw for both Option C and from Lowry and Beauheim (2004) are listed in Table 16. Given the fact that the leakage sources between the two scenarios are very different (a large recharge area in the northern part of the modeling domain for

Lowry and Beauheim (2004) versus a more distributed source for Option C), the results are quite similar, with the means and medians showing a 31% difference outside of Nash Draw and a 6% difference within Nash Draw. The ratio of the mean S_s within Nash Draw to the mean S_s outside Nash Draw for Option C is 7.7, whereas it was 5.7 in Lowry and Beauheim (2004). This consistent difference may indicate that the T-field calibration of McKenna and Hart (2003) could be improved by using more than a single value of S_s over the entire model domain.

Table 15. Relative error, ε , of each T-field sorted by best (d01r06) to worst (d04r08) for Option C.

T-field	ε (m)	T-field	ε (m)	T-field	ε (m)	T-field	ε (m)
d01r06	0.312	d03r09	0.373	d11r09	0.388	d09r08	0.408
d01r08	0.327	d02r07	0.376	d08r06	0.391	d09r07	0.409
d22r02	0.338	d04r03	0.377	d09r05	0.391	d22r08	0.409
d04r06	0.339	d11r01	0.377	d13r02	0.393	d03r07	0.413
d01r02	0.340	d22r05	0.379	d21r02	0.393	d13r01	0.413
d22r04	0.342	d13r06	0.379	d08r05	0.395	d08r01	0.417
d21r04	0.352	d12r02	0.379	d03r10	0.396	d12r07	0.418
d05r07	0.352	d21r10	0.380	d22r07	0.396	d06r04	0.441
d12r01	0.356	d13r03	0.381	d09r10	0.398	d04r02	0.463
d09r02	0.358	d08r03	0.382	d03r06	0.398	d07r05	0.468
d08r07	0.360	d04r05	0.383	d06r10	0.401	d06r06	0.471
d03r03	0.360	d22r06	0.384	d10r07	0.402	d07r08	0.500
d11r02	0.362	d21r06	0.384	d13r05	0.403	d04r10	0.734
d02r10	0.363	d06r07	0.384	d12r09	0.404	d05r05	0.776
d13r07	0.370	d12r03	0.387	d10r08	0.405	d04r07	0.815
d02r02	0.370	d12r06	0.388	d10r10	0.406	d04r08	0.886
d09r06	0.372						

Table 16. Comparison of specific storage values (m^{-1}) from Lowry and Beauheim (2004) and Option C.

Statistic	Lowry and Beauheim (2004)		Option C	
	S_s^{ND}	S_s	S_s^{ND}	S_s
Average	5.24×10^{-5}	9.25×10^{-6}	4.91×10^{-5}	6.40×10^{-6}
Median	4.31×10^{-5}	6.24×10^{-6}	4.72×10^{-5}	3.02×10^{-6}
Maximum	2.13×10^{-4}	5.09×10^{-5}	9.99×10^{-5}	5.55×10^{-5}
Minimum	9.43×10^{-6}	2.40×10^{-7}	3.28×10^{-6}	1.02×10^{-8}
Std. Dev.	4.17×10^{-5}	1.01×10^{-5}	2.51×10^{-5}	8.91×10^{-6}

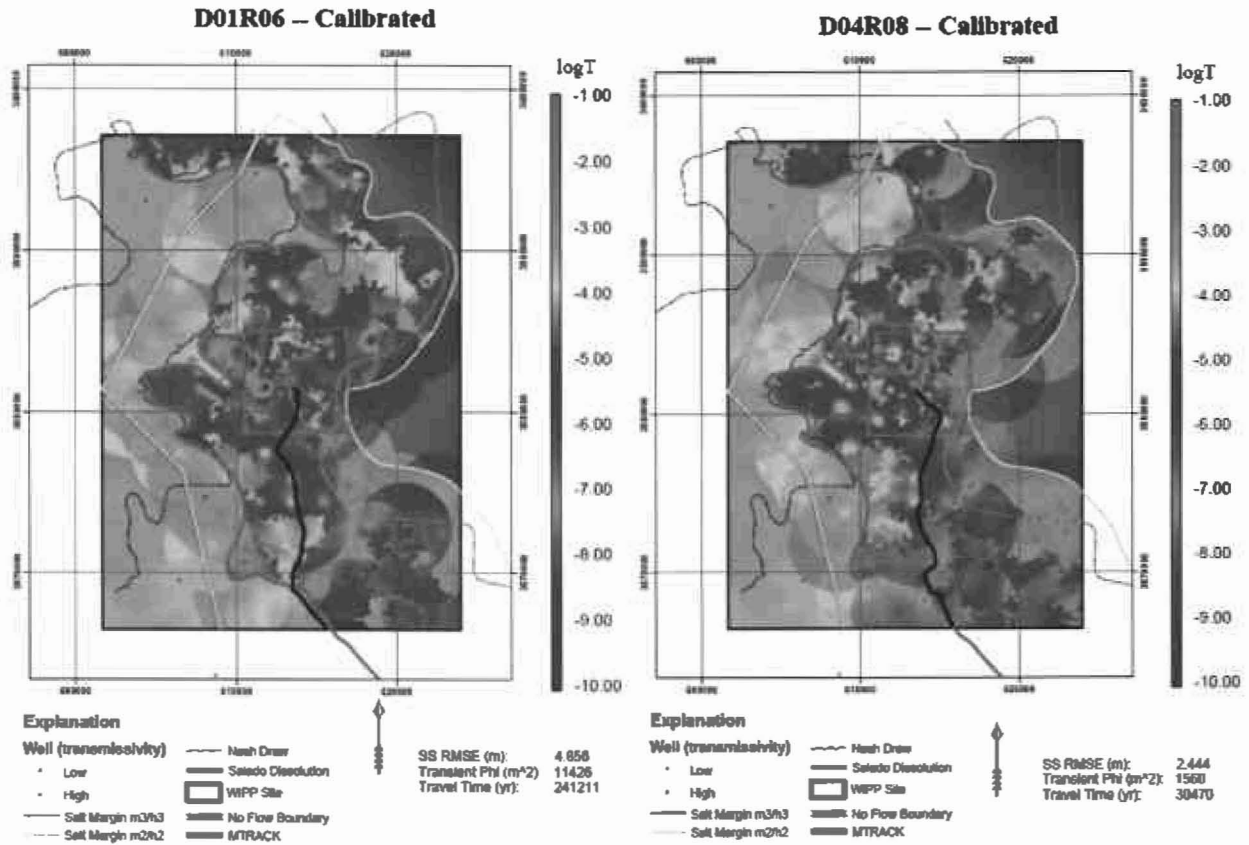


Figure 12. Comparison of the best-fit T-field (d01r06) and the worst-fit T-field (d04r08) for Option C.

Figure 13 shows the data slopes versus the calibrated slopes for T-field d01r06. As compared to Options A and B, the slopes are not as biased and tend to be closer to the 1:1 line. This indicates the influence of S_s on temporal water-level dynamics. However, like Option B, the range of simulated head rises was much less than that shown by the data (0.135 to 0.198 m/yr for Option C versus 0.073 to 0.229 m/yr for the data).

To gain some understanding of the error associated with the calibration process, we compare the percentage contribution of each monitoring well to ε (Table 17) for three T-fields and the averaged case. The three T-fields are d01r06 (best fit), d04r08 (worst fit), and d12r06 (median fit). Looking at the four worst-fit wells for each case, only P-14 is common across all four cases with WIPP-13, WIPP-25 and H-7b1 being common across three of the four cases. The difficulty in fitting P-14 and WIPP-25 may again point to a conceptual model problem or mischaracterization in that area of the model, especially since this area was difficult to fit with Options A and B as well as in Lowry and Beauheim (2004). The difficulty in fitting H-7b1 may indicate that Nash Draw cannot be treated as homogeneous from north to south. We are uncertain why WIPP-13 proved to be more difficult to fit under Option C than it was under Option B. For the average case, wells WIPP-13 and H-7b1 are the two most difficult to fit and account for 33.3% of the total error. For d01r06 and d12r06, WIPP-13 and H-7b1 together account for 44.5% and 41.7%, respectively, of the total error. The worst overall case, d04r08,

was able to fit these two wells very well, but had difficulty fitting most of the other wells. A contour plot showing the normalized error for the average case and for T-fields d01r06, d12r06, and d04r08 is shown in Figure 14. The hard-to-fit WIPP-13 and H-7b1 wells can easily be seen in the average, d01r06, and d12r06 plots, while the d04r08 plot shows the good fits in those areas.

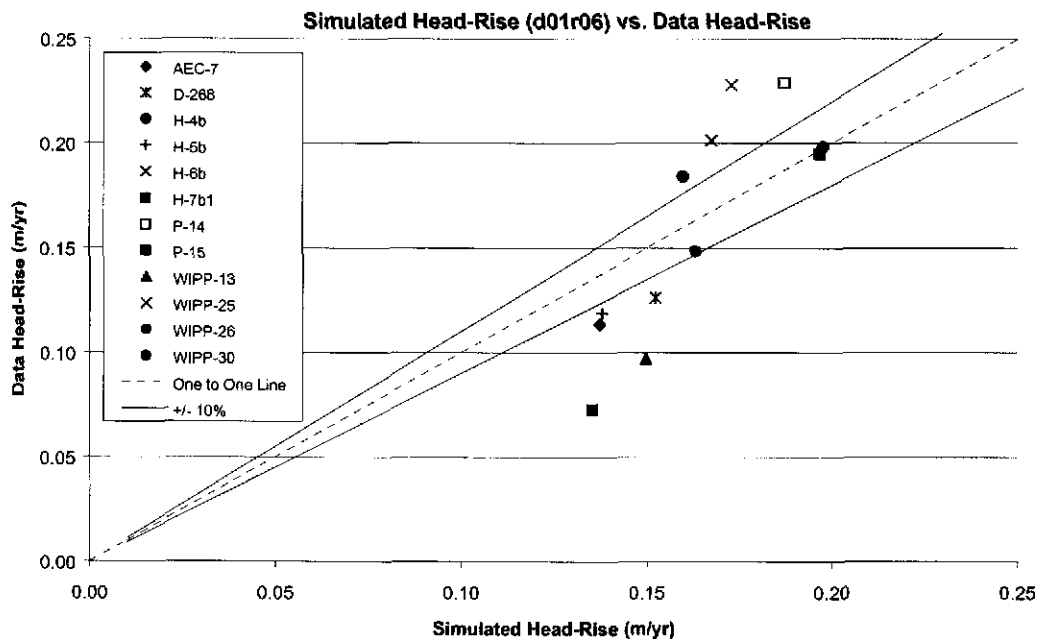


Figure 13. Simulated head-rise for T-field d01r06, Option C, versus data head-rise.

Table 17. Percentage contribution of each well to the total error for the average case, T-field d01r06 (best fit), T-field d12r06 (median case) and T-field d04r08 (worst fit) for Option C. The results for the four worst-fitting wells for each case are in bold.

Well #	Average	d01r06	d12r06	d04r08
AEC-7	2.20%	3.73%	0.02%	5.70%
D-268	5.50%	4.48%	4.24%	1.72%
H-4b	6.65%	0.00%	10.73%	11.10%
H-5b	5.60%	2.40%	7.07%	3.61%
H-6b	6.51%	7.66%	3.01%	13.37%
H-7b1	17.02%	26.01%	23.86%	0.01%
P-14	12.53%	11.76%	11.23%	17.88%
P-15	5.28%	0.02%	7.63%	10.49%
WIPP-13	16.23%	18.44%	17.81%	0.89%
WIPP-25	12.86%	20.14%	6.34%	18.26%
WIPP-26	3.75%	1.42%	5.19%	3.33%
WIPP-30	5.88%	3.93%	2.86%	13.66%

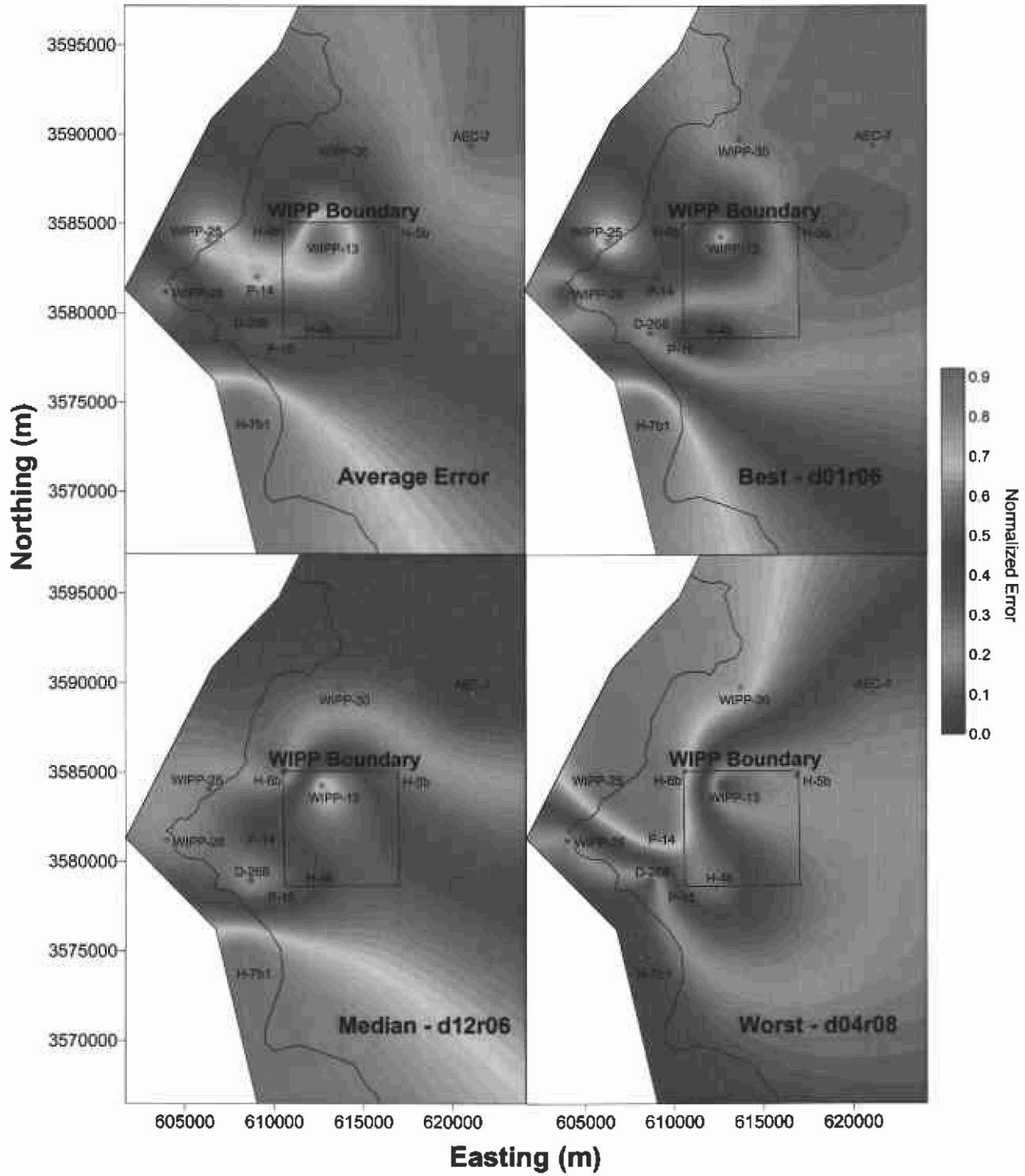


Figure 14. Contour plots of the normalized ϵ value as calculated at each well for Option C.

To assess the long-term implications of leakage to the Culebra, an additional set of runs was made with the Option C calibration parameters with a total simulation time of 115 years (15 years from 1989 to 2004, plus 100 years into the future). Plots for the filtered T-fields for each monitoring well are shown in Appendix T. On each plot, the data slope that was fitted to from year 9 through year 15 is shown as a continuous line from the origin to year 15. Note that the vertical placement of this data-slope line is arbitrary. In most cases, the rate of water-level rise decreases significantly after year 15, with comparatively little rise occurring over the next 100 years. Figure 15 is a histogram of the maximum additional water-level rise at the 12 wells considered for the 100 simulated years after year 15 for the filtered T-fields of Option C. In the vast majority of cases, the additional rise is less than 8 m, with a mean of 2.02 m and a median of 1.53 m (shown as the red and green vertical lines, respectively, in Figure 15). Unless the specific storage values are much less than those calibrated in Option C, or the $1.069 \times 10^{-6} \text{ m}^{-1}$ used in Option A, these long-term simulations indicate that the potential for additional water-level rises may be limited.

Option - C

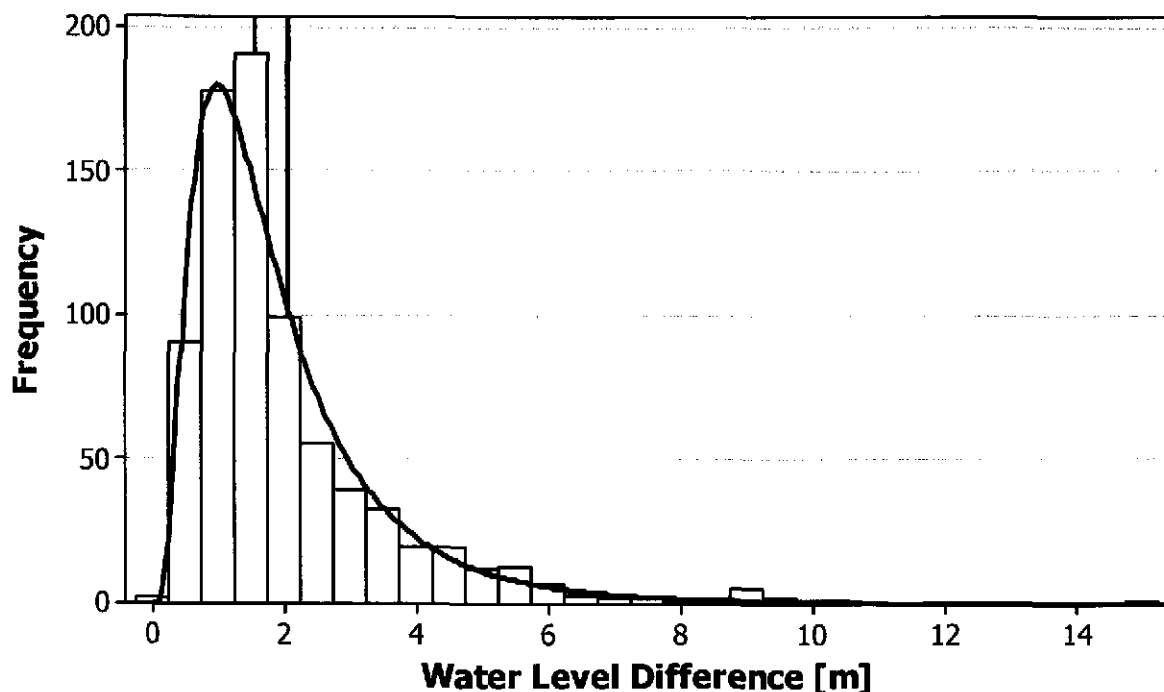


Figure 15. Histogram of the maximum additional water level rise for the last 100 years of the long-term simulations. The vertical green and red lines represent the median (1.53 m) and mean (2.02 m) values, respectively.

6 Discussion

Comparisons of the leakage rate for each group of boreholes as well as the minimum and maximum ϵ values for each option are shown in Table 18. For all three options, the leakage rate for the Upper group of boreholes was the most consistent, ranging from 2.93×10^{-4} to 8.00×10^{-4} m^3/s . Leakage rates for the other three groups show a variability of two to three orders of magnitude among the different options. The total leakage rate was about one order of magnitude higher for Options B and C than for Option A, primarily because the early transient period, in which most of the head rise occurred, was excluded from the calibration process for Options B and C. With this early period excluded, more leakage was required to match the late-time head rise.

Table 18. Comparison of mean calibration parameters for all three options. Percentages show percent of leakage from that group to the total leakage.

Parameter	Option		
	A	B	C
Leakage in Upper Group (m^3/s)	2.93×10^{-4} (66.5%)	8.00×10^{-4} (25.6%)	3.64×10^{-4} (28.5%)
Leakage in Mid Group (m^3/s)	6.39×10^{-7} (0.1%)	7.24×10^{-8} (0.0%)	2.42×10^{-5} (1.9%)
Leakage in Nash Draw Group (m^3/s)	7.09×10^{-5} (16.1%)	3.62×10^{-8} (0.0%)	$7.09 \times 10^{-5*}$ (5.5%)
Leakage in Lower Group (m^3/s)	7.63×10^{-5} (17.3%)	2.32×10^{-3} (74.4%)	8.18×10^{-4} (64.1%)
Total Leakage (m^3/s)	4.41×10^{-4}	3.12×10^{-3}	1.28×10^{-3}
ϵ min (m)	0.510	0.745	0.312
ϵ max (m)	0.698	1.458	0.886

*Fixed as the average from Option A

Figure 16 shows comparisons of the cumulative distribution functions (CDF's) for the major calibration parameters as well as the maximum simulated water-level rise for each option. In addition, a log-normal distribution is fit to each CDF (dotted lines). Overall, the CDF's from Option C are the most uniform and fit the log-normal model the best. For the Mid group, Option A is almost bi-modal showing a gap for the per well natural-log leakage rate from about -16 to -22, with the upper 20% of the values being greater than -16. This indicates that for a certain set

of T-fields, leakage from the Mid group of wells has a somewhat greater influence on the water-level rise. The same phenomenon can be seen in the Lower group for both Options A and B, where the lower 10% of the values is distinct from the rest of the distribution. The implication is that most (~90%) of the T-fields modeled in Options A and B require a relatively high rate of flow from the Lower group. With regards to S_s , the range of calibrated values for the area outside of Nash Draw is much greater than the range within Nash Draw. This means the model is more sensitive to the S_s values inside of Nash Draw than outside it.

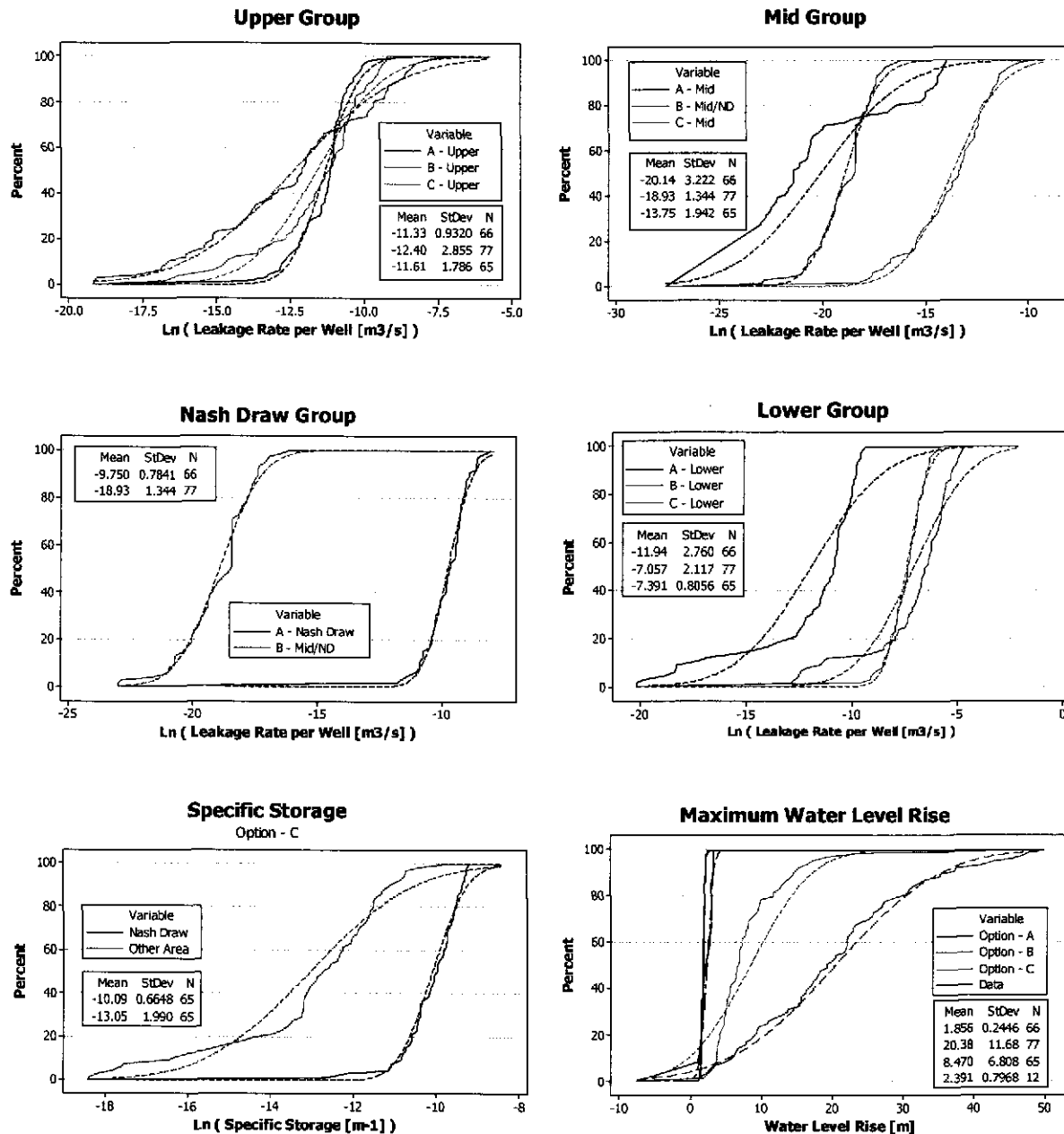


Figure 16. Cumulative distribution functions of the major calibration parameters and the maximum simulated water level rise for Options A, B, and C.

Examining the distributions of the maximum simulated water-level rise, Option A shows a very small range of values as compared to Options B and C. This is because Option A calibrated to the rate of water-level rise for the entire 15-year period, forcing the results into this narrow range. Conversely, Options B and C used the rate of water-level rise between simulation years 9 and 15, with no bounds on the total rise for the 15-year simulation. As a comparison, the CDF of the 15-year water-level rise from the linearized data from the 12 monitoring wells is plotted in blue (ranges from 1.09 to 3.44 m).

Examination of the ϵ values in Table 18 indicates that Option C had the best-fitting calibrations with the majority of the T-fields (61 of the 65 qualified calibrations) having ϵ values that were less than the minimum from either Option A or Option B. Overall, the Option C fits were much more accurate than the fits from the other options.

The contribution to the total leakage from the Upper group of boreholes for Option A was much higher than for Options B or C (66.4% for Option A versus 25.6% and 28.5 % for Options B and C, respectively). Conversely, the contribution by the Lower group was 17.3%, 74.4%, and 64.1% for Options A, B, and C, respectively. This highlights the difference between the two conceptual models (full-time calibration and late-time calibration) and means that if the water-level rise is in quasi-steady-state, a significant amount of leakage must be entering the Culebra from a source south of the WIPP site.

The amounts of leakage listed in Table 18 are not large, and are not unreasonable when compared to the capacities of the potential sources. Taking the Option C results as an example, the average total leakage through the Upper group of boreholes is only 3.64×10^{-4} m³/s, which is equivalent to 5.8 gallons per minute (gpm) or 9.3 acre-ft/yr, distributed among 16 boreholes. Lowry and Beauheim (2004) indicate that 1100 acre-ft/yr of water may be infiltrating from the Intrepid East tailings pile into the upper groundwater system in the vicinity of the Upper group, over 100 times the amount calculated to be leaking through the Upper group boreholes. The average total leakage through the Mid group of boreholes is only 2.42×10^{-5} m³/s, or 0.38 gpm, distributed among six boreholes. This is within the capacity of the Magenta in this area (but see the discussion in the next paragraph). The fixed leakage through the three boreholes in the Nash Draw group totaled 7.09×10^{-5} m³/s, or 1.12 gpm. Lambert and Robinson (1984) reported pumping 34 gpm from the Magenta at WIPP-25, so the Magenta (or Dewey Lake where saturated) could easily be the source of the leakage through the Nash Draw group of boreholes. The average total leakage through the single borehole in the Lower group is 8.18×10^{-4} m³/s, or 13.0 gpm. A Dewey Lake water table is present in this area (Powers and Richardson, 2004). Beauheim and Ruskauff (1998) report that the Dewey Lake could be pumped at a rate of 12 gpm in well WQSP-6A with only 3 psi of drawdown. Hence, the Dewey Lake could plausibly be providing 13 gpm to a leaky borehole.

With respect to the Mid group of boreholes, monitoring points on the nearby NW and NE corners of the WIPP site (wells H-6 and H-5, respectively) show Magenta heads rising in a manner similar to those in the Culebra, which is the opposite of what would be expected if Magenta water were leaking into the Culebra. The Dewey Lake does not appear to be saturated in any zone with significant permeability in this region, so no driving force seems to be present above the Magenta. Given these observations and the low leakage rates calculated by the model, the boreholes in the Mid group may not, in fact, be leaking. The observed rises in both Culebra

and Magenta heads in the vicinity of the Mid group of boreholes may be explained by pressure propagation from the Upper group of boreholes.

The modeling results show that a balance must be achieved between leakage in the Upper group of boreholes and in the Lower and (to a much lesser extent) Nash Draw groups of boreholes in order to produce the observed head rise in the 12 monitoring wells. If no water is leaking through the Lower borehole, then heads to the south of the WIPP site are too low and the observed water-level rise cannot be reproduced in the middle part of the modeling domain. As discussed above, the required amount of leakage could plausibly be leaking from the Dewey Lake to the Culebra through the Lower group borehole. As a conceptual model alternative to the potentially leaking Lower group borehole, however, the Culebra could instead (or also) be receiving natural recharge southwest of the WIPP site close to H-7b1, where we believe it to be unconfined.

We would expect the leaky-borehole scenario to require less water to match the observed water-level rise than the tailings-pile scenario investigated by Lowry and Beauheim (2004) because it distributes the source, allowing head rises to occur in the south without the water having to come from the north. The tailings-pile scenario, on the other hand, relied only on inflow from the northern portion of the model domain. The mean leakage rate from the tailings-pile recharge scenario from Lowry and Beauheim (2004) is $2.88 \times 10^{-3} \text{ m}^3/\text{s}$ (73.6 acre-ft/yr). This value is similar to the total leakage rates from Options B and C for the leaky-borehole scenario. However, the tailings-pile-scenario modeling used the Option A method of trying to match the head rise over the entire simulation period to the linearized hydrographs. Had that modeling used the Option B or Option C method of fitting to only the last six years' data, an order of magnitude more leakage may well have been required. We note also that the tailings-pile scenario introduces water into the Culebra at essentially the same location as the Upper group of boreholes in the leaky-borehole scenario. Even using the Option A method of calibration, the tailings-pile scenario required an order of magnitude more leakage at the north end of the model domain than did the leaky-borehole scenario.

7 Summary and Conclusions

This analysis report describes the activities of Task 3 of AP-110, "Analysis Plan for Evaluation of Culebra Water-Level-Rise Scenarios" (Beauheim, 2003a). The purpose of this Task is to evaluate the possibility that observed rising water levels in the Culebra Dolomite Member of the Rustler Formation near the Waste Isolation Pilot Plant (WIPP) are due to leakage into the Culebra of water from units above the Culebra (Magenta and/or Dewey Lake) through poorly plugged and abandoned boreholes.

The basis of this analysis relies on a numerical model of the WIPP area, with the same grid layout and boundary conditions as that used in McKenna and Hart (2003). Hydrograph data from 12 wells in the WIPP area, which were first converted to linearized rates of water-level rise over time, were used to calibrate four groups of boreholes (Figure 5) that were identified as poorly plugged or abandoned (Powers, 2004). One hundred calibrations were completed, each using a different T-field generated from separate calibrations in McKenna and Hart (2003).

Three different sets of calibrations were completed, comprising Options A, B, and C. Option A calibrated the leakage rates of the four groups of boreholes by fitting the simulated head rise over 15 years to that of the data head-rise slopes, using a constant value of specific storage across the entire domain. Results from Option A showed high rates of head rise in the first few years of the simulation with relatively little change over the last 10 years. Thus, Option B calibrated the leakage rates of three groups of boreholes (two of the low-sensitivity groups from Option A were combined) by fitting the simulated head rise over the last 6 years of the 15-year simulation to the data head-rise slopes. Option B also assumed a constant value of specific storage across the modeling domain. The assumption underlying Option B is that the field measurements are reflecting a quasi-steady-state condition where rapid changes in water levels due to initial stresses on the system occurred prior to water level monitoring in the area and have now leveled out to a consistent head rise over time. To explore the effect of specific storage on the calibrations, Option C calibrated leakage rates to three groups of boreholes (one group was fixed to the average from Option A) and two specific storage parameters (one inside Nash Draw, the other outside Nash Draw) by fitting the simulated head rise over the last 6 years of the 15-year simulation to the data head-rise slopes. The merging of two borehole groups (Mid and Nash Draw) for Option B and fixing the leakage rate for the Nash Draw group in Option C were done to limit the number of adjustable parameters to aid in attaining more robust and accurate calibrations.

The calibration results from all the options were filtered to ensure none of the calibrated leakage rates reached their respective maximum or minimum allowable limit and that no single group of boreholes accounted for 100% of the leakage to the Culebra. Exceptions for Option A were made based on the root mean squared error (ϵ) if the Mid group of boreholes reached its minimum and the ϵ value was less than 0.70 m. Option B also had an additional filtering criterion that omitted a calibration if the total head rise for the 15-year simulation was greater than or equal to 50 m. Filtering of the 100 T-fields for Options A, B, and C resulted in 66, 77, and 65 qualified calibrations, respectively.

Of the three options, Option C provided the best and most consistent fits across the qualified calibrations. Error analysis shows that all options had difficulty in fitting the hydrographs from wells P-14 and WIPP-25. This is a similar finding to that of the investigation of the tailings-pile scenario (Lowry and Beauheim, 2004). The agreement between this analysis and that of Lowry and Beauheim (2004) indicates that the geologic model and/or the T-field calibrations in the area of P-14 and WIPP-25 may be inaccurate and should be examined more closely.

The calibrations showed leakage through the Lower and Upper groups of boreholes to be of most importance. Leakage through the Nash Draw group was minor, while leakage through the Mid group was insignificant (and may be zero).

Given the uncertainties and limitations in the model and available data, we conclude that leakage from units above the Culebra through poorly plugged and abandoned boreholes is a plausible explanation for the observed water-level changes in and around the WIPP site. However, the Intrepid East tailings pile may well be the source of the water leaking through the Upper group of boreholes, so a combination of the tailings-pile and leaky-borehole scenarios is probably the best explanation for the water-level rises. Also, natural recharge south of the WIPP where the Culebra is unconfined could provide the water ascribed to the Lower group borehole in these calculations.

Calibration of the T-fields to the observed water-level rises could undoubtedly be improved by such things as allowing specific storage to vary on a cell-by-cell basis, allowing leakage rates to vary among boreholes in a group, and by making the water-level-rise calibration an integral part of the overall T-field calibration. However, these improvements would not alter the conclusion that leaky boreholes can plausibly be causing, or contributing to, the observed water-level rise. Accordingly, we consider the objective of this investigation to have been met.

References:

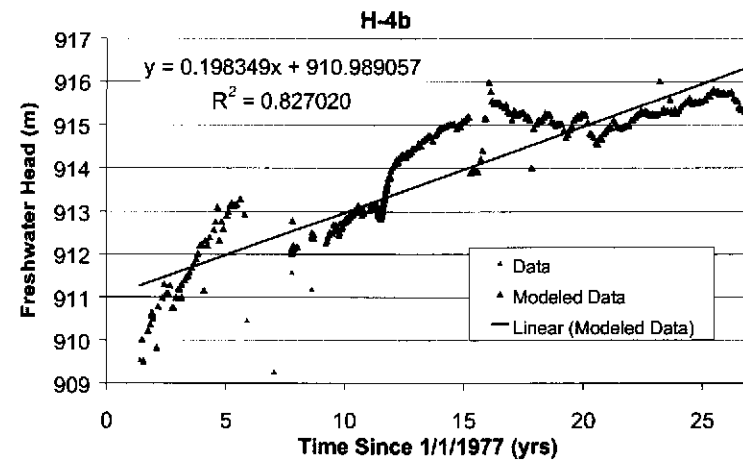
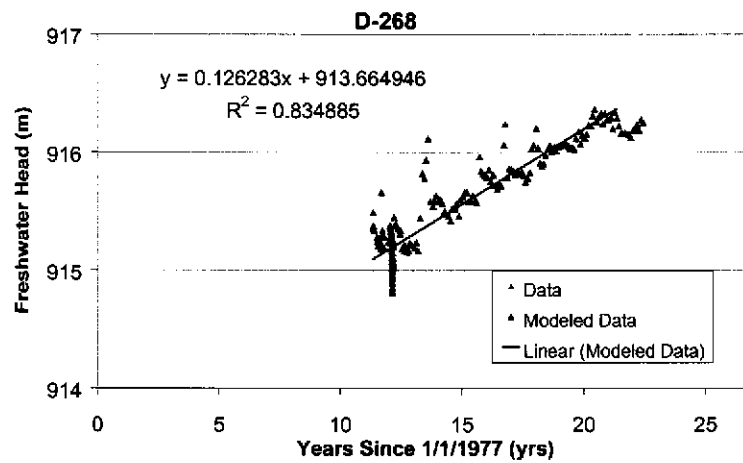
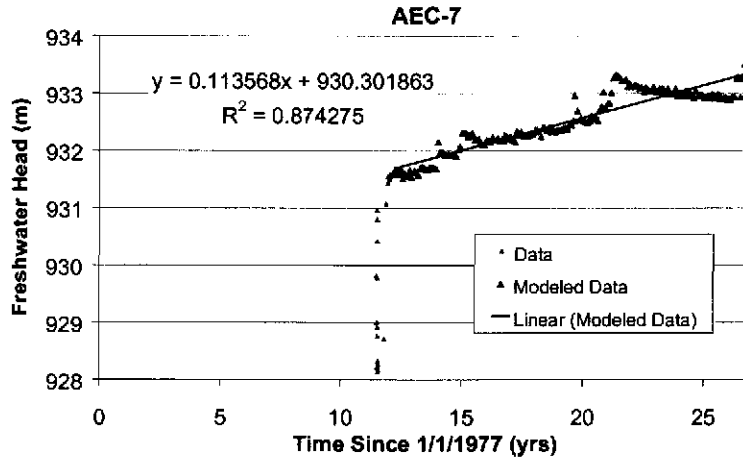
- Beauheim, R.L. 2002. Analysis Plan for Evaluation of the Effects of Head Changes on Calibration of Culebra Transmissivity Fields. AP-088, Rev. 1, 12/06/02, 11 pp., ERMS# 524785.
- Beauheim, R.L. 2003a. Analysis Plan for Evaluation of Culebra Water-Level-Rise Scenarios. AP-110, Rev. 0, 11/11/03, 27 pp., ERMS# 532799.
- Beauheim, R.L. 2003b. Analysis Report for AP-100 Task 1: Development and Application of Acceptance Criteria for Culebra Transmissivity (T) Fields. Carlsbad, NM: SNL, ERMS# 531136.
- Beauheim, R.L., and G.J. Ruskauff. 1998. *Analysis of Hydraulic Tests of the Culebra and Magenta Dolomites and Dewey Lake Redbeds Conducted at the Waste Isolation Pilot Plant Site*. SAND98-0049. Albuquerque, NM: Sandia National Laboratories.
- DOE (U.S. Department of Energy). 1996. *Title 40 CFR Part 191 Compliance Certification Application for the Waste Isolation Pilot Plant*. DOE/CAO-1996-2184. Carlsbad, NM: US DOE Waste Isolation Pilot Plant, Carlsbad Area Office.
- DOE (U.S. Department of Energy). 2004. *Title 40 CFR Part 191 Compliance Recertification Application for the Waste Isolation Pilot Plant, March 2004*. DOE/WIPP 2004-3231. Carlsbad, NM: US DOE Waste Isolation Pilot Plant, Carlsbad Field Office.
- Doherty, J. 2002. *Manual for PEST; 5th Edition*. Watermark Numerical Computing, Australia.
- EEG (Environmental Evaluation Group). 2002. Letter from Matthew Silva, Director, EEG, to Dr. Inés Triay, Manager, Carlsbad Field Office, DOE, dated August 6, 2002. Albuquerque, NM: Environmental Evaluation Group.
- EPA (U.S. Environmental Protection Agency). 2002. Letter from Frank Marcinowski, Director, Radiation Protection Division, U.S. EPA, to Dr. Inés Triay, Manager, Carlsbad Field Office, DOE, dated August 6, 2002. Washington, DC: U.S. Environmental Protection Agency, Office of Air and Radiation.
- GMS. 2004. Groundwater Modeling System: Developed by the Environmental Modeling Research Laboratory of Brigham Young University in partnership with the U.S. Army Engineer Waterways Experiment Station, Vicksburg, MS 39180. <http://chl.wes.army.mil/software/gms/default.htm>.
- Harbaugh, A.W., E. Banta, M.C. Hill, and M. McDonald. 2000. MODFLOW 2000: The U.S. Geological Survey Modular Ground-Water Model – User Guide to Modularization Concepts and the Ground-Water Flow Process. U.S. Geological Survey, Reston, VA, Open File Report 00-92, 121pp.

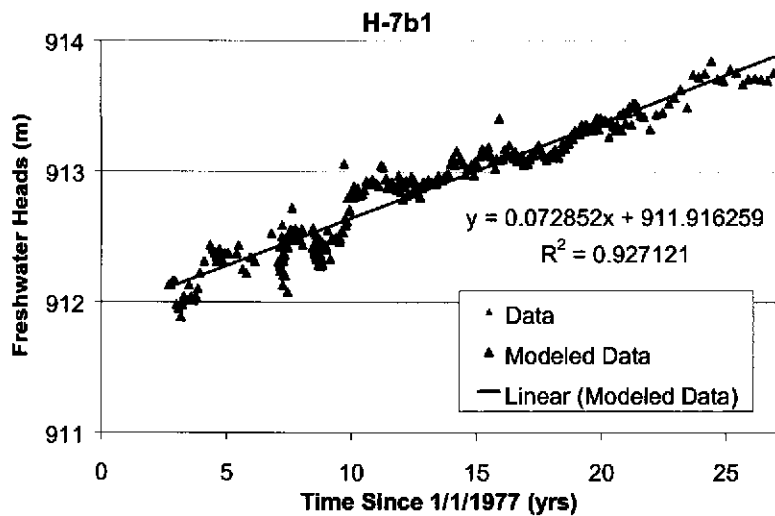
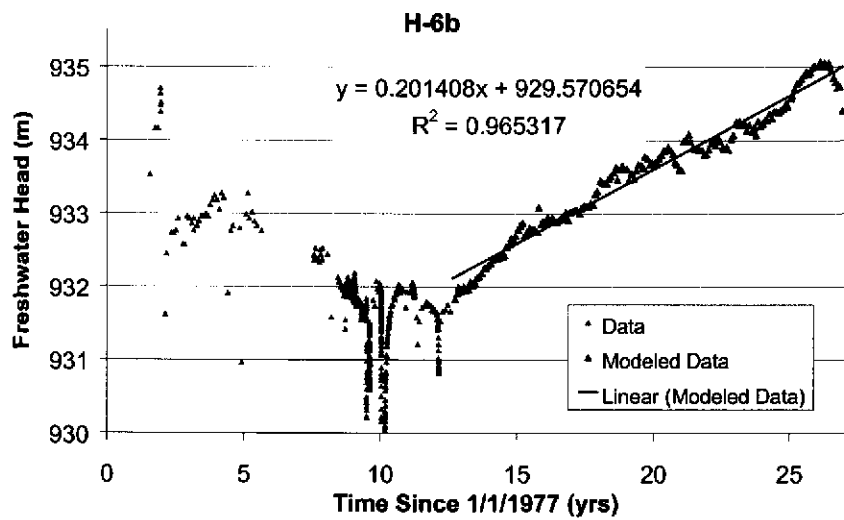
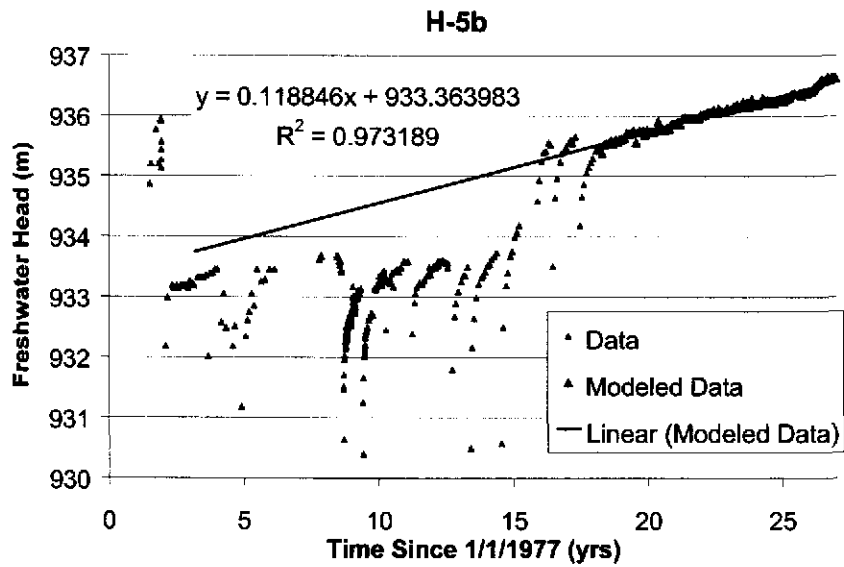
- Holt, R.M., and L. Yarbrough. 2003. Addendum 2 to Analysis Report, Task 2 of AP-088, Estimating Base Transmissivity Fields. ERMS# 529416. Carlsbad, NM: Sandia WIPP Records Center.
- Hydro Geo Chem, Inc. 1985. *WIPP Hydrology Program, Waste Isolation Pilot Plant, SENM, Hydrologic Data Report #1*. SAND85-7206. Albuquerque, NM: Sandia National Laboratories.
- INTERA Technologies, Inc. 1986. *WIPP Hydrology Program, Waste Isolation Pilot Plant, Southeastern New Mexico, Hydrologic Data Report #3*. SAND86-7109. Albuquerque, NM: Sandia National Laboratories.
- INTERA Technologies, Inc., and Hydro Geo Chem, Inc. 1985. *WIPP Hydrology Program, Waste Isolation Pilot Plant, Southeastern New Mexico, Hydrologic Data Report #2*. SAND85-7263. Albuquerque, NM: Sandia National Laboratories.
- Kehrman, R.F. 2002. Compliance Recertification Application Monitoring Data, Volume Two. Carlsbad, NM: Westinghouse TRU Solutions LLC. Copy on file in the Sandia WIPP Records Center under ERMS# 527193.
- Lowry, T.S., and R.L. Beauheim. 2004. Analysis Report, Task 2 of AP-110, Evaluation of Water-Level Rise in the Culebra Due to Recharge from Refining Process Water Discharged onto Potash Tailings Piles, ERMS# 536239. Carlsbad, NM: Sandia WIPP Records Center.
- McKenna, S.A., and D. Hart. 2003. Analysis Report, Task 4 of AP-088, Conditioning of Base T-Fields to Transient Heads. ERMS# 531124. Carlsbad, NM: Sandia WIPP Records Center.
- Mercer, J.W., and B.R. Orr. 1979. *Interim Data Report on the Geohydrology of the Proposed Waste Isolation Pilot Plant Site, Southeast New Mexico*. Water Resources Investigations Report 79-98. Albuquerque, NM: U.S. Geological Survey.
- Powers, D.W. 2004. Analysis Report, Task 1A of AP-110, Identify Potash Holes Not Sealed Through the Culebra with Cement, and Units to Which the Culebra Might Be Connected. ERMS# 535377. Carlsbad, NM: Sandia WIPP Records Center.
- Powers, D.W., and R.G. Richardson. 2004. *Basic Data Report for Drillhole SNL-12 (C-2954) (Waste Isolation Pilot Plant)*. DOE/WIPP 03-3295. Carlsbad, NM: WIPP MOC.
- Richey, S.F. 1986. *Hydrologic-Test Data from Wells at Hydrologic-Test Pads H-7, H-8, H-9, and H-10 Near the Proposed Waste Isolation Pilot Plant, Southeastern New Mexico*. Open-File Report 86-413. Albuquerque, NM: U.S. Geological Survey.
- Richey, S.F. 1987a. *Preliminary Hydrologic Data for Wells Tested in Nash Draw, Near the Proposed Waste Isolation Pilot Plant, Southeastern New Mexico*. Open-File Report 87-37. Albuquerque, NM: U.S. Geological Survey.

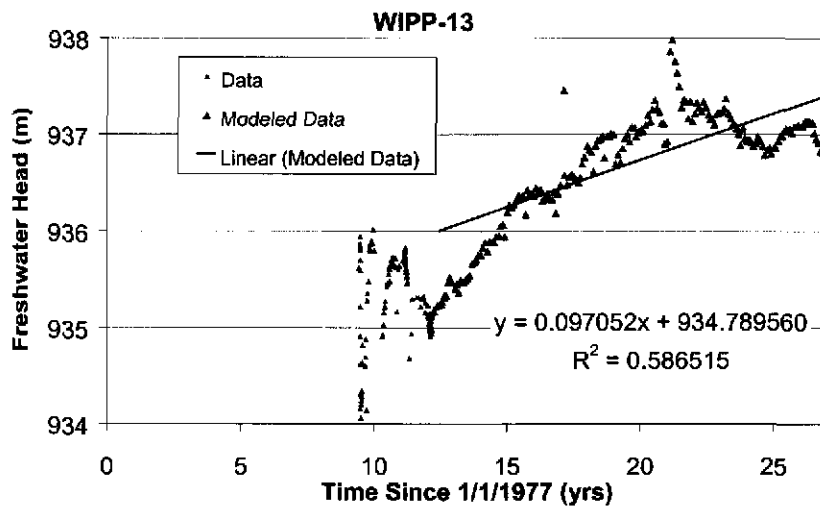
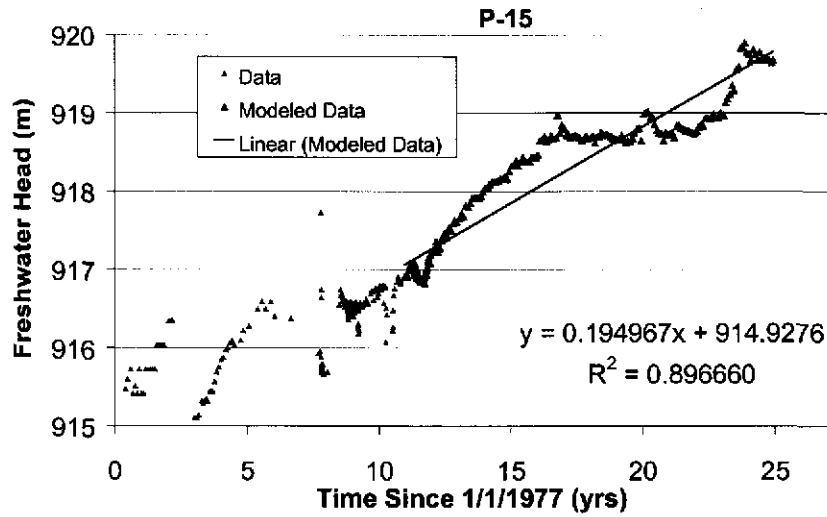
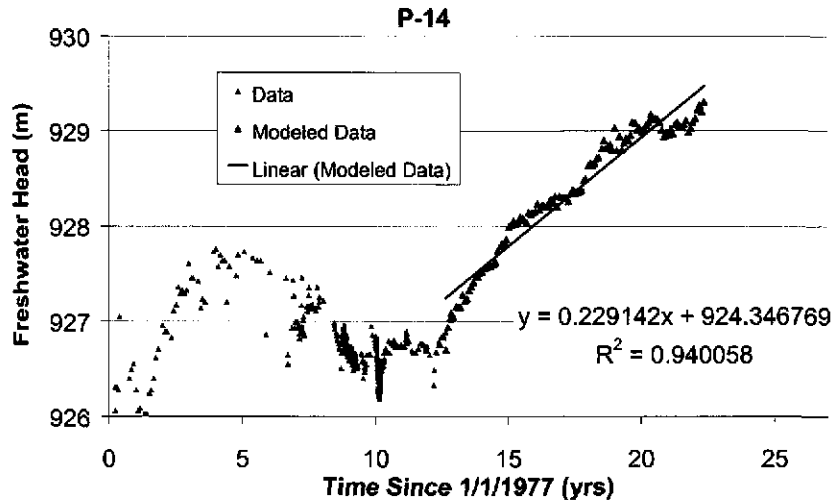
- Richey, S.F. 1987b. *Water-Level Data from Wells in the Vicinity of the Waste Isolation Pilot Plant, Southeastern New Mexico*. Open-File Report 87-120. Albuquerque, NM: U.S. Geological Survey.
- Silva, M.K. 1996. *Fluid Injection for Salt Water Disposal and Enhanced Oil Recovery as a Potential Problem for the WIPP: Proceedings of a June 1995 Workshop and Analysis*. EEG-62. Albuquerque, NM: Environmental Evaluation Group.
- SNL (Sandia National Laboratories). 2001. Sandia National Laboratories Annual Compliance Monitoring Parameter Assessment. ERMS# 501162. Carlsbad, NM: Sandia WIPP Records Center.
- SNL (Sandia National Laboratories). 2003. Program Plan, WIPP Integrated Groundwater Hydrology Program, FY03-09, Revision 0. ERMS# 526671. Carlsbad, NM: Sandia WIPP Records Center.
- Stensrud, W.A., M.A. Bame, K.D. Lantz, A.M. LaVenu, J.B. Palmer, and G.J. Saulnier, Jr. 1987. *WIPP Hydrology Program, Waste Isolation Pilot Plant, Southeastern New Mexico, Hydrologic Data Report #5*. SAND87-7125. Albuquerque, NM: Sandia National Laboratories.
- Stensrud, W.A., M.A. Bame, K.D. Lantz, T.L. Cauffman, J.B. Palmer, and G.J. Saulnier, Jr. 1988a. *WIPP Hydrology Program, Waste Isolation Pilot Plant, Southeastern New Mexico, Hydrologic Data Report #6*. SAND87-7166. Albuquerque, NM: Sandia National Laboratories.
- Stensrud, W.A., M.A. Bame, K.D. Lantz, J.B. Palmer, and G.J. Saulnier, Jr. 1988b. *WIPP Hydrology Program, Waste Isolation Pilot Plant, Southeastern New Mexico, Hydrologic Data Report #7*. SAND88-7014. Albuquerque, NM: Sandia National Laboratories.
- Stensrud, W.A., M.A. Bame, K.D. Lantz, J.B. Palmer, and G.J. Saulnier, Jr. 1990. *WIPP Hydrology Program, Waste Isolation Pilot Plant, Southeastern New Mexico, Hydrologic Data Report #8*. SAND89-7056. Albuquerque, NM: Sandia National Laboratories.
- Theis, C.V. 1935. "The relation between the lowering of the piezometric surface and the rate and duration of discharge of a well using groundwater storage," *Trans. Amer. Geophys. Union*, 2:519-524.

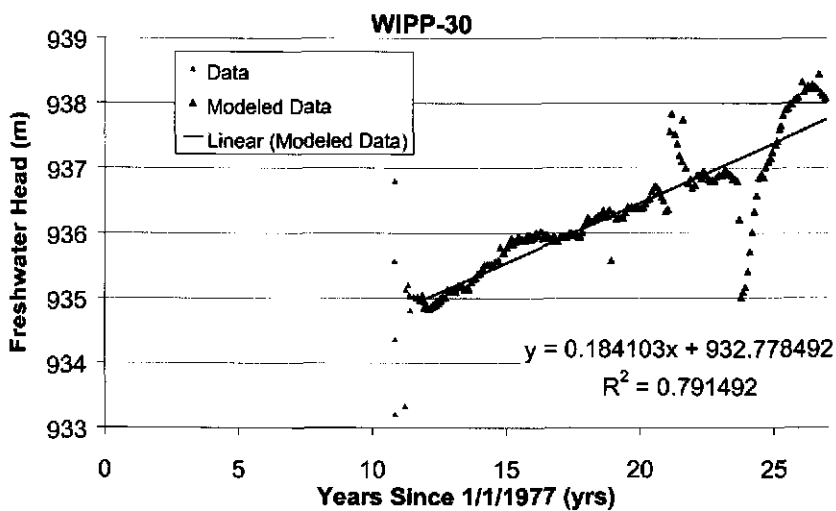
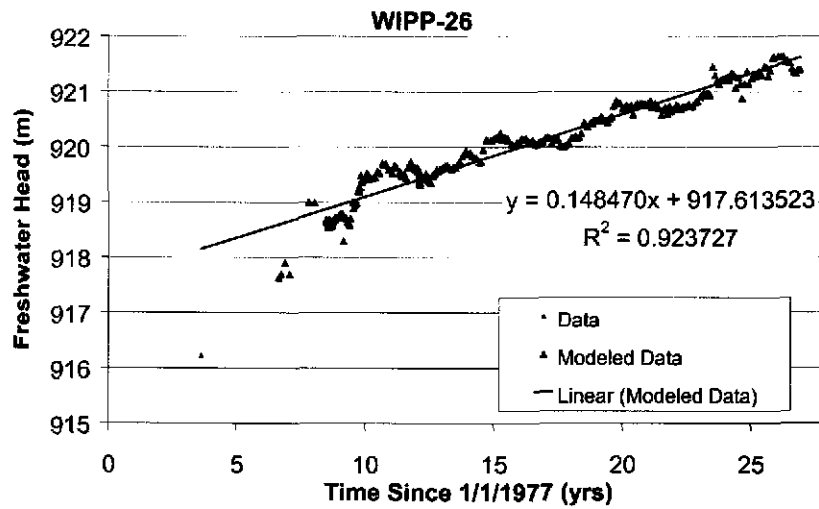
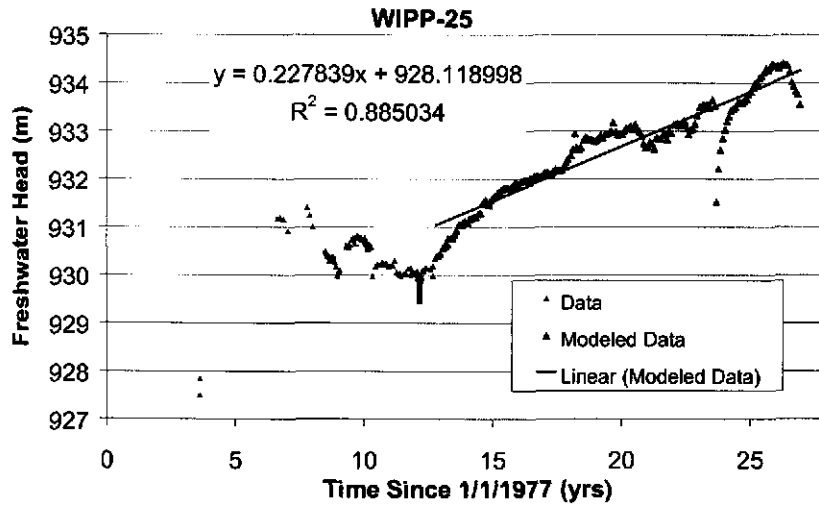
Appendix A: Fitted Well Data for Calibration

Each chart shows the raw data for each well, the fitted trend line, the equation of the fitted line, and the R^2 value of the fitted line. Data that are excluded from the regression are plotted in red. Each plot is scaled to emphasize the portions of the data that are used in the linear regression.









Appendix B: FORTRAN Utility Code - T_Field.f90

```
!This program reads in the calibrated transmissivity values  
!from AP-088 and writes them to a MODFLOW layer-property-flow  
!file. The transmissivities are converted to conductivities  
!by dividing by the aquifer thickness.
```

```
!TSL - 8-12-04
```

```
INTEGER, PARAMETER :: ncol=224,nrow=307,nlay=1
```

```
REAL, PARAMETER :: thick=7.75
```

```
REAL*8 HkHet(ncol,nrow,nlay),xdum
```

```
REAL*8 cond(ncol,nrow,nlay)
```

```
CHARACTER runnum*6,Tfile*10,path*30
```

```
CHARACTER pstor(ncol,nrow,nlay)*14
```

```
DATA path/'/home3/tslowry/wipp/Tfields'/
```

```
READ(*,*)runnum
```

```
Tfile=runnum//'.mod'
```

```
OPEN(50,file=TRIM(ADJUSTL(path))//'/Tfile,status='old')
```

```
DO j=1,nrow
```

```
    READ(50,*)(HkHet(i,j,1),i=1,ncol)
```

```
END DO
```

```
OPEN(70,file='LBH1.lpf',status='unknown')
```

```
WRITE(70,'(a15)')'15 -888.0 0'
```

```
WRITE(70,'(a1)')'0'
```

```
WRITE(70,'(a1)')'0'
```

```
WRITE(70,'(a4)')'-1.0'
```

```
WRITE(70,'(a1)')'1'
```

```
WRITE(70,'(a1)')'0'
```

```
WRITE(70,'(a23)')"INTERNAL 1 (free) 0"
```

```
DO j=1,nrow
```

```
    WRITE(70,'(224e20.11)')(HkHet(i,j,1)/thick,i=1,ncol)
```

```
END DO
```

```
WRITE(70,'(a13)')"CONSTANT 1.0"
```

```
WRITE(70,'(a19)')"CONSTANT 0.0"
```

```
WRITE(70,'(a19)')"CONSTANT 1.2903e-6"
```

```
CLOSE(70)
```

```
STOP
```

```
END
```

Appendix C: FORTRAN Utility Code – Get_heads.f90

```
!This program reads in a MODFLOW *.hed file from a steady-state
!simulation, extracts the heads, and writes them to a new
!MODFLOW basic input file called LBH1_new.ba6 as the starting heads.
!The new basic input file will be used for the transient
!calibration runs.
!TSL - 8-12-04
```

```
REAL, PARAMETER :: tconv=86400*365
INTEGER, PARAMETER :: nx=224,ny=307
INTEGER, PARAMETER :: numwells=12
```

```
REAL*8 heads(nx,ny)
INTEGER ix(numwells),jy(numwells),ibound(nx,ny)
CHARACTER*80 hedFile,ba6File,outFile,yinFile
```

```
!Well locations by cell indices
```

```
!Well Name  i      j
!AEC-7      195    79
!D-268      71     184
!H-4b       107    188
!H-5b       152    124
!H-6b       89     122
!H-7b1      65     226
!P-14       74     153
!P-15       90     185
!WIPP-13    110    130
!WIPP-25    47     132
!WIPP-26    24     161
!WIPP-30    121    75
```

```
DATA ix/195,71,107,152,89,65,74,90,110,47,24,121/
DATA jy/79,184,188,124,122,226,153,185,130,132,161,75/
```

```
hedFile="LBH1.hed"
ba6File="LBH1.ba6"
outFile="LBH1_new.ba6"
yinFile="Y_Int.txt"
```

```
OPEN(10,file=TRIM(ADJUSTL(hedFile)),status='old')
OPEN(15,file=TRIM(ADJUSTL(ba6File)),status='old')
OPEN(20,file=TRIM(ADJUSTL(outFile)),status='unknown')
OPEN(30,file=TRIM(ADJUSTL(yinFile)),status='unknown')
```

```
!Read in heads
READ(10,*)
DO j=1,ny
  READ(10,*)(heads(i,j),i=1,nx)
END DO
CLOSE(10)
```

```
!Get starting heads
```

```
!Skip header lines
DO i=1,4
```

```
      READ(15,*)
END DO

!READ IBOUND array
DO j=1,ny
  READ(15,*)(ibound(i,j),i=1,nx)
END DO
CLOSE(15)

!Write out ba6 file
WRITE(20,'(a22)')"#WIPP Water Level Rise"
WRITE(20,'(a16)')"#PEST Simulation"
WRITE(20,'(a4)')"FREE"
WRITE(20,'(a19)')"INTERNAL 1 (free) 0"
DO j=1,ny
  WRITE(20,'(224i3)')(ibound(i,j),i=1,nx)
END DO
WRITE(20,'(a11)')"-999.000000"
WRITE(20,'(a19)')"INTERNAL 1 (free) 0"
DO j=1,ny
  WRITE(20,'(224f10.4)')(heads(i,j),i=1,nx)
END DO
CLOSE(20)

!Write out y-intercepts (starting head at each well)
DO iw=1,numwells
  WRITE(30,'(f9.4)')heads(ix(iw),jy(iw))
END DO
CLOSE(30)

STOP
END
```


Appendix D: FORTRAN Utility Code – exhdsdrw_scratch.f90

```
!This program reads in a MODFLOW *.hed and *.drw file and extracts the
!heads and drawdowns at selected nodes in the domain. The MODFLOW
!output files must be located in the scratch/temp/pest directory of
!the executing slave computer. It then writes the output to
!to an output file called wellhdsdrw.txt. It will also calculate
!the root mean squared error between the simulated drawdowns and the
!observed drawdowns. This program is called from the script,
!LBH1_run.sh, which executes MODFLOW within each PPEST calibration.
!TSL - 7-15-04
```

```
REAL, PARAMETER :: tconv=86400*365
INTEGER, PARAMETER :: nx=224,ny=307,nper=15
INTEGER, PARAMETER :: numwells=12
```

```
REAL*8 heads(nx,ny,nper),drw(nx,ny,nper)
REAL*8 sheads(numwells)
REAL*8 time(nper)
REAL slp(numwells),yint(numwells)
REAL resid(numwells,nper)
INTEGER ix(numwells),jy(numwells)
CHARACTER*7 wellname(numwells)
CHARACTER*80 hedFile,drwFile,ba6File,outFile,RSEFile,yinFile
```

```
!Well locations by cell indices
```

!Well Name	i	j
!AEC-7	195	79
!D-268	71	184
!H-4b	107	188
!H-5b	152	124
!H-6b	89	122
!H-7b1	65	226
!P-14	74	153
!P-15	90	185
!WIPP-13	110	130
!WIPP-25	47	132
!WIPP-26	24	161
!WIPP-30	121	75

```
!Slopes from Data
```

! AEC-7	0.113568t + 930.301863
! D-268	0.126283t + 913.664946
! H-4b	0.198349t + 910.989057
! H-5b	0.118846t + 933.363983
! H-6b	0.201408t + 929.570654
! H-7b	0.072852t + 911.916259
! P-14	0.229142t + 924.346769
! P-15	0.194967t + 914.927600
! Wipp-13	0.097052t + 934.789560
! Wipp-25	0.227839t + 928.118998
! Wipp-26	0.148470t + 917.613523
! WIPP-30	0.184103t + 932.778492

```
DATA ix/195,71,107,152,89,65,74,90,110,47,24,121/
DATA jy/79,184,188,124,122,226,153,185,130,132,161,75/
```

```
DATA wellname/"AEC-7", "D-268", "H-4b", "H-5b", "H-6b", &  
      "H-7b1", "P-14", "P-15", "WIPP-13", "WIPP-25", "WIPP-26", "WIPP-30" /  
DATA slp/0.113568, 0.126283, 0.198349, 0.118846, 0.201408, &  
      0.072852, 0.229142, 0.194967, 0.097052, 0.227839, 0.148470, 0.184103 /
```

```
hedFile="/home/scratch/temp/pest/LBH1.hed"  
drwFile="/home/scratch/temp/pest/LBH1.drw"  
ba6File="/home/scratch/temp/pest/LBH1.ba6"  
outFile="wellhdsdrw.txt"  
RSEFile="RSE.txt"  
yinFile="../../Y_Int.txt"
```

```
OPEN(10, file=TRIM(ADJUSTL(hedFile)), status='old')  
OPEN(15, file=TRIM(ADJUSTL(drwFile)), status='old')  
OPEN(20, file=TRIM(ADJUSTL(outFile)), status='unknown')
```

```
DO ip=1, nper  
  !Read in heads  
  READ(10, *) i1, i2, time(ip)  
  DO j=1, ny  
    READ(10, *) (heads(i, j, ip), i=1, nx)  
  END DO  
END DO  
CLOSE(10)
```

```
DO ip=1, nper  
  !Read in drawdowns  
  READ(15, *)  
  DO j=1, ny  
    READ(15, *) (drw(i, j, ip), i=1, nx)  
  END DO  
END DO  
CLOSE(15)
```

```
!Output results  
WRITE(20, '(14a10)') "Time (sec)", (wellname(iw), iw=1, numwells)  
DO ip=1, nper  
  
WRITE(20, '(e10.5, 13f10.4)') time(ip), (heads(ix(iw), jy(iw), ip), iw=1, numwells)  
END DO  
WRITE(20, *)  
DO ip=1, nper  
  WRITE(20, '(e10.5, 13f10.4)') time(ip), (drw(ix(iw), jy(iw), ip), iw=1, numwells)  
END DO  
  
CLOSE(20)
```

```
!Get starting heads  
OPEN(30, file=TRIM(ADJUSTL(ba6file)), status='old')
```

```
!Skip header lines  
DO i=1, 4  
  READ(30, *)  
END DO
```

```
!Skip IBOUND array and starting head headers  
DO j=1, ny+2
```

```
        READ(30,*)
END DO

!Read in heads
DO j=1,ny
    READ(30,*)(heads(i,j,1),i=1,nx)
END DO
CLOSE(30)

!Get heads at each well
DO iw=1,numwells
    sheads(iw)=heads(ix(iw),jy(iw),1)
END DO

!Get y-intercept values (starting heads at each well)
OPEN(35,file=yinFile,status='old')
DO iw=1,numwells
    READ(35,*)yint(iw)
END DO
CLOSE(35)

!Calculate differences in drawdowns
rsum=0
DO ip=1,nper
    DO iw=1,numwells
        ddown=sheads(iw)-(slp(iw)*time(ip)/tconv+yint(iw))
        resid(iw,ip)=(ddown-drw(ix(iw),jy(iw),ip))*(ddown-
drw(ix(iw),jy(iw),ip))
        rsum=rsum+resid(iw,ip)
    END DO
END DO

RSE=rsum/(iw*ip)

OPEN(40,file=RSEFile,status='unknown')
WRITE(40,*)RSE
CLOSE(40)

STOP
END
```

Appendix E: FORTRAN Utility Code – mfrun.f90

```
!This program reads the calibrated well leakage rates from the compiled  
!output file well.out, and writes them to a MODFLOW WEL input file  
!for use in the final calibrated MODFLOW run.
```

```
!TSL - 10-8-04  
INTEGER, PARAMETER :: ncol=224,nrow=307,nlay=1  
INTEGER, PARAMETER :: numfields=100  
INTEGER, PARAMETER :: numwells=26,numgrps=4  
REAL, PARAMETER :: thick=7.75  
REAL*8 HkHet(ncol,nrow,nlay),xdum  
REAL*8 qwell(numwells),qgrp(numgrps)  
INTEGER kcoord(numwells),jcoord(numwells),icoord(numwells)  
CHARACTER runnum*6,t_field*6,Tfile*10,path*30  
CHARACTER pstor(ncol,nrow,nlay)*14  
CHARACTER arun(numwells)*6,adum*4  
CHARACTER wname(numwells)*4  
DATA path/'/home3/tslowry/wipp/Tfields'/  
!DATA jcoord/5,8,8,9,13,15,15,16,16,17,24,24,24,32,40,41,89,104,&  
!      105,106,117,120,121,142,210,237/  
DATA jcoord/8,9,8,13,17,16,16,24,24,24,41,40,32,89,106,105,104,&  
      121,120,117,142,210,237,5,15,15/  
!DATA icoord/128,104,144,137,108,121,130,112,144,96,105,128,&  
!      144,161,153,128,120,138,121,105,26,138,105,32,57,122/  
DATA icoord/104,137,144,108,96,112,144,105,128,144,128,153,161,&  
      120,105,121,138,105,138,26,32,57,122,128,121,130/  
  
kcoord=1  
DATA wname/"4_1","4_2","4_3","4_4","4_5","4_6","4_7","4_8","4_9",&  
      "4_10","4_11","4_12","4_13","4_14","4_15","4_16","4_17",&  
      "4_18","4_19","4_20","4_21","4_22","4_23","5_1","5_2","5_3"/  
!Read in conductivity field  
READ(*,*)runnum  
!runnum="d01r04"  
Tfile=runnum//'.mod'  
OPEN(50,file=TRIM(ADJUSTL(path))//'/'/Tfile,status='old')  
DO j=1,nrow  
    READ(50,*)(HkHet(i,j,1),i=1,ncol)  
END DO  
  
!Get pumping rates from Pest output  
OPEN(85,file='well.out',status='old')  
ip=1  
iruns=numfields*numgrps  
DO i=1,iruns  
    READ(85,*)qgrp(ip),arun(ip),t_field  
    IF(t_field.eq.runnum.and.ip.eq.1)THEN  
        DO ip=2,numgrps  
            READ(85,*)qgrp(ip),arun(ip)  
        END DO  
    EXIT  
ENDIF  
END DO  
CLOSE(85)  
  
!Write new *.lpf file
```

```
OPEN(70,file='LBH1.lpf',status='unknown')
WRITE(70,'(a15)')'15 -888.0 0'
WRITE(70,'(a1)')'0'
WRITE(70,'(a1)')'0'
WRITE(70,'(a4)')'-1.0'
WRITE(70,'(a1)')'1'
WRITE(70,'(a1)')'0'
WRITE(70,'(a23)')"INTERNAL 1 (75e20.11) 0"
DO j=1,nrow
  WRITE(70,'(75e20.11)')(HkHet(i,j,1)/thick,i=1,ncol)
END DO
WRITE(70,'(a13)')"CONSTANT 1.0"
WRITE(70,'(a13)')"CONSTANT 1.0"
WRITE(70,'(a19)')"CONSTANT 1.2903e-6"

CLOSE(70)

!Assign flow rate to appropriate well
DO i=1,numwells
  IF(i.gt.1.and.i.le.13)THEN
    wflow=qgrp(1)
  ELSEIF(i.gt.13.and.i.le.19)THEN
    wflow=qgrp(2)
  ELSEIF(i.gt.19.and.i.le.22)THEN
    wflow=qgrp(3)
  ELSEIF(i.eq.23)THEN
    wflow=qgrp(4)
  ELSE
    wflow=qgrp(1)
  ENDIF
  qwell(i)=wflow
END DO

!Write new *.wel file
OPEN(80,file='LBH1.wel',status='unknown')
WRITE(80,'(a5)')'26 15'
WRITE(80,'(a4)')'26 0'
DO iw=1,numwells

WRITE(80,'(i2,2i4,2x,e13.7,a6)')kcoord(iw),jcoord(iw),icoord(iw),qwell(iw),wn
ame(iw)
END DO

STOP
END
```

Appendix F: FORTRAN Utility Code – cut.f90

!This program is run after the final MF2K calibrated run. It successively
 !goes to each T-field directory and reads the output from exhdsdrw,
 !called!wellhdsdrw.txt. It will read the output for all T-fields and then
 !recompile it into a single file call wellobstxt, located in the base
 !simulation directory. wellobstxt is suitable for import to MS Excel for
 !visualization.

```
INTEGER, PARAMETER :: numwells=12,nper=15,nobs=100
REAL*8 time(nper,nobs),heads(numwells,nper,nobs),drw(numwells,nper,nobs)
REAL*8 rse(nobs)
CHARACTER*10 head1,wellname(numwells,nobs)
CHARACTER file1*100,file2*100,trun(nobs)*6
```

```
OPEN(10,file='Goodruns_100.txt',status='old')
DO io=1,nobs
  READ(10,*)trun(io)
  print *,trun(io),io
  file1='/home3/tslowry/wipp/lkybrhl/'//trun(io)//'/wellhdsdrw.txt'
  OPEN(20,file=TRIM(ADJUSTL(file1)),status='old')
  READ(20,'(14a10)')head1,(wellname(iw,io),iw=1,numwells)
  DO ip=1,nper
  READ(20,'(e10.5,13f10.4)')time(ip,io),(heads(iw,ip,io),iw=1,numwells)
  END DO
  READ(20,*)
  DO ip=1,nper
    READ(20,'(e10.5,13f10.4)')tdum,(drw(iw,ip,io),iw=1,numwells)
  END DO
  CLOSE(20)
  file2='/home3/tslowry/wipp/lkybrhl/'//trun(io)//'/RSE.txt'
  OPEN(50,file=TRIM(ADJUSTL(file2)),status='old')
  READ(50,*)rse(io)
  CLOSE(50)
END DO
CLOSE(10)
```

```
OPEN(30,file='wellobstxt',status='unknown')
DO iw=1,numwells
  WRITE(30,'(a10)')wellname(iw)
  WRITE(30,'(a10,100a10)')"Time (sec)",(trun(io),io=1,nobs)
  WRITE(30,'(101a10)')(" 0 ",io=1,nobs+1)
  DO ip=1,nper
    WRITE(30,'(e10.5,100f10.4)')time(ip,1),(drw(iw,ip,io),io=1,nobs)
  END DO
  WRITE(30,*)
END DO
```

```
OPEN(40,file='RSE_tot.txt',status='unknown')
DO io=1,nobs
  WRITE(40,'(f10.6,3x,a6)')rse(io),trun(io)
END DO
CLOSE(40)
STOP
END
```

Appendix G: Linux Shell Script – Ppest_run.sh

```
#!/bin/bash
RUNS=`cat Goodruns.txt`
THISDIR=`pwd`

#This script controls the entire PPEST run sequence across
#all T-fields.

outFile=run.out

for Runs in $RUNS
do
#Clean up files from last run
  cd ppest1
  clean.sh
  cd $THISDIR
  echo $Runs > runnum.out

#Generate new *.lpf and *.tmp files
  echo $Runs | T_Field

#Run steady-state model
  mf2k LBH1_steady.nam
  echo "mf2k" $Runs >> $outFile

#Extract new starting heads to new *.ba6 file
  Get_heads
  mv LBH1.ba6 LBH1_old.ba6
  mv LBH1_new.ba6 LBH1.ba6
  echo "Get_heads" $Runs >> $outFile

#Setup and run PEST
  cd ppest1
  runpest.sh
  echo "runpest" $Runs >> $outFile
  sleep 60s
  cd $THISDIR

#Find out of the jobs are still running
  JRun=`qstat | grep -E 'pslave|pmaster' | awk 'END{print NR}'`

#Stay in this loop until the que is clear
  while [ $JRun -gt 0 ]
  do
    echo $JRun $Runs >> $outFile
    sleep 30s
    JRun=`qstat | grep -E 'pslave|pmaster' | awk 'END{print NR}'`
  done

done
```

Appendix H: Linux Shell Script – clean.sh

```
rm -rf slave*/*  
rm -f 04*.out  
rm -f LBH1*.*  
rm -f jacob.*  
rm -f pest.*  
rm -f pmaster.sh
```

```
#This script removes the directories, output, and temporary files  
#from the previous PPEST simulation.
```


Appendix I: Linux Shell Script – runpest.sh

```
#!/bin/bash
#This script controls the setup sequence for the PPEST
#run.

setup.sh
TDir="/home3/tslowry/wipp/lkybrhl"
SLAVES=`ls -d slave* | grep -vw slave1`
PDir=$TDir/ppest1

TFiles=$(sed $TDir/LBH1.nam -e '/^#/d' | awk '{print $3}')
FILES=`cat $TDir/filelist.modflow | sed "s@^@$TDir/@g"`

for Slave in $SLAVES
do
    cd $Slave
    pfile=pslave.sh
    SDir=$PDir/$Slave
    echo '#PBS -N pslave
#PBS -j oe
#PBS -q half
#PBS -S /bin/bash

mkdir /home/scratch/temp /home/scratch/temp/pest 2>/dev/null

cd '$PDir'
cp '$FILES' /home/scratch/temp/pest/
cd '$SDir'

pslave < LBH1_run.in
rm -rf /home/scratch/temp
' > ${pfile}
    qsub $pfile
    cd $PDir
done
qsub pmaster.sh
```

Appendix J: Linux Shell Script – setup.sh

```
#!/bin/bash
SLAVES="slave1 slave2 slave3 slave4 slave5 slave6 slave7 slave8"
THISDIR=`pwd`
FILES=`cat ../filelist.master`

#This script creates the slave directories and populates the directories
#with the appropriate files, listed in filelist.slave.

for File in $FILES
do
    cp ../$File $THISDIR
done
for Slave in $SLAVES
do
    mkdir $THISDIR/$Slave 2>/dev/null
    FILES=`cat ../filelist.slave`
    for File in $FILES
    do
        cp ../$File $THISDIR/$Slave
    done
done
cd $THISDIR
```

Appendix K: Linux Shell Script – pslave.sh

```
#PBS -N pslave
#PBS -j oe
#PBS -q half
#PBS -S /bin/bash

mkdir /home/scratch/temp /home/scratch/temp/pest 2>/dev/null

cd /home3/tslowry/wipp/lkybrhl/ppest1
cp /home3/tslowry/wipp/lkybrhl/LBH1.dis /home3/tslowry/wipp/lkybrhl/LBH1.ba6
/home3/tslowry/wipp/lkybrhl/LBH1.oc /home3/tslowry/wipp/lkybrhl/LBH1.lpf
/home3/tslowry/wipp/lkybrhl/LBH1.lmg /home3/tslowry/wipp/lkybrhl/LBH1.nam
/home/scratch/temp/pest/
cd /home3/tslowry/wipp/lkybrhl/ppest1/slave2

pslave < LBH1_run.in
rm -rf /home/scratch/temp
```

Appendix L: Linux Shell Script – pmaster.sh

```
#PBS -N pmaster
#PBS -j oe
#PBS -q half
#PBS -S /bin/bash
MASTERDIR="/home3/tslowry/wipp/lkybrhl/ppest1"
FILES=`cat /home3/tslowry/wipp/lkybrhl/filelist.modflow`
cd /home/scratch
mkdir temp
cd temp
mkdir pest
cd $MASTERDIR/slave1
for File in $FILES
do
    echo $File
    cp ../../$File /home/scratch/temp/pest/
done
pslave < LBH1_run.in &> slave1.out &
cd $MASTERDIR
ppest LBH1
wait
Runs=`cat ../runnum.out`

#Get flow rates at each well and write to separate file
echo `tail -4l LBH1.sen | grep -i w1 | awk '{print $3}'` " Upper " $Runs >>
../well.out
echo `tail -4l LBH1.sen | grep -i w2 | awk '{print $3}'` " Mid " $Runs >>
../well.out
echo `tail -4l LBH1.sen | grep -i w3 | awk '{print $3}'` " NDraw " $Runs >>
../well.out
echo `tail -4l LBH1.sen | grep -i w4 | awk '{print $3}'` " Lower " $Runs >>
../well.out

mv LBH1.rec ../$Runs.rec
rm -rf /home/scratch/temp

#Update finish code to tell master script it is time to move on
echo "1" > ../rundone.out
```

Appendix M: Linux Shell Script – mfrun.sh

```
#!/bin/sh
RUNS=`cat Goodruns.txt`
THISDIR=`pwd`

#This script sets up and runs the final calibrated MODFLOW
#run. This occurs for all T-fields after all the PPEST
#calibrations are complete.

for Runs in $RUNS
do

#Set-up *.wel file with calibrated leakage rates
echo $Runs | mfrun

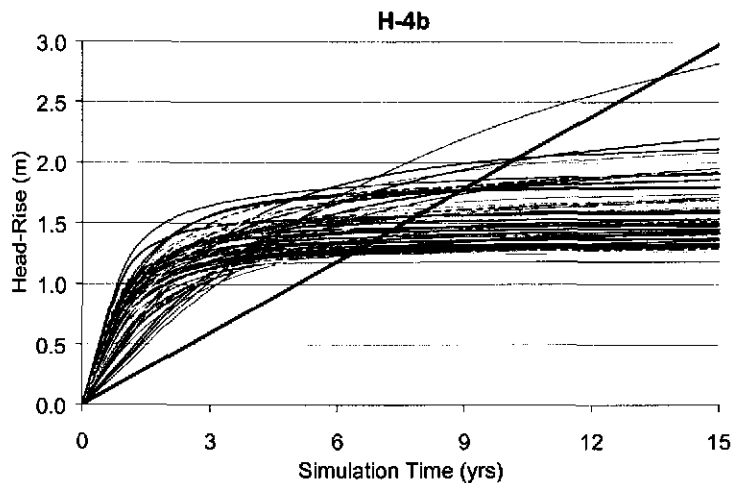
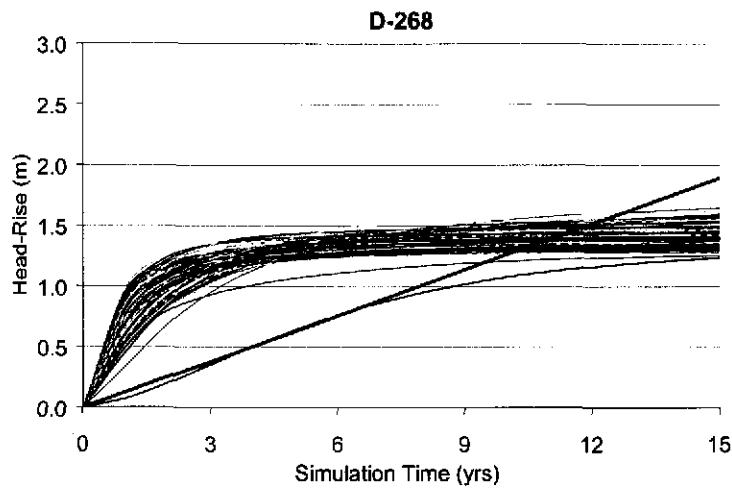
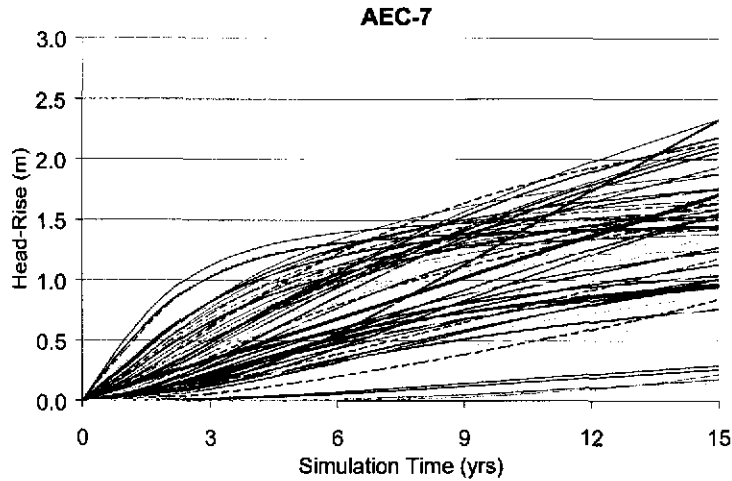
#Make new directory and copy files
mkdir $Runs
cp LBH1.ba6 $Runs
cp LBH1.lpf $Runs
cp LBH1.oc $Runs
cp LBH1.lmg $Runs
cp LBH1_home.nam $Runs
cp LBH1_steady.nam $Runs
cp LBH1.dis $Runs
cp LBH1_steady.dis $Runs
cp LBH1.wel $Runs

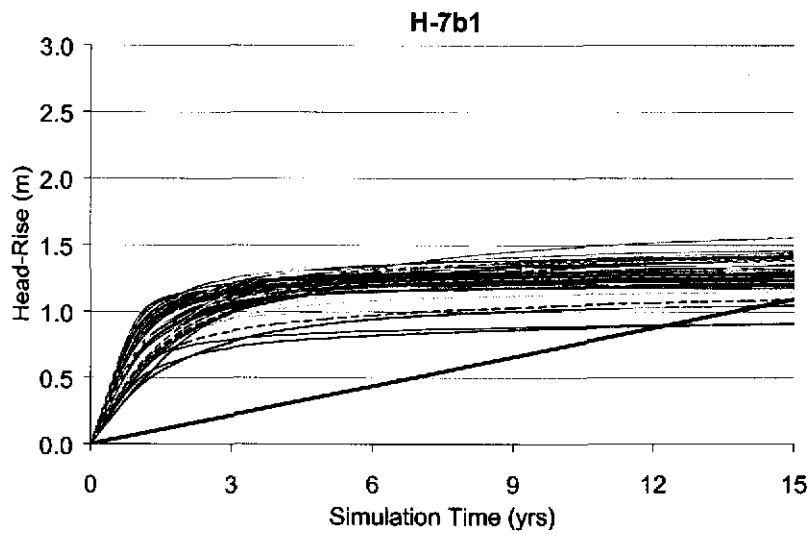
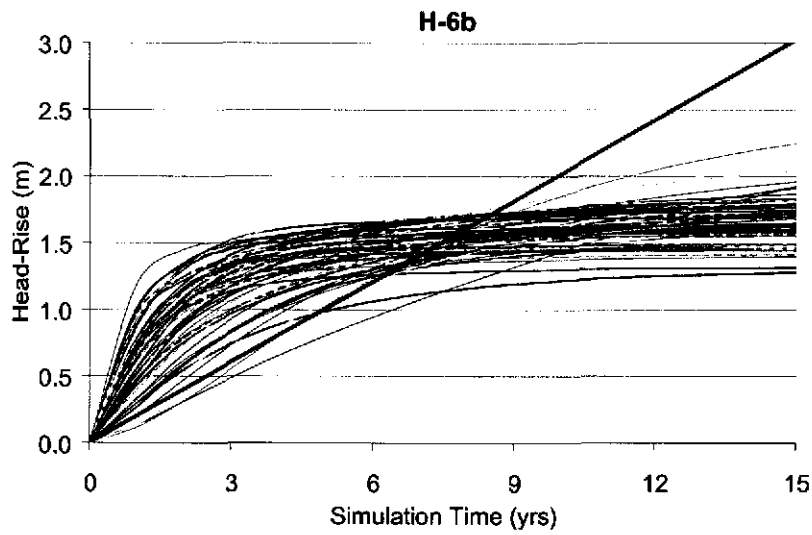
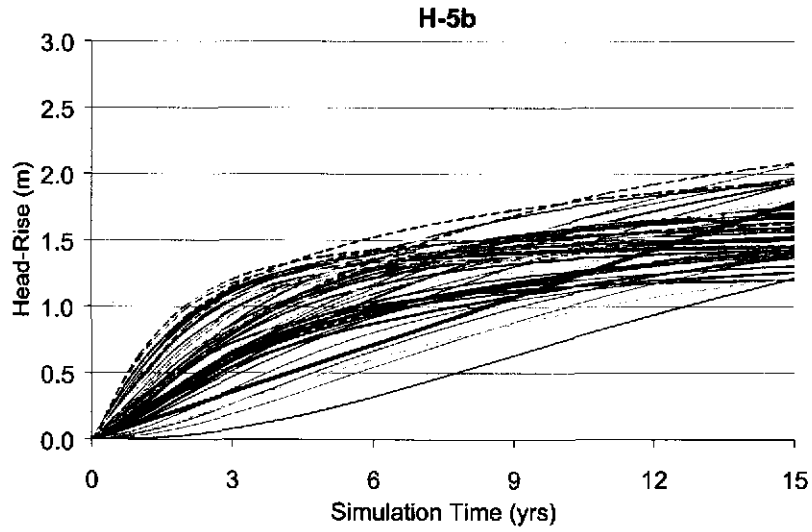
#Create new que file
runFile=$Runs.sh
echo '#PBS -N mfrun' > ${runFile}
echo '#PBS -j oe' >> ${runFile}
echo '#PBS -k oe' >> ${runFile}
echo '#PBS -q half' >> ${runFile}
echo '#PBS -S /bin/bash' >> ${runFile}
echo ' ' >> ${runFile}
echo '# Run steady-state model' >> ${runFile}
echo 'cd /home3/tslowry/wipp/lkybrhl/'$Runs >> ${runFile}
echo 'mf2k LBH1_steady.nam' >> ${runFile}
echo '# Re-write new starting heads' >> ${runFile}
echo 'Get_heads' >> ${runFile}
echo 'mv LBH1.ba6 LBH1_old.ba6' >> ${runFile}
echo 'mv LBH1_new.ba6 LBH1.ba6' >> ${runFile}
echo '# Run transient model' >> ${runFile}
echo 'mf2k LBH1_home.nam' >> ${runFile}
echo '# Get heads and drawdowns at each well location' >> ${runFile}
echo 'exhdsdrw' >> ${runFile}
mv $runFile $Runs
cd $THISDIR/$Runs
chmod u+x $runFile

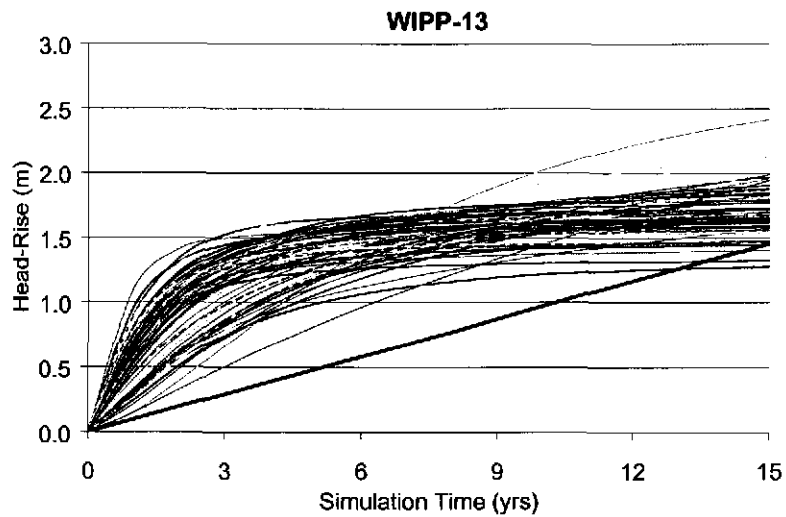
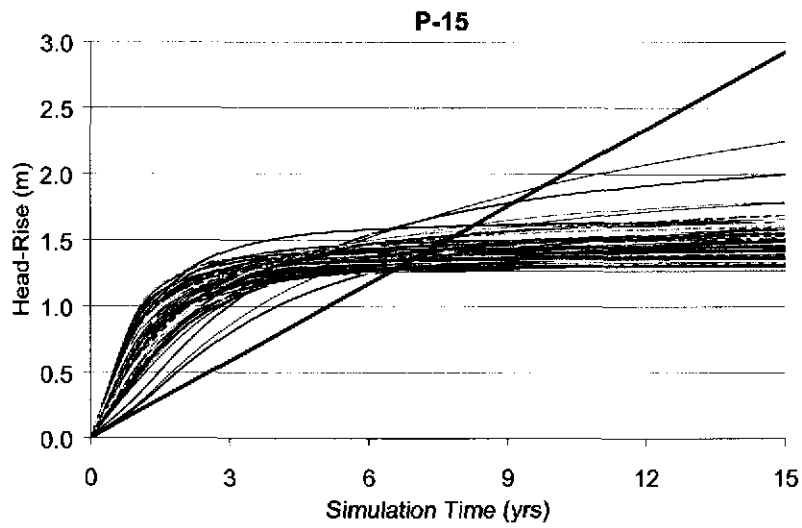
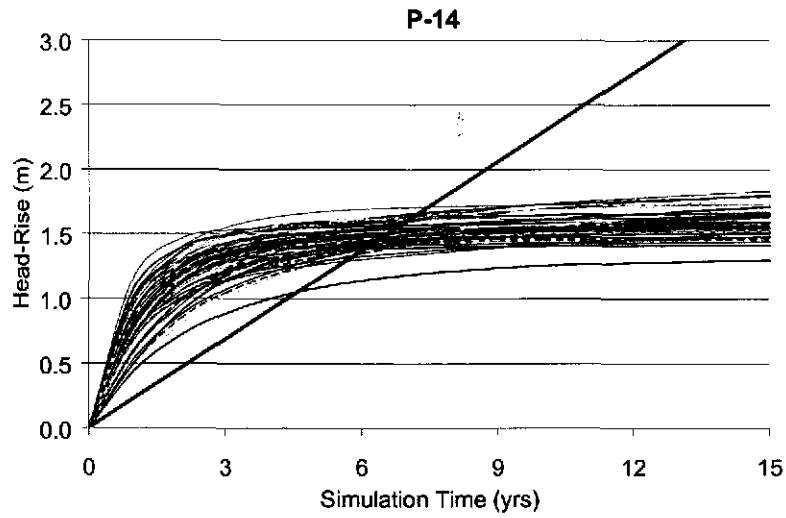
#Que run file
qsub $runFile
cd $THISDIR
done
```

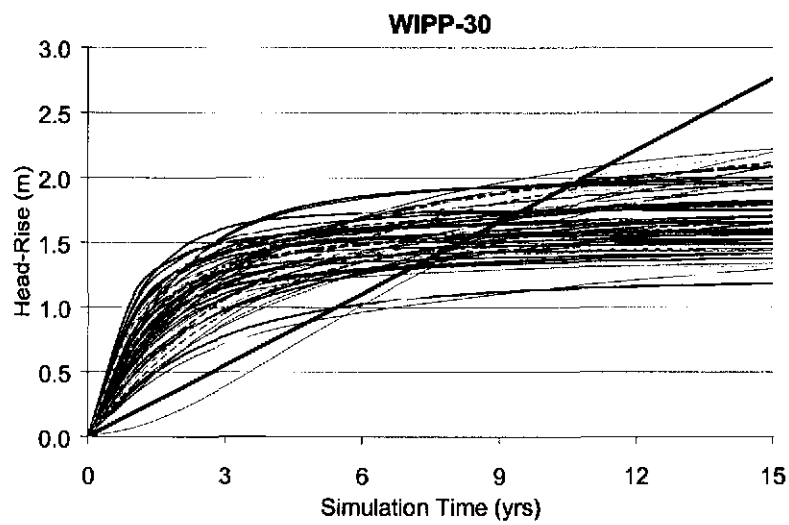
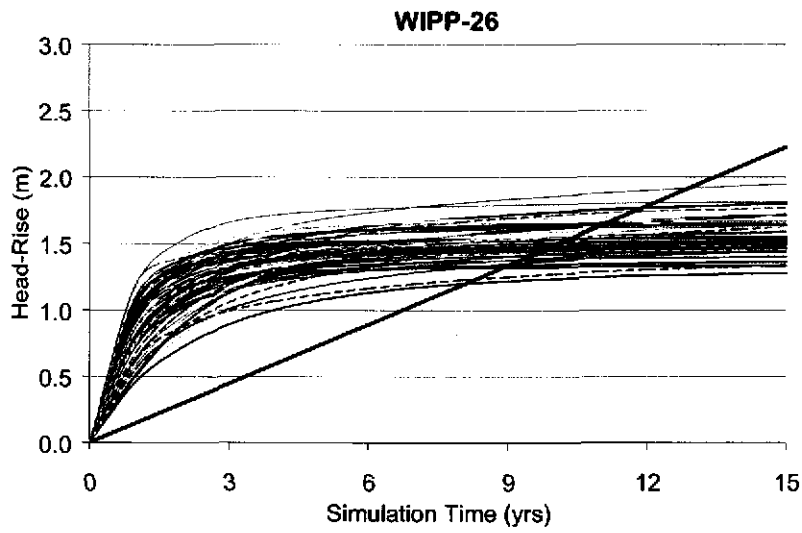
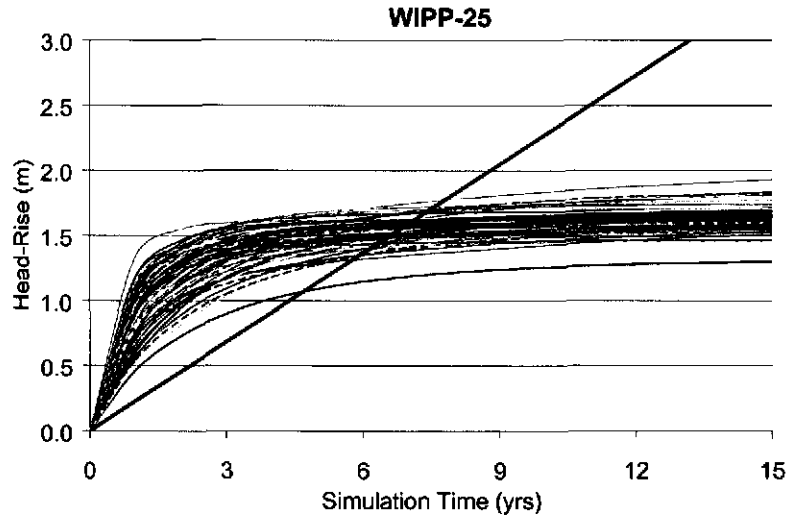
Appendix N: Option A Calibrated Filtered Head Rises

Each plot shows the head rise for each T-field using the calibrated parameters. The thick red line in each plot represents the slope of the head rise calculated from the data shown in Appendix A.









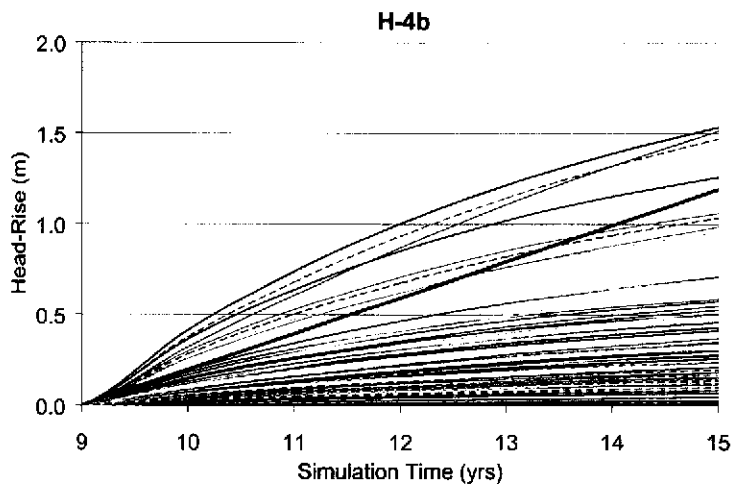
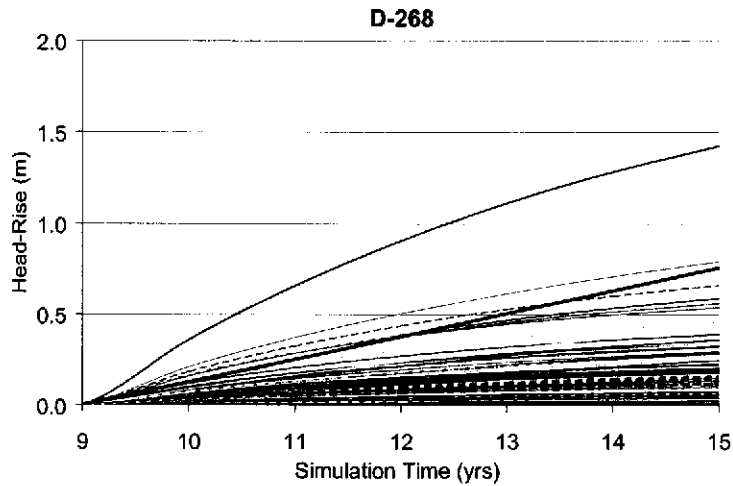
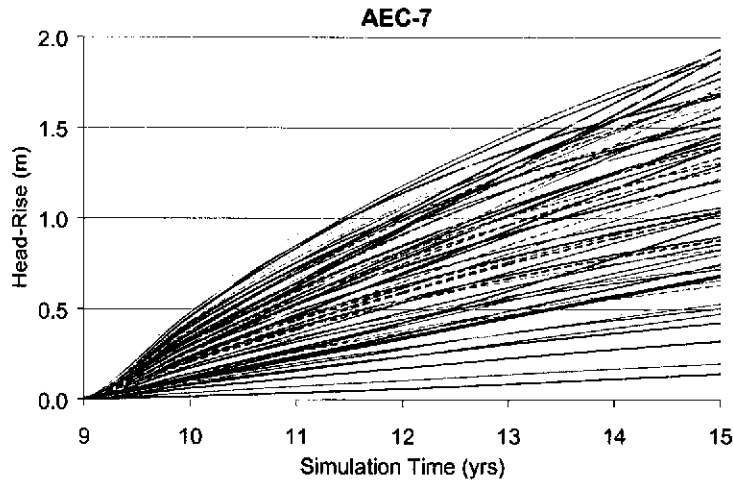
Appendix O: Option A Calibration Results

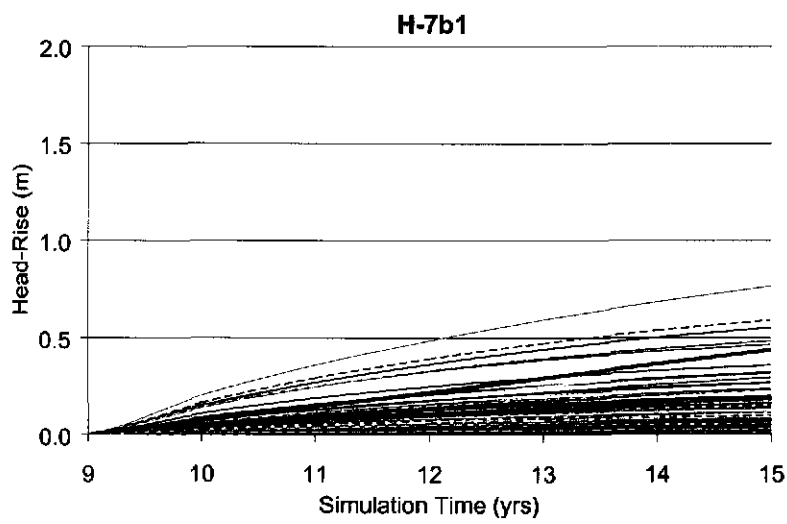
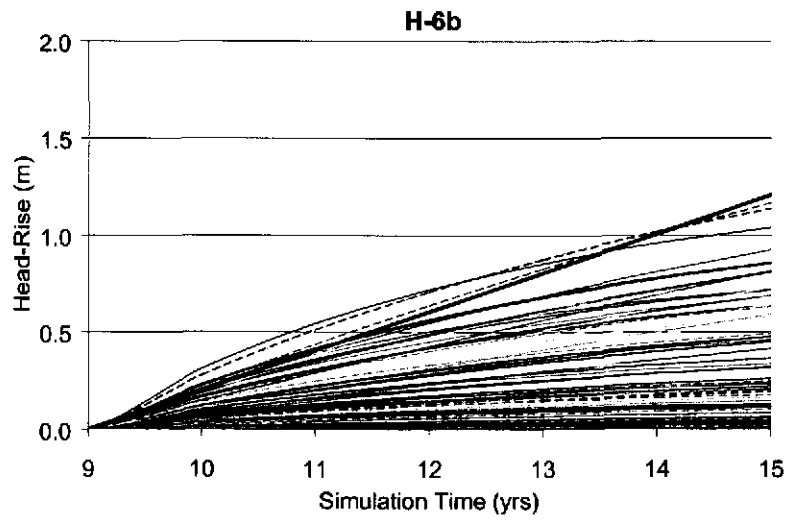
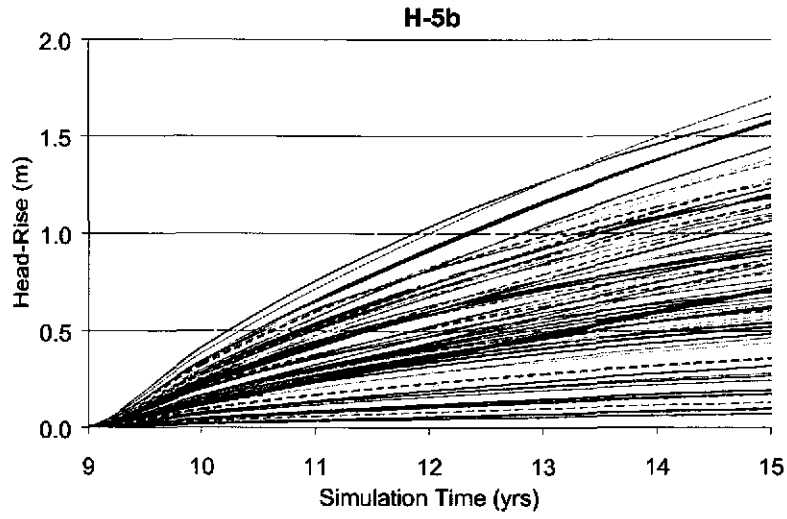
T-Field	Leakage Rate per Well (m ³ /s)			
	Upper	Mid	Nash Draw	Lower
d01r02	8.32E-07	7.81E-07	9.03E-06	3.59E-05
d01r06	2.69E-06	9.04E-09	4.49E-05	1.80E-04
d01r07	5.21E-06	9.74E-10	2.01E-05	1.16E-05
d01r08	3.24E-05	1.16E-09	2.17E-06	2.21E-04
d01r10	1.22E-05	4.92E-10	2.30E-05	8.90E-05
d02r02	5.01E-06	4.44E-07	1.02E-05	1.62E-05
d02r07	5.45E-06	2.24E-10	2.26E-05	4.49E-05
d02r10	1.56E-05	1.00E-10	4.07E-06	3.42E-05
d03r03	1.80E-06	5.57E-07	2.42E-05	5.50E-05
d03r06	1.62E-05	1.03E-10	3.11E-05	1.13E-04
d03r07	4.06E-05	1.00E-10	2.05E-05	8.18E-05
d03r09	1.63E-05	1.56E-10	5.17E-08	5.70E-05
d03r10	1.48E-05	1.23E-10	6.86E-05	3.10E-04
d04r02	1.56E-05	1.00E-10	1.32E-05	1.90E-05
d04r03	1.72E-05	1.00E-10	3.10E-08	8.14E-05
d04r05	1.05E-05	1.10E-09	6.87E-05	5.83E-05
d04r06	3.31E-06	4.84E-08	2.71E-05	8.50E-05
d04r07	1.18E-05	5.00E-10	5.44E-05	6.64E-05
d04r08	1.37E-05	1.61E-10	2.29E-05	3.15E-05
d04r10	1.61E-06	1.79E-08	4.95E-05	1.80E-05
d05r01	1.38E-05	1.00E-10	2.30E-05	7.60E-06
d05r02	2.84E-05	4.73E-10	1.58E-05	3.10E-05
d05r03	3.21E-05	1.00E-10	1.60E-05	5.48E-05
d05r05	1.45E-05	1.00E-10	1.87E-05	3.49E-05
d05r07	1.50E-05	1.11E-09	1.24E-06	1.38E-04
d06r02	1.22E-05	2.94E-07	5.93E-05	1.07E-04
d06r03	4.41E-05	1.00E-10	8.48E-07	1.88E-04
d06r04	1.67E-05	6.84E-07	1.19E-05	1.91E-05
d06r07	1.34E-05	6.55E-10	3.26E-05	6.20E-05
d06r10	1.08E-05	1.00E-10	1.86E-05	7.97E-05
d07r01	7.61E-06	1.00E-10	3.71E-05	4.09E-05
d07r02	5.50E-05	5.47E-07	4.93E-06	9.78E-05
d07r05	4.27E-05	3.06E-07	9.88E-06	1.14E-04
d07r07	6.15E-06	5.92E-08	4.26E-05	3.70E-05
d07r08	3.75E-06	6.55E-10	2.41E-05	9.00E-06
d07r09	3.62E-05	1.00E-10	3.47E-06	8.43E-05
d07r10	2.12E-05	3.11E-07	8.55E-05	2.77E-05
d08r01	1.44E-05	8.23E-07	6.70E-09	8.55E-05
d08r03	2.23E-05	3.82E-10	1.96E-05	4.47E-05
d08r04	2.00E-05	2.30E-09	1.90E-07	1.05E-04
d08r05	1.02E-05	5.94E-07	3.58E-05	2.14E-05
d08r06	1.91E-05	1.02E-09	1.73E-09	8.86E-05
d08r07	2.61E-06	5.31E-07	4.48E-05	2.13E-05
d08r09	1.58E-05	1.88E-10	2.38E-09	3.24E-05
d09r02	1.98E-05	3.34E-10	4.52E-06	1.24E-04
d09r03	1.60E-05	1.00E-10	7.38E-05	8.91E-05

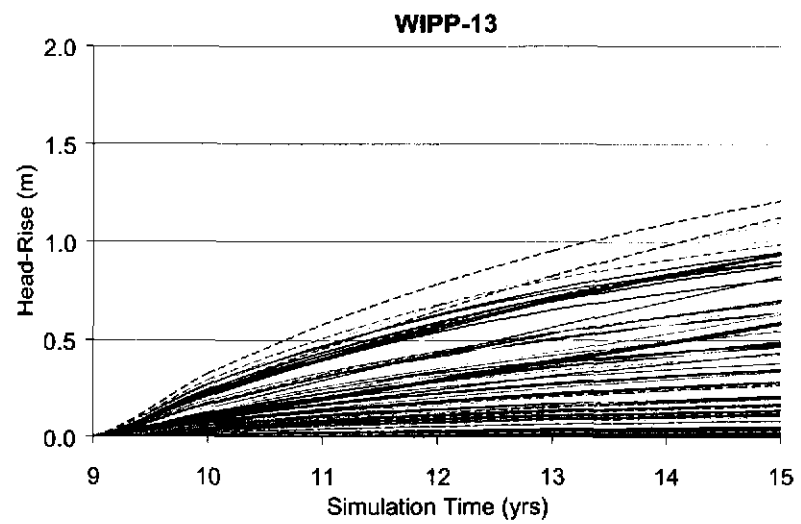
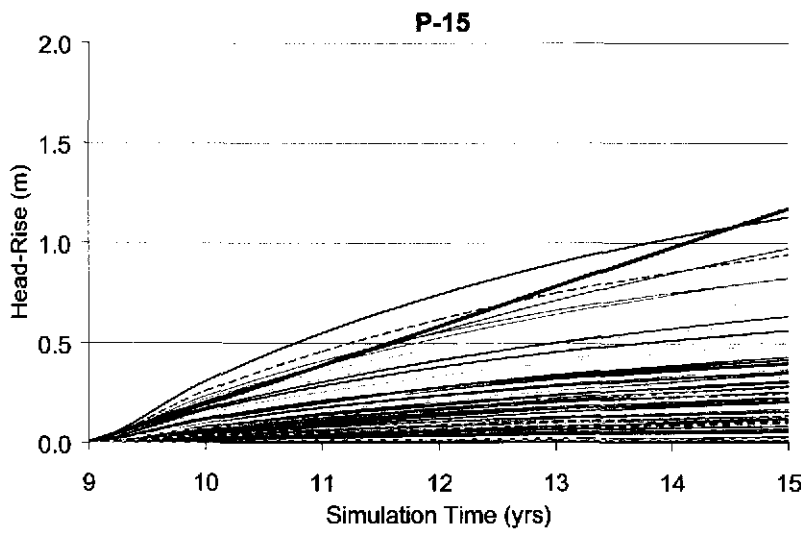
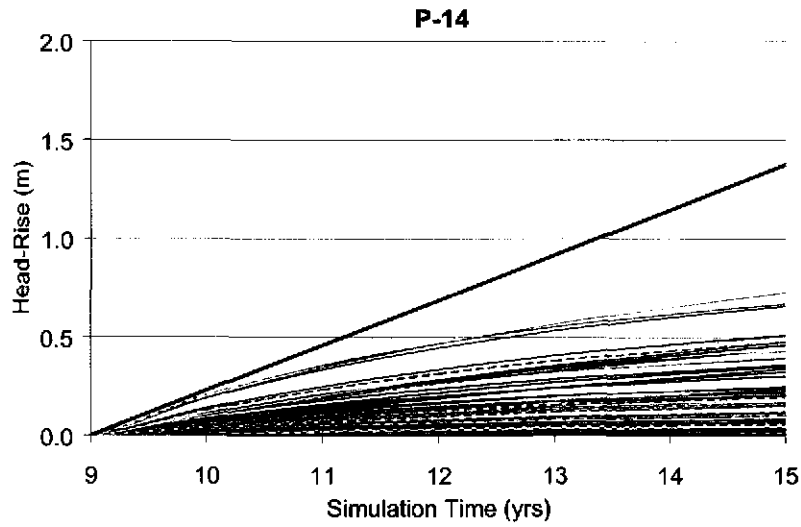
d09r04	5.65E-06	6.81E-07	4.92E-05	2.12E-05
d09r05	1.30E-05	1.00E-10	2.49E-05	5.43E-05
d09r06	6.67E-06	6.03E-09	5.59E-05	4.02E-05
d09r07	4.97E-06	1.32E-10	1.10E-05	4.16E-05
d09r08	2.21E-05	2.14E-10	1.13E-08	9.78E-05
d09r10	4.33E-06	1.99E-09	4.94E-06	6.64E-05
d10r03	2.60E-05	8.98E-10	4.01E-05	1.38E-04
d10r04	1.35E-05	1.00E-10	5.40E-05	1.20E-04
d10r08	1.29E-05	5.00E-10	2.04E-05	9.55E-05
d10r10	1.98E-04	1.00E-10	1.07E-08	1.18E-04
d11r01	1.72E-05	5.00E-10	3.36E-06	5.18E-05
d11r02	1.69E-05	1.00E-10	7.13E-06	7.89E-05
d11r07	2.13E-05	2.32E-07	2.22E-05	2.99E-05
d11r08	2.59E-05	1.70E-09	4.16E-07	1.90E-04
d11r10	1.77E-05	3.90E-10	6.94E-06	1.79E-04
d12r01	2.31E-05	7.73E-08	1.11E-08	9.27E-05
d12r02	2.53E-06	1.00E-10	5.48E-05	7.79E-05
d12r07	1.09E-05	1.24E-09	4.63E-05	3.50E-05
d12r08	6.59E-06	1.00E-10	4.55E-05	9.57E-05
d22r02	3.10E-06	1.00E-09	1.16E-05	6.31E-05

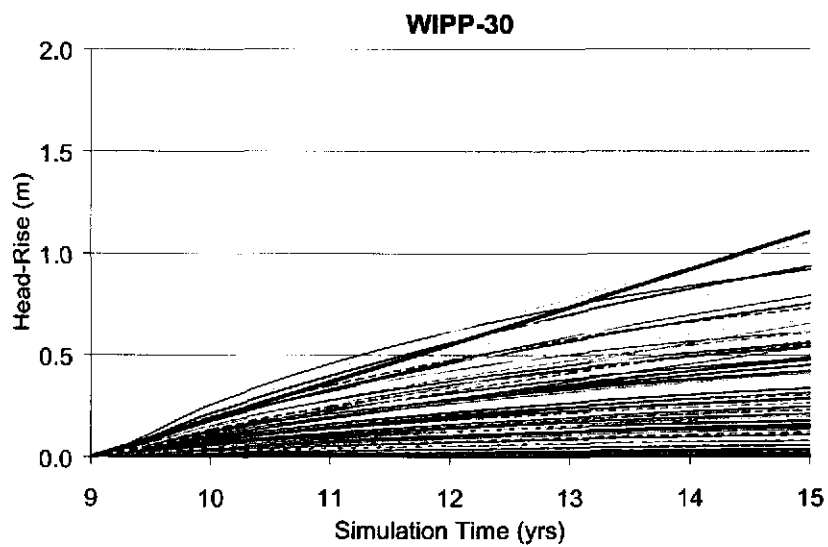
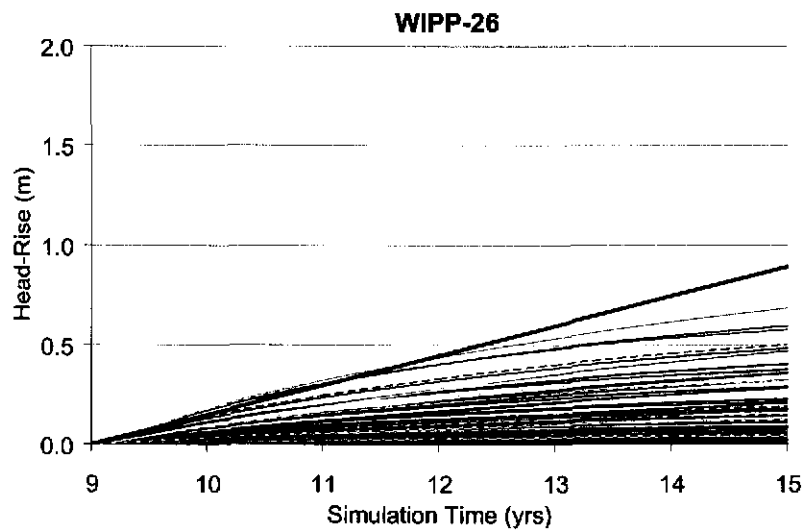
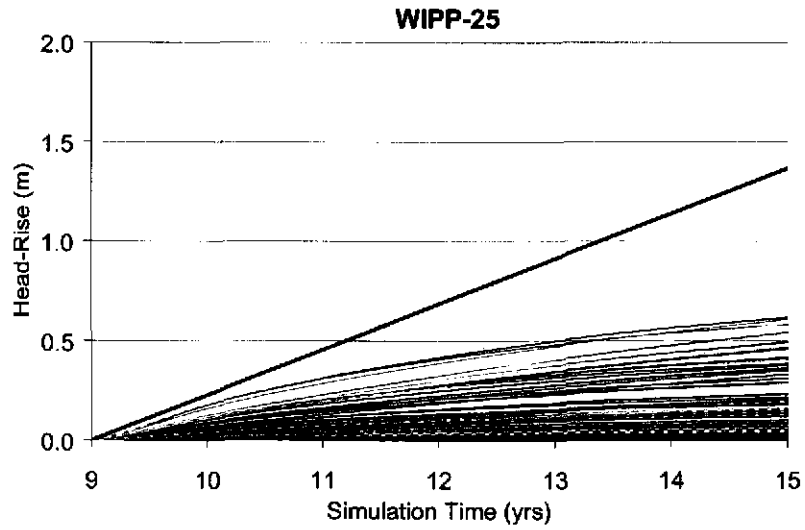
Appendix P: Option B Calibrated Filtered Head Rises

Each plot shows the head rise for each T-field using the calibrated parameters. The thick red line in each plot represents the slope of the head rise calculated from the data shown in Appendix A.









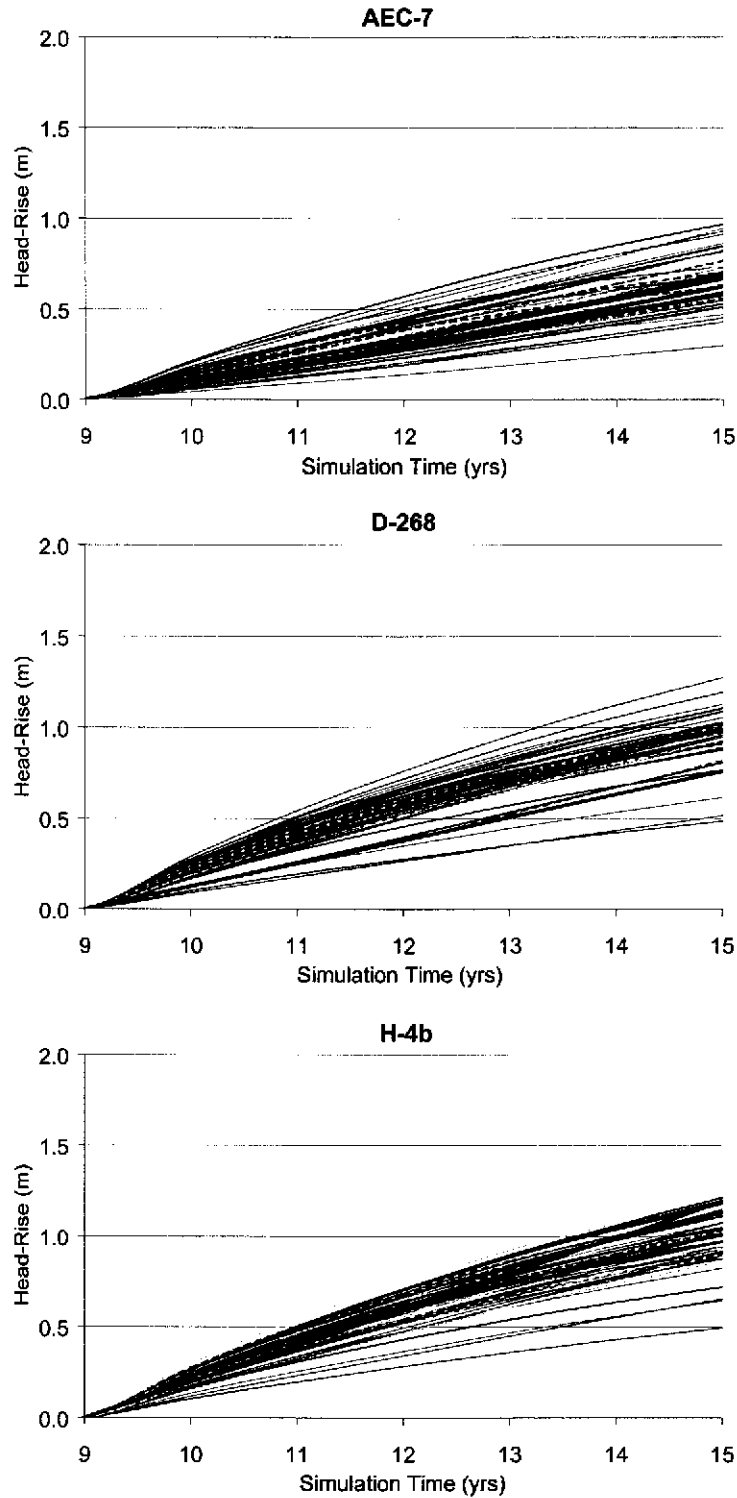
Appendix Q: Option B Calibration Results

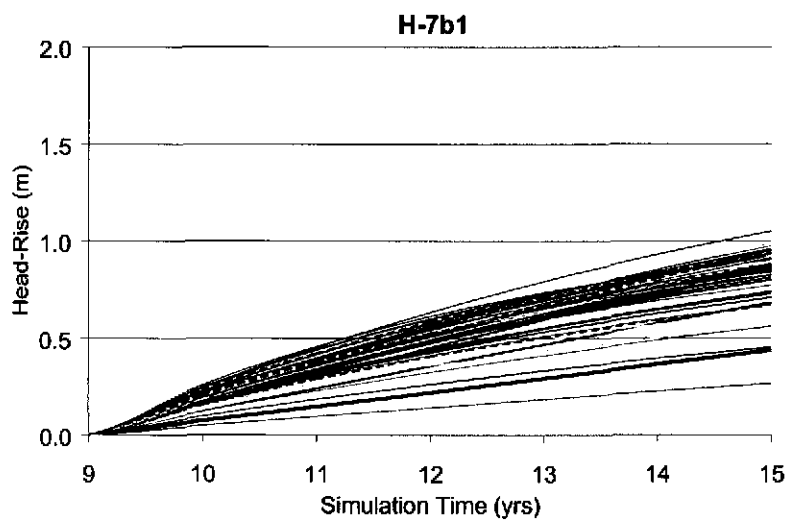
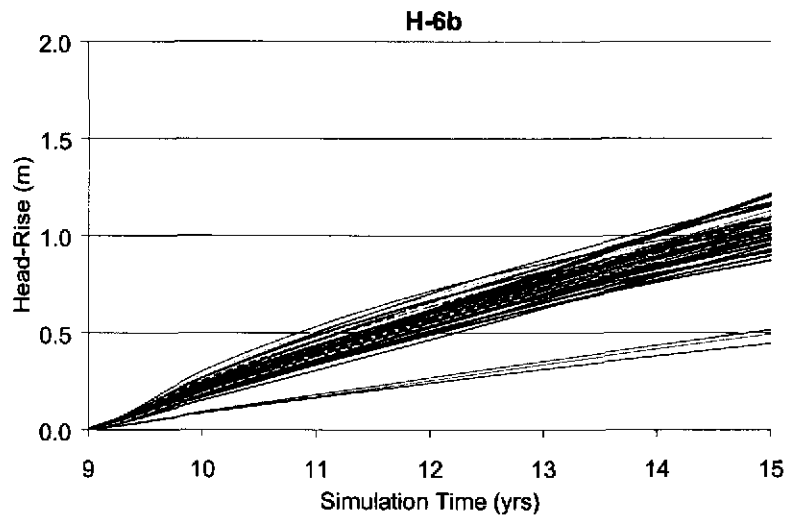
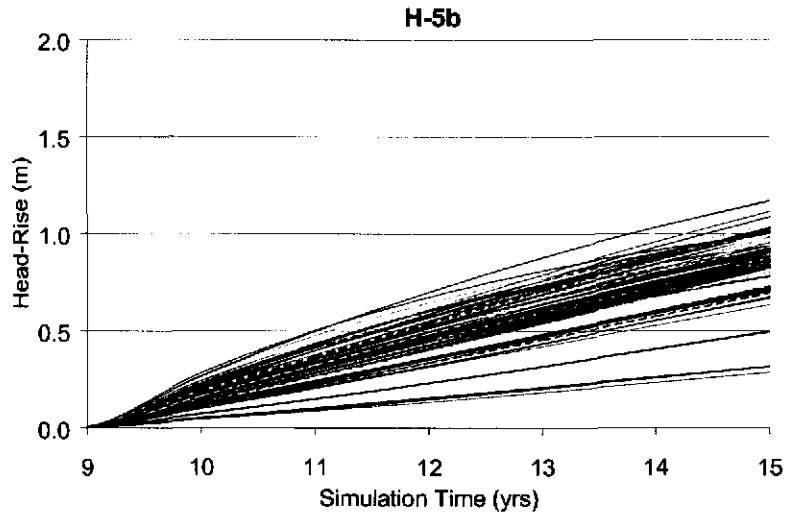
T-Field	Leakage Rate per Well (m ³ /s)		
	Upper	Mid / Nash Draw	Lower
d01r02	3.70E-06	2.00E-09	6.74E-04
d01r07	2.01E-07	2.81E-09	1.70E-03
d01r08	9.51E-05	4.00E-09	6.31E-03
d01r10	5.72E-07	2.86E-08	3.59E-03
d02r02	1.95E-07	1.00E-09	9.50E-04
d02r07	7.04E-07	2.86E-08	1.06E-03
d02r10	4.67E-06	1.00E-08	5.91E-04
d03r03	3.11E-08	2.55E-08	1.26E-03
d03r06	1.92E-06	2.11E-09	5.75E-03
d03r07	6.44E-05	1.03E-09	1.21E-05
d03r09	5.25E-05	2.09E-08	4.20E-06
d03r10	1.38E-06	3.11E-09	6.90E-03
d04r02	2.69E-07	1.19E-10	4.15E-04
d04r03	9.25E-06	1.00E-08	2.96E-03
d04r05	3.08E-07	9.41E-10	4.90E-03
d04r06	1.15E-06	1.80E-08	3.39E-03
d04r08	6.30E-06	8.92E-09	2.31E-03
d04r10	1.98E-08	2.00E-08	1.36E-03
d05r02	3.25E-05	2.24E-08	8.74E-05
d05r03	5.05E-05	9.96E-10	1.02E-05
d05r05	7.53E-06	1.00E-08	3.92E-04
d05r07	8.87E-05	1.00E-08	1.18E-03
d06r02	4.68E-08	8.41E-09	2.56E-03
d06r03	1.15E-05	1.00E-08	3.25E-03
d06r04	5.50E-06	1.00E-08	8.00E-04
d06r06	5.90E-06	2.68E-09	8.83E-03
d06r07	2.51E-05	3.70E-09	8.63E-04
d07r01	7.90E-07	9.41E-08	3.33E-03
d07r02	7.60E-04	4.47E-08	3.81E-06
d07r05	1.81E-04	1.00E-08	2.89E-03
d07r07	5.96E-08	1.00E-08	6.94E-04
d07r08	5.57E-08	8.00E-10	1.98E-03
d07r09	1.76E-04	1.06E-10	2.91E-06
d07r10	9.36E-07	3.51E-08	3.62E-04
d08r01	6.31E-05	3.76E-09	3.57E-04
d08r02	9.16E-06	1.00E-08	9.81E-04
d08r03	5.00E-06	1.00E-08	6.50E-04
d08r04	4.56E-08	2.46E-08	1.92E-03
d08r05	6.49E-06	6.76E-08	1.70E-03

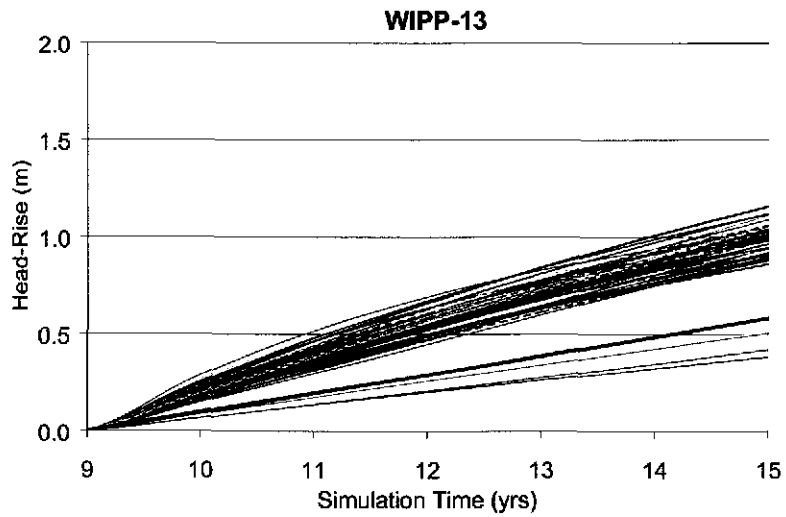
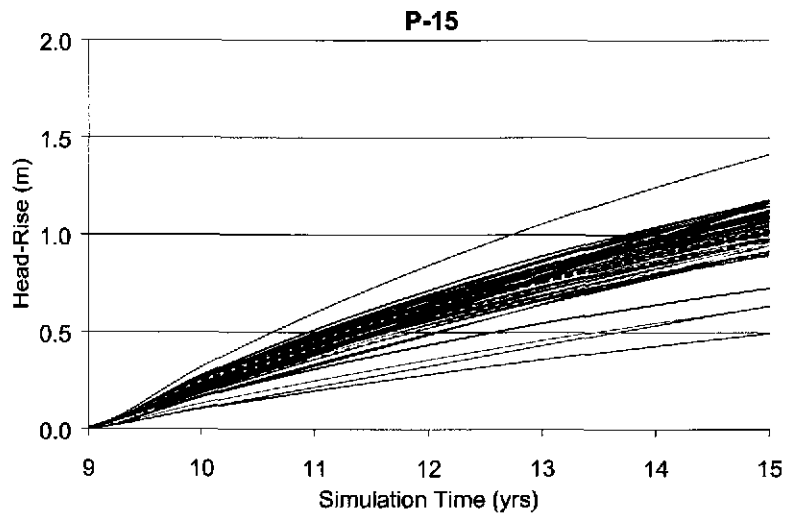
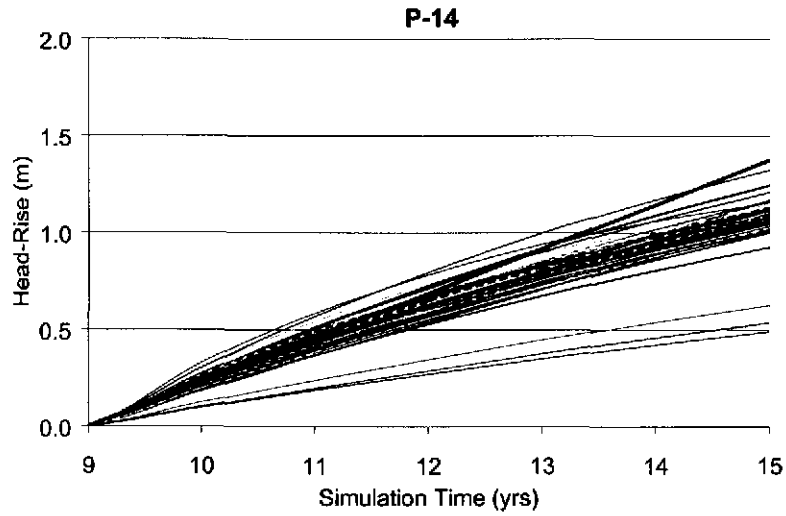
d08r06	2.41E-06	1.46E-08	2.08E-04
d08r09	6.99E-06	1.00E-08	2.11E-04
d09r02	1.06E-04	2.00E-09	5.70E-04
d09r05	1.02E-04	2.16E-08	2.50E-06
d09r10	5.34E-09	9.63E-09	1.20E-03
d10r02	1.07E-06	1.44E-09	1.02E-02
d10r07	2.42E-04	2.80E-08	2.13E-03
d10r08	4.68E-06	2.46E-09	3.18E-03
d10r10	2.22E-04	4.00E-09	3.80E-03
d11r01	2.11E-07	1.94E-08	1.47E-03
d11r06	4.37E-04	3.42E-09	1.27E-03
d11r07	2.70E-04	3.89E-10	3.47E-06
d11r08	4.71E-09	1.42E-08	5.30E-03
d11r10	2.60E-07	5.25E-09	7.75E-03
d12r01	6.24E-06	1.98E-09	1.63E-03
d12r02	5.45E-05	4.47E-08	3.18E-03
d12r03	6.23E-05	1.33E-09	1.13E-03
d12r05	6.59E-06	3.55E-09	4.04E-03
d12r06	8.70E-07	9.66E-09	1.48E-03
d12r07	2.35E-05	1.00E-08	7.05E-03
d12r08	1.35E-07	2.07E-09	2.59E-03
d13r01	1.07E-07	2.86E-09	2.84E-03
d13r02	1.05E-05	1.34E-08	2.02E-03
d13r05	1.01E-06	6.29E-09	1.08E-03
d13r08	6.32E-07	4.47E-09	3.23E-03
d21r01	1.91E-04	7.99E-10	8.01E-04
d21r02	1.21E-04	7.23E-10	5.56E-06
d21r03	1.48E-04	1.79E-09	1.40E-05
d21r05	1.96E-06	1.00E-08	8.24E-03
d21r07	2.45E-06	5.42E-09	4.04E-03
d21r10	1.62E-05	1.79E-08	4.97E-03
d22r02	1.04E-07	4.00E-09	1.84E-03
d22r05	2.69E-07	4.99E-09	2.68E-04
d22r06	9.27E-05	1.34E-08	1.35E-04
d22r07	4.41E-06	7.01E-09	4.98E-03
d22r08	1.18E-05	1.00E-08	1.97E-03
d22r09	5.53E-06	1.00E-08	3.12E-03
d22r10	2.08E-05	2.97E-08	3.63E-03

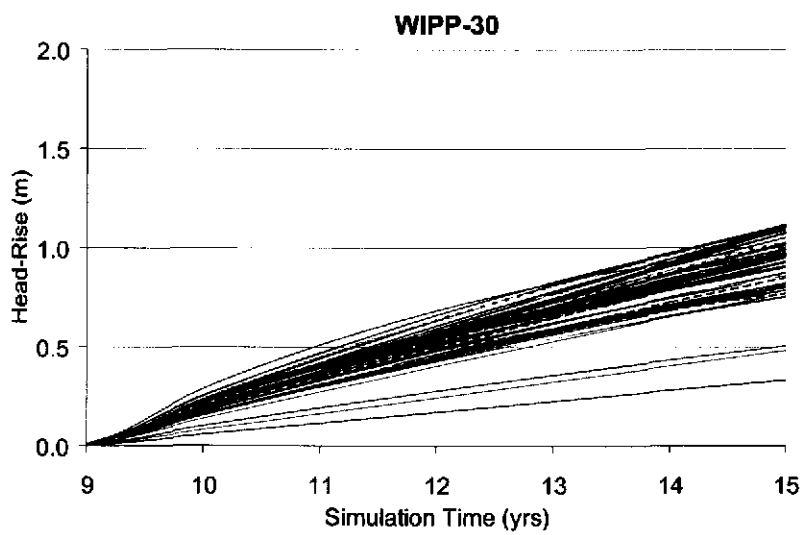
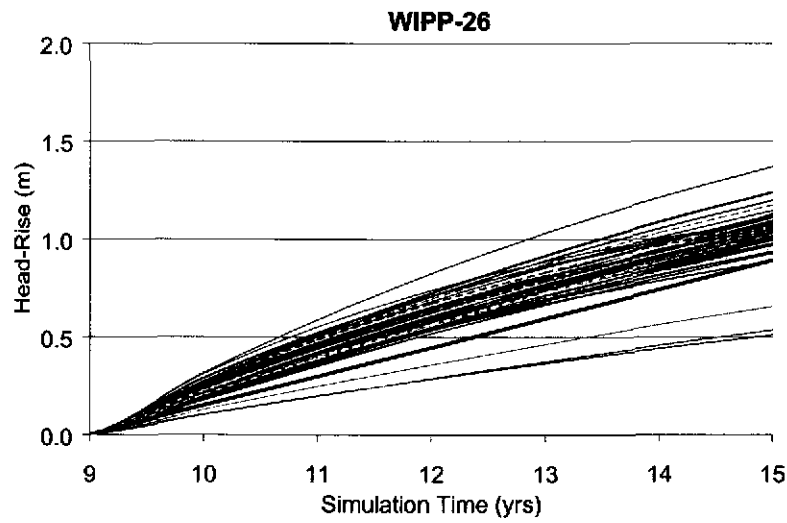
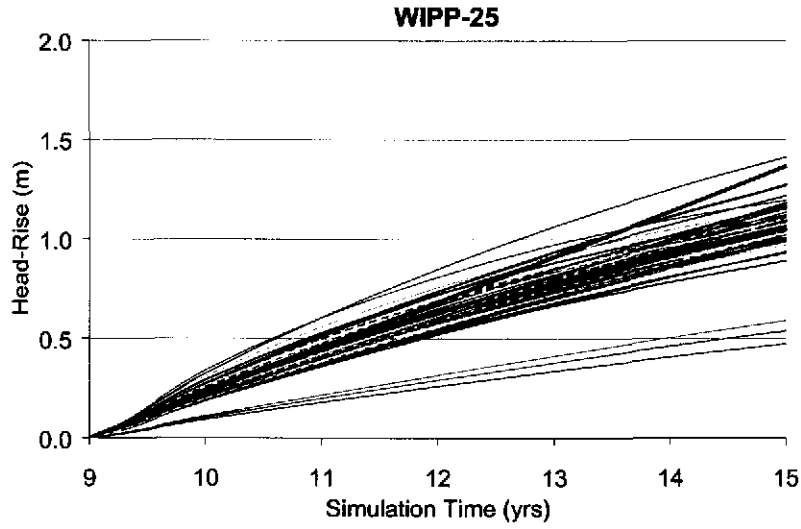
Appendix R: Option C Calibrated Filtered Head Rises

Each plot shows the head rise for each T-field using the calibrated parameters. The thick red line in each plot represents the slope of the head rise calculated from the data shown in Appendix A.









Appendix S: Option C Calibration Results

T-Field	Leakage Rate per Well (m ³ /s)*			Specific Storage (m ⁻¹)	
	Upper	Mid	Lower	S _s ND	S _s
d01r02	1.25E-05	3.31E-06	1.13E-04	4.72E-05	4.81E-06
d01r06	2.29E-05	4.32E-07	1.82E-03	3.91E-05	2.17E-05
d01r08	2.79E-05	3.42E-06	2.49E-03	6.01E-05	7.20E-06
d02r02	2.28E-05	1.08E-06	1.09E-04	1.96E-05	9.34E-06
d02r07	5.84E-06	1.32E-06	8.74E-04	2.91E-05	4.33E-07
d02r10	8.62E-05	1.04E-06	1.40E-04	7.03E-05	1.01E-05
d03r03	4.71E-06	2.32E-07	7.71E-04	2.42E-05	4.41E-06
d03r06	3.45E-07	2.73E-07	1.32E-03	7.19E-05	1.42E-06
d03r07	1.78E-06	1.79E-08	1.33E-03	5.68E-05	1.35E-06
d03r09	5.97E-06	2.03E-06	4.48E-04	3.16E-05	2.12E-06
d03r10	9.71E-05	5.56E-07	2.22E-03	9.02E-05	9.07E-06
d04r02	1.20E-05	5.66E-08	2.18E-04	3.13E-05	8.78E-07
d04r03	8.48E-06	6.90E-06	7.07E-04	3.77E-05	3.51E-06
d04r05	1.21E-06	1.11E-08	2.98E-03	4.86E-05	2.24E-08
d04r06	4.90E-06	2.01E-06	1.02E-03	4.35E-05	7.98E-06
d04r07	2.11E-06	7.26E-07	6.24E-04	8.67E-05	1.81E-08
d04r08	1.26E-07	2.30E-08	2.00E-04	5.18E-05	5.82E-06
d04r10	8.38E-06	1.64E-06	3.75E-04	8.69E-05	8.83E-06
d05r05	5.01E-05	5.30E-08	7.19E-05	4.74E-05	9.97E-06
d05r07	6.86E-06	1.52E-06	1.09E-03	4.28E-05	1.56E-05
d06r04	2.42E-05	5.06E-06	1.87E-04	2.18E-05	1.85E-06
d06r06	7.18E-06	2.05E-07	1.70E-03	6.98E-05	1.10E-05
d06r07	9.93E-05	1.91E-07	1.69E-03	3.14E-05	1.02E-08
d06r10	2.65E-05	1.85E-07	6.55E-04	6.72E-05	2.83E-06
d07r05	7.12E-08	8.36E-06	1.03E-03	7.59E-05	1.31E-08
d07r08	1.57E-05	1.12E-05	3.91E-04	2.47E-05	1.66E-07
d08r01	2.74E-05	2.44E-06	3.98E-04	3.09E-05	1.78E-06
d08r03	3.47E-05	3.33E-06	5.49E-04	5.97E-05	3.15E-07
d08r05	3.95E-07	5.94E-07	1.52E-03	3.26E-05	2.41E-08
d08r06	1.20E-05	1.52E-06	9.04E-04	6.57E-05	1.98E-06
d08r07	1.26E-06	1.88E-06	1.04E-03	3.28E-06	1.88E-05
d09r02	7.17E-05	8.36E-07	6.44E-04	5.40E-05	1.39E-05
d09r05	1.67E-05	1.47E-05	7.25E-04	8.37E-05	1.20E-06
d09r06	1.77E-05	2.24E-08	1.02E-03	4.39E-05	9.86E-06
d09r07	2.67E-07	2.39E-07	3.86E-04	1.43E-05	4.12E-06
d09r08	2.87E-05	5.33E-06	6.57E-04	7.82E-05	1.90E-06
d09r10	3.18E-06	4.02E-06	2.54E-04	2.84E-05	2.10E-06
d10r07	2.40E-05	1.10E-05	1.49E-03	9.63E-05	5.69E-07
d10r08	1.08E-05	1.06E-05	9.75E-04	7.57E-05	4.73E-06
d10r10	2.29E-05	4.04E-06	1.83E-03	7.39E-05	1.07E-06
d11r01	4.56E-05	1.81E-06	2.12E-04	5.89E-05	2.49E-06
d11r02	8.24E-05	3.01E-06	2.76E-04	2.86E-05	1.25E-05
d11r09	3.55E-05	3.29E-07	5.81E-04	1.51E-05	5.55E-05

d12r01	3.44E-05	1.65E-06	5.75E-04	5.90E-05	2.35E-06
d12r02	5.14E-08	1.52E-07	1.40E-03	5.42E-05	8.54E-06
d12r03	6.79E-05	3.92E-08	4.00E-04	9.99E-05	1.76E-06
d12r06	2.95E-05	7.64E-07	2.72E-04	9.41E-05	8.30E-08
d12r07	3.39E-05	7.01E-07	7.38E-04	9.47E-05	2.20E-07
d12r09	1.70E-05	4.31E-06	3.59E-04	4.24E-05	1.85E-06
d13r01	8.35E-06	2.49E-06	1.02E-03	6.83E-05	2.57E-06
d13r02	4.02E-06	4.42E-06	7.93E-04	6.25E-05	1.82E-06
d13r03	9.59E-06	2.57E-05	2.88E-04	3.13E-05	6.95E-06
d13r05	4.76E-06	7.85E-06	3.56E-04	2.17E-05	1.23E-05
d13r06	2.22E-05	7.82E-08	2.68E-04	1.54E-05	2.09E-05
d13r07	2.15E-05	1.77E-05	1.44E-03	4.01E-05	1.87E-06
d21r02	1.58E-05	9.74E-06	9.08E-04	4.74E-05	6.03E-06
d21r04	6.15E-05	1.87E-07	2.85E-04	2.04E-05	2.16E-05
d21r06	7.63E-05	4.10E-06	7.39E-04	5.11E-06	3.06E-05
d21r10	4.02E-06	1.10E-06	1.31E-03	3.81E-05	3.02E-06
d22r02	4.32E-07	3.97E-07	4.82E-04	1.92E-05	3.48E-06
d22r04	1.44E-05	7.27E-06	7.99E-04	2.91E-05	5.70E-06
d22r05	6.05E-07	5.73E-07	6.08E-04	2.57E-05	1.13E-07
d22r06	9.88E-06	4.36E-06	4.80E-04	2.54E-05	6.75E-06
d22r07	3.18E-06	5.12E-05	1.07E-03	5.85E-05	7.02E-08
d22r08	4.86E-05	4.07E-08	5.27E-04	8.92E-05	4.37E-06

***The Nash Draw Group was fixed at a rate of $2.36 \times 10^{-5} \text{ m}^3/\text{s}$.**

Appendix T: Option C Long-Term Simulations (115 yr)

